UNIVERSITY OF CALIFORNIA
RIVERSIDE

Dynamic Rupture and Ground Motion Modeling on Realistically Complex Strike-Slip Faults

A Dissertation submitted in partial satisfaction
of the requirements for the degree of

Doctor of Philosophy

in

Geological Sciences

by

Julian Charles Lozos

June 2013

Dissertation Committee:
Dr. David D. Oglesby, Chairperson
Dr. James N. Brune
Dr. James H. Dieterich
Dr. Gareth J. Funning

The Dissertation of Julian Charles Lozos is approved:

Committee Chairperson

University of California, Riverside

Acknowledgments

This dissertation would have never come together without the help of a huge supporting cast of people. I am incredibly grateful and thankful for all the technical, interpretational, and emotional support I have received over the past five years. I wish I could name everyone who helped, but that could turn into something as long as another entire chapter.

Starting with the obvious: thanks to the Southern California Earthquake Center and the US Geological Survey Earthquake Hazards Program for funding the grants that supported this research and kept me fed and housed over the course of said research.

In terms of technical support, I cannot thank Michael Barall enough. Michael is the author of FaultMod, the dynamic rupture code used in three of the four chapters of this dissertation. Not only did he write some adaptations to the code to specifically tailor it for the types of problems I was working on, but he was incredibly patient and helpful with all of my questions and problems and 2 AM emails. This project literally would not have happened, at least not in the way presented here, without him. On a related note, I would like to thank Ben Duan, author of EQDyna, which I used in chapter one. Several people helped me with other aspects of code setup: thanks to Phil Maechling, for helping me get the SCEC CVM up and running; to Jacqui Gilchrist, for modifying FaultMod to read in stress states from an external file; and to Kenny Ryan, for setting up the creeping patch geometry in FaultMod.

There are many people that contributed to the science itself, in terms of interpretation, of suggesting things for me to model, and of suggesting new extensions and directions for ideas I already had:

Thanks to Jim Dieterich, for many things. First, for long conversations about the details of friction laws, their implementation, and their meaning in dynamics. Second, for getting extremely excited about a small detail of my MS thesis that ultimately became chapter one of this dissertation. Third, for being a member of my dissertation committee and the head of my quals committee. And fourth, for that trip to Hawaii.

Thanks to Gareth Funning, who, in addition to being on my dissertation and quals committees, also happened to teach the very first earth science course I ever took. His guidance on science, on how to not stress out so much, and on having a thicker skin about commentary, all from day one, has been invaluable. Gareth is also responsible for my getting into modeling aseismic creep, and I look forward to continued collaborations on this.

Thanks to Jim Brune. One of my first conversations with him was about how it was interesting that there were so many precariously balanced rocks near the stepover in the San Jacinto Fault. This conversation effectively led to one MS thesis chapter, two dissertation chapters, and my beginning to model ground motion to begin with. Jim also was on both my quals committee and my dissertation committee. Thanks for the fieldwork opportunities as well!

Thanks to Kim Olsen, for helping take the San Jacinto ground motion models to the next level, from qualitative descriptions to quantitative analyses with risk

implications. Kim has been extremely helpful in model setup and interpretation, and has had the patience of a saint while all of my own models have taken far longer than I told him they would.

I would also like to thank Ruth Harris, Tom Rockwell, Glenn Biasi, Delphine Fitzenz, and Nate Onderdonk for helpful conversations in the interpretation of my work and the development of future models; Nick Beeler and Brian Kilgore for the opportunity to do experimental work on friction that informed this dissertation, even though it is not a formal chapter; Bahram Mobasher, for being on my quals committee; and Yaron Finzi and an anonymous reviewer, for commentary on a subset of chapter two results that became a Geophysical Research Letters paper.

A huge number of people were immensely emotionally supportive through the course of this work. Enormous thanks to the whole Earthquake Physics group at UC Riverside - especially those who have had to spend time in the same lab space as me - and to the rest of the department as well. I am also thankful for everyone who has played music with me over my time at UCR; that has also played a big role in keeping me sane and focused.

There is a glaring omission in all of these previous paragraphs, and that is because the person in question fits in pretty much every category that deserves thanks, and including him above would have crowded out other important people from their paragraphs. That person is David Oglesby. No wording is going to do the gratitude I have for David even close to justice. David has been a fantastic scientific advisor: he started out giving me ideas straight out and guiding me through their interpretation, and ended

up sitting back and encouraging the ideas I have developed for my own work and discussing interpretation with me like a colleague rather than a teacher. He has helped me with setup, with pacing, with interpretation, and with editing. He has encouraged me to present at meetings from day one, and to publish things as I finish them. He made sure I developed the skillset I need to be a good seismologist, whether through his own instruction or a careful choice of classes, despite my coming into this department with no relevant background. Related to that point, perhaps most importantly, he gave me the chance to become a scientist at all. I imagine many advisors would have seen someone with a music background trying to switch into science and made them go do another bachelor's, but David gave me the benefit of the doubt. It certainly paid off for me, and I hope it did for him. Throughout the past five years, David has been a scientific and academic advisor, but also a strong emotional support and a good friend. I am beyond lucky to have had him guide me through my years in this department, and through the work that became this dissertation.

Lastly, a special thank you to Pete Sadler. Pete is the first person I met in the Earth Sciences department at UCR. He was also glad to help a music student make the switch to being a science student, and he pushed me to work the hardest that I could to make that change, all the while providing feedback, guidance, and emotional support. Pete is also the person who first directed me to David's office, and the rest, as they say, is history.

ABSTRACT OF THE DISSERTATION

Dynamic Rupture and Ground Motion Modeling
on Realistically Complex Strike-Slip Faults

by

Julian Charles Lozos

Doctor of Philosophy, Graduate Program in Geological Sciences
University of California, Riverside, June 2013
Dr. David D. Oglesby, Chairperson

Faults are complex structures: they are geometrically complex, and have variable stress conditions and frictional behaviors along their length. In addition, faults exist in heterogeneous settings, in terms of surrounding geology, and in terms of regional and local stresses. These individual types of heterogeneity all contribute to complex dynamic rupture behaviors and ground motion distributions, as inferred from observational data and supported by previous modeling studies. In this study, we investigate the effects of individual types of complexity, and we combine different types of heterogeneity in order to enhance the realism of models of real-world faults.

We use the finite element method to conduct dynamic rupture models of earthquakes on faults with complex geometry, initial stresses, frictional parameters, and surrounding geology, and with combinations of these factors, in order to investigate the effects of this complexity on fault interactions, rupture extent, and ground motion. In particular, we investigate the effect of critical weakening distance on the ability of

rupture to propagate through a discontinuity in the fault trace, the effect of a small fault between the larger strands of a stepover on the ability of rupture to jump the stepover, and how zones of aseismic creep affect rupture through locked portions of the same fault. We also construct realistically complex models of the northern San Jacinto Fault, California, incorporating realistic geometry, velocity structure, and combined regional and stochastic stress fields.

We find that the distribution of complexity of any type on the fault, which leads to heterogeneous fault strength, has the primary controlling effect on rupture behavior. The relative strength or weakness of the fault, rather than the actual value, is most important. We also find that the balance of the energy budget is crucial; if too much energy is redirected into fracture, rupture stops. Lastly, we find that each type of complexity affects rupture in its own way, but it is difficult to separate out the effects of individual factors in a model that incorporates many types of heterogeneity. We therefore emphasize the importance of including as many types of realistic complexity as feasible when modeling real faults.

Table of Contents

List of Figures

Chapter 1:

Chapter 2:

Chapter 3:

Chapter 4:

List of Tables

Chapter 1:

Chapter 2:

Chapter 3:

Chapter 4:

Introduction

Fault systems in nature incorporate many types and many scales of complexity and heterogeneity. Geometrical complexities are evident from surface trace mapping and seismicity relocation alike: fault planes are seldom actually planar, and a fault system may include multiple branching or discontinuous strands, each of which may incorporate changes in strike, and slip-surface-scale roughness. Stress state complexity arises in many ways, including the way a regional stress orientation resolves onto complex fault geometry, the interacting kinematics of neighboring faults, and the local changes in stress induced by earthquakes on nearby faults or adjacent fault segments. Complexity of the geologic setting surrounding the faults may pre-date the faulting, but by their very nature, faults also bring different rock units in contact with each other. Complexity of frictional behavior is most evident on faults that sustain both aseismic creep and coseismic rupture, but variation in these properties exists on fully locked faults as well. Each of these types of complexity in and of itself can affect the rupture behavior of a fault, and the ground motion resulting from that rupture. However, the complexity of real world ruptures arises from a combination of all of these individual types of heterogeneity. It is therefore important not just to consider individual effects, but the combination of these effects, when describing, parameterizing, or modeling rupture behavior on realistically complex fault systems.

There has already been a large body of research conducted on each of these individual components of complexity. The effect of fault geometry on rupture behavior and extent is a particularly well-studied topic. Geologic assessment of historic surface

rupture traces suggests that over 75% of earthquake ruptures have at least one endpoint at a previously mapped geometrical complexity in the fault trace (Wesnousky, 2008). However, many historic ruptures, including the 1992 M7.3 Landers (Sieh *et al*., 1993), 1999 M7.9 Denali (Dreger *et al*., 2004), 2008 M8.0 Wenchuan (Zhang *et al*., 2010), and 2010 M7.2 El Mayor-Cucapah (Rymer *et al*., 2011) events all negotiated large bends, branches, stepovers, or mapped delineations between named fault zones. Dynamic rupture modeling has been a particularly prevalent tool for investigating how geometrical complexity affects rupture propagation and endpoints. There exist many studies isolating the effect of a single type of complexity, such as disconnected stepovers between parallel faults (Harris *et al*., 1991; Harris and Day, 1993; Aochi *et al*., 2000; Oglesby, 2008), parallel faults with another fault linking them at some angle (Magistrale and Day, 1999; Oglesby, 2005; Lozos *et al*., 2011), and fault branches (Kame *et al*., 2003; Duan and Oglesby, 2007). However, these studies isolate the effect of the specific type of complexity by using faults that are otherwise planar. There have also been several modeling studies that investigate how a rough or wavy fault trace affects rupture behavior (Dunham *et al.*, 2011; Shi and Day, 2013), but these studies do not incorporate larger scale breaks and bends in the fault. The modeling studies with the most realistic complexity have been ones that aim to match the rupture processes of historic earthquakes, such as the 1992 M7.3 Landers (Olsen *et al*., 1997), 1999 M7.1 Hector Mine (Oglesby *et al*., 2003), and 2002 M7.9 Denali (Dreger *et al.*, 2004; Oglesby *et al*., 2004) events. These studies have been successful at recreating large-scale features of rupture velocity, slip rate, and slip distribution seen in observational data. There is agreement

among these studies, however, that simplifications to the fault geometry and initial stress state are likely responsible for mismatches between details in the models and the observational data, and that incorporation of more realistic geometrical and stress complexities into future models will likely produce better fits to the observations.

The effect of stress state on rupture behavior has been studied from several different angles. Many of the aforementioned modeling studies on how geometrical complexity affects rupture behavior also address issues of stress state. Harris and Day (1993) found that higher initial stress values, leading to faster rupture velocities, allowed rupture to propagate through wider stepovers. Lozos *et al.* (2011) found that fault strength is extremely sensitive to the fault's orientation within a regional stress field. Oglesby (2005) found that dynamic stress transfer, on top of the general kinematics of a fault stepover, may be what determines whether or not rupture can propagate through a geometrical complexity. There is also a growing body of work designed specifically to look the effects of stress complexity on rupture behavior. Dieterich and Smith (2009) describe the stress distribution that arises from a rupture on a wavy fault, and how the heterogeneity compounds itself with successive rupture cycles. Gilchrist *et al*. (2012) conducted both dynamic and quasi-dynamic models of faults with an arbitrary heterogeneous initial stress distribution, and found that this heterogeneity controls rupture behavior within a single event and over multiple earthquake cycles. Andrews and Barall (2011) incorporated a random self-similar stress distribution into models of planar faults, and found that different asperity distributions produced very different rupture patterns. All of these studies highlight the importance of stress complexity in rupture behavior,

though, as with the geometry-specific studies, they do not focus on the combined effect of stress with other complex parameters.

The effect of a complex geologic setting and velocity structure has not been investigated as extensively as the effects of fault geometry or stress state. A realistic regional velocity structure is commonly incorporated into kinematic models of scenario earthquakes (Olsen *et al*., 2006; Jones *et al*., 2008; Graves *et al*., 2011). These being kinematic models, however, their rupture length and slip distribution is pre-determined, so these studies can only speak as to how the velocity structure affects ground motion, not rupture behavior. There have been many dynamic modeling studies addressing the issue of a bimaterial interface across a fault (Harris and Day, 1997; Andrews and Ben Zion, 1997; Cochard and Rice, 2000; Shi and Ben Zion, 2006; Ma and Beroza, 2008; Dalguer and Day, 2009; Lozos *et al*., 2013), but a smooth contact between only two materials is still vastly simplified when compared to a natural velocity structure, and the majority of these studies do not consider the effect of fault geometry or stress heterogeneity within a complex material setting. The most complex studies incorporating both geometrical and geological effects are recreations of historical events (e.g. Olsen *et al.*, 1997), rather than investigation of those effects without the goal of achieving a specific scenario as a result.

Studies of the effect of frictional regime – more specifically, the interaction between seismic and aseismic slip, and between rate-weakening and rate-strengthening friction (Dieterich, 1992) – on rupture behavior are also more limited, and tend to be focused on specific faults or specific historic events. Kinematic (Aagaard *et al*., 2010)

and statistical (Aagaard *et al*., 2012) models of the partially-creeping Hayward fault use a complex pattern of creep and locking, and low coseismic slip through the creeping zones, but neither of these conclusions incorporate the full dynamics of rupture. Kanu and Johnson (2011) modeled creep events on the Hayward, but not in the context of a larger seismic rupture. Recent dynamic modeling studies of megathrust earthquakes (Noda and Lapusta, 2013; Dunham and Kozdon, 2013) suggest that rate-strengthening parts of the megathrust may able to weaken enough, whether by thermal weakening or by time-dependent changes in normal stress, to engage in coseismic slip. Ryan *et al*.'s (2013) more generalized dynamic models of subduction zones shows that the presence of a rate-strengthening patch on an otherwise rate-weakening fault changes the peak slip and slip distribution, regardless of whether or not coseismic slip propagates into that patch. Similar studies have not previously been conducted on other types of faults.

The present work seeks to fill several gaps in the existing literature, and to combine many levels of fault zone complexity into a single, more realistic set of models. The first chapter addresses the issue of how dynamic fault weakening is parameterized, by testing how the choice of dynamic weakening distance effects the ability of rupture to propagate through both connected and disconnected stepovers of variable bend angle and separation between segments. The second chapter investigates whether a small complexity in a larger fault system can have a controlling effect on rupture through the entire system; more specifically, we test whether or not the presence of a small fault segment within a larger disconnected stepover can aid or inhibit propagation through the stepover. In the third chapter, we conduct dynamic rupture models on the Claremont –

Casa Loma stepover of the northern San Jacinto Fault in southern California, incorporating realistic complexity in fault geometry, initial stress state, and material setting. The fourth and final chapter is a parameter study of the effects of a creeping patch of variable size within a locked strike-slip fault, or a locked patch of variable size within a creeping strike-slip fault, on the ability of rupture to propagate across the fault and into the creeping region. Through all four of these studies, we gain further insight into how these individual types of complexity, and the interactions between them, influence the physics of dynamic rupture propagation and cessation.

References

Aagaard, B.T., R.W. Graves, D.P. Schwartz, D.A. Ponce, and R.W. Graymer (2010). Ground-motion modeling of Hayward Fault scenario earthquakes, part I: construction of the suite of scenarios, *Bulletin of the Seismological Society of America* **100**, 2927-2944.

Aagaard, B.T., J.J. Lienkaemper, and D.P. Schwartz (2012). Probabilistic estimates of surface coseismic slip and afterslip for Hayward Fault earthquakes, *Bulletin of the Seismological Society of America* **102**, 961-979.

Andrews, D. J., and Y. Ben-Zion (1997). Wrinkle-like slip pulse on a fault between different materials, *Journal of Geophysical Research* **102,** 553–571.

Andrews, D. J., and M. Barall (2011). Specifying initial stress for dynamic heterogeneous earthquake source models, *Bulletin of the Seismological Society of America* **101**, 2408-2417.

Aochi, H., and E. Fukuyama (2002). Three-dimensional nonplanar simulation of the 1992 Landers earthquake, *Journal of Geophysical Research* **107,** doi:10.1029/2001JB001456.

Cochard, A. and J. Rice (2000). Fault rupture between dissimilar materials: Ill-posedness, regularization, and slip-pulse response, *Journal of Geophysical Reasearch* **105,** 25 891–25 907.

Dalguer, L. A., and S. M. Day (2009). Asymmetric rupture of large aspect-ration faults at bimaterial interfaces, *Geophysical Research Letters* **36**, doi:10.1029/2009GL040303.

Dieterich, J. H. (1992). Earthquake nucleation on faults with rate-and-state-dependent strength, *Tectonophysics* **211**, 115-134.

Dieterich, J. H., and D. E. Smith (2009). Nonplanar faults: mechanics of slip and off-fault damage, *Pure and Applied Geophysics* **166**, 1799-1816.

Dreger, D. S., D. D. Oglesby, R. Harris, N. Ratchkovski, and R. Hansen (2004). Kinematic and dynamic rupture models of the November 3, 2002 Mw7.9 Denali, Alaska earthquake, *Geophysical Research Letters* **31**, doi:10.1029/2003GL018333.

Duan, B., and D. D. Oglesby (2007). Nonuniform prestress from prior earthquakes and the effect on dynamics on branched fault systems, *Journal of Geophysical Research* **112**, B05308, doi:10.1029/2006JB004443.

Dunham, E. M., D. Belanger, L. Cong, and J. E. Kozdon (2011). Earthquake ruptures with strongly rate-weakening friction and off-fault plasticity, part 2: nonplanar faults, *Bulletin of the Seismological Society of America* **101**, 2308-2322.

Gilchrist, J. J., J. H. Dieterich, K. B. Richards-Dinger, and D. D. Oglesby (2012). "Using a multi-cycle earthquake simulator to specify initial conditions for modeling rupture dynamics." American Geophysical Union Fall Meeting, Moscone Center, San Francisco, California. Conference presentation.

Graves, R., T. H. Jordan, S. Callaghan, E. Deelman, E. Field, G. Juve, C. Kesselman, P. Maechling, G. Mehta, K. Milner, D. Okaya, P. Small, and K. Vahi (2011). CyberShake: a physics-based seismic hazard model for southern California, *Pure and Applied Geophysics* **168**, 367-381.

Harris, R. A., R. J. Archuleta, and S. M. Day (1991). Fault steps and the dynamic rupture process - 2-D numerical simulations of a spontaneously propagating shear fracture, *Geophysical Research Letters* **18,** 893-896.

Harris, R. A., and S. M. Day (1993). Dynamics of fault interaction: parallel strike-slip faults, *Journal of Geophysical Research* **98,** 4461-4472.

Harris, R. A., and S. M. Day (1997). Effects of a low-velocity zone on dynamic rupture, *Bulletin of the Seismological Society of America* **87**, 1267-1280.

Jones, L. M., R. Bernknopf, D. Cox, J. Goltz, K. Hudnut, D. Mileti, S. Perry, D. Ponti, K. Porter, M. Reichle, H. Seligson, K. Shoaf, J. Treiman, and A. Wein (2008). The ShakeOut scenario, *U.S. Geological Survey Open File Report 2008-1150*.

Kame, N., J. R. Rice, and R. Dmowska (2003). Effects of pre-stress state and rupture velocity on dynamic fault branching, *Journal of Geophysical Research* **108,** 2265, doi: 10.1029/2002JB002189.

Kanu, C., and K. Johnson (2011). Arrest and recovery of frictional creep on the southern Hayward fault triggered by the 1989 Loma Prieta, California, earthquake and implications for future earthquakes, *Journal of Geophysical Research* **116**, doi:10.1028/2010JB007927.

Kozdon, J. E., and E. M. Dunham (2013). Rupture to the trench: dynamic rupture simulations of the 11 March 2011 Tohoku earthquake, *Bulletin of the Seismological Society of America* **103**, 1275-1289.

Lozos, J. C., D. D. Oglesby, B. Duan, and S. G. Wesnousky (2011). The effects of fault bends on rupture propagation: a geometrical parameter study, *Bulletin of the Seismological Society of America* **101***,* 385-398.

Lozos, J. C., D. D. Oglesby, and J. N. Brune (2013). The effects of fault stepovers on ground motion, *Bulletin of the Seismological Society of America* **103**, doi: 10.1785/0120120223.

Ma S., and G. C. Beroza (2008). Rupture dynamics on a bimaterial interface for dipping faults, *Bulletin of the Seismological Society of America* **98,** 1642-1658.

Magistrale, H., and S. M. Day (1999). 3D simulations of multi-segment thrust fault rupture, *Geophysical Research Letters* **26,** 2093-2096.

Noda, H., and N. Lapusta (2013). Stable creeping fault segments can become destructive as a result of dynamic weakening, *Nature* **493**, 518-521.

Oglesby, D.D., and S.M. Day (2001). Fault geometry and dynamics of the 1999 Chi-Chi (Taiwan) earthquake, *Bulletin of the Seismological Society of America* **91***,* 1099-1111.

Oglesby, D. D., S. M. Day, Y.-G. Li, and J. E. Vidale (2003). The 1999 Hector Mine earthquake: the dynamics of a branched fault system, *Bulletin of the Seismological Society of America* **93,** 2459-2476.

Oglesby, D. D., D. S. Dreger, R. A. Harris, N. Ratchkovski, and R. Hansen (2004). Inverse kinematic and forward dynamic models of the 2002 Denali Fault earthquake, Alaska, *Bulletin of the Seismological Society of America* **94**, S214-S233.

Oglesby, D. D. (2005). The dynamics of strike-slip step-overs with linking dip-slip faults, *Bulletin of the Seismological Society of America* **95,** 1604-1622.

Oglesby, D. D. (2008). Rupture termination and jump on parallel offset faults, *Bulletin of the Seismological Society of America* **98**, 440-447.

Olsen, K. B., R. Madariaga, and R. J. Archuleta (1997). Three-dimensional dynamic simulation of the 1992 Landers earthquake, *Science* **278**, 834-838.

Olsen, K. B., S. M. Day, J. B. Minster, Y. Cui, A. Chourasia, M. Faerman, R. Moore, P. Maechling, and T. Jordan (2006). Strong shaking in Los Angeles expected from southern San Andreas earthquake, *Geophysical Research Letters* **33**, doi: 10.1029/2005GL025472.

Ryan, K. J., D. D. Oglesby, and E. L. Geist (2013). "Modeling rupture with heterogeneous prestress and through stable sliding zones, and implications for an Alaskan-Aleutian megathrust earthquake." Seismological Society of America

Annual Meeting, Salt Palace Convention Center, Salt Lake City, Utah. Conference presentation.

Rymer, M.J., J.A. Treiman, K.J. Kendrick, J.J. Lienkaemper, R.J. Weldon, R. Bilham, M. Wei, E.J. Fielding, J.L. Hernandez, B.P.E. Olson, P.J. Irvine, N. Knepprath, R.R. Sickler, X. Tong, and M.E. Siem (2011). Triggered surface slips associated with the 2010 El Mayor-Cucapah , Baja California, Mexico earthquake, *U.S. Geological Survey Open File Report 2010-1333.*

Shi, Z., and Y. Ben-Zion (2006). Dynamic rupture on a bimaterial interface governed by slip- weakening friction, *Geophysical Journal International*, doi: 10.1111/j.1365-246X.2006.02853.

Shi, Z., and S. M. Day (2013). "Validation of dynamic rupture simulations for high-frequency ground motion." Seismological Society of America Annual Meeting, Salt Palace Convention Center, Salt Lake City, Utah. Conference presentation.

Sieh, K., L. Jones, E. Hauksson, K. Hudnut, D. Eberhart-Phillips, T. Heaton, S. Hough, K. Hutton, H. Kanamori, A. Lilje, S. Lindvall, S. McGill, J. Mori, C. Rubin, J. Spotila, J. Stock, H.Thio, J. Tremain, B. Wernicke, and J. Zachariasen (1993). Near-field investigations of the Landers earthquake sequence, April to July 1992. *Science*, **260**, 171-176.

Wesnousky, S. G. (2008). Displacement and geometrical characteristics of earthquake surface ruptures: issues and implications for seismic-hazard analysis and the process of earthquake rupture, *Bulletin of the Seismological Soceity of America* **98**, 1609-1632.

Zhang, Y., W. Feng, L. Xu, C. Zhou, and Y. Chen (2008). Spatio-temporal rupture process of the 2008 great Wenchuan earthquake, *Science in China Series D: Earth Science* **52**, 145-154.

Chapter 1: The Effects of d_0 on Rupture Propagation on Fault Stepovers

Introduction

Slip on a fault occurs when shear stress overcomes the fault's strength, as determined by its static coefficient of friction and the surrounding normal stress. In order for self-sustaining rupture propagation to occur, a patch of the fault larger than a certain critical size must also weaken to this sliding frictional value (Ida, 1972; Palmer and Rice, 1973; Andrews, 1976a; Day, 1982). This weakening to a frictional state that allows for sliding does not happen instantaneously. Laboratory experiments on shear stress response to displacement suggest that this weakening process requires a certain amount of time – and therefore a certain slip distance – to occur (Dieterich *et al.*, 1978; Dieterich, 1981), and that the critical patch size required for self-sustaining rupture depends upon that critical weakening distance (Day, 1982). This critical weakening distance becomes important in describing the rupture process of shear cracks and seismic faults (Ida, 1972; Das and Aki, 1977; Andrews, 1976a, 1976b; Day, 1982).

While there is some expression of this critical weakening distance in many friction laws, its implementation is simplest and easiest to interpret in a slip-weakening criterion coupled with Coulomb friction (Andrews, 1976b; Das and Aki, 1977; Day, 1982). This criterion states simply that fault strength weakens from its static value to its dynamic value as the faults slips some critical distance d_0 (Figure 1.1). This critical distance in turn is a factor in determining the size of the fault patch that must weaken in order for self-sustaining rupture to occur (Day, 1982). The more energy required to fracture the fault, the larger the critical patch size necessary to achieve self-sustaining

Figure 1.1.

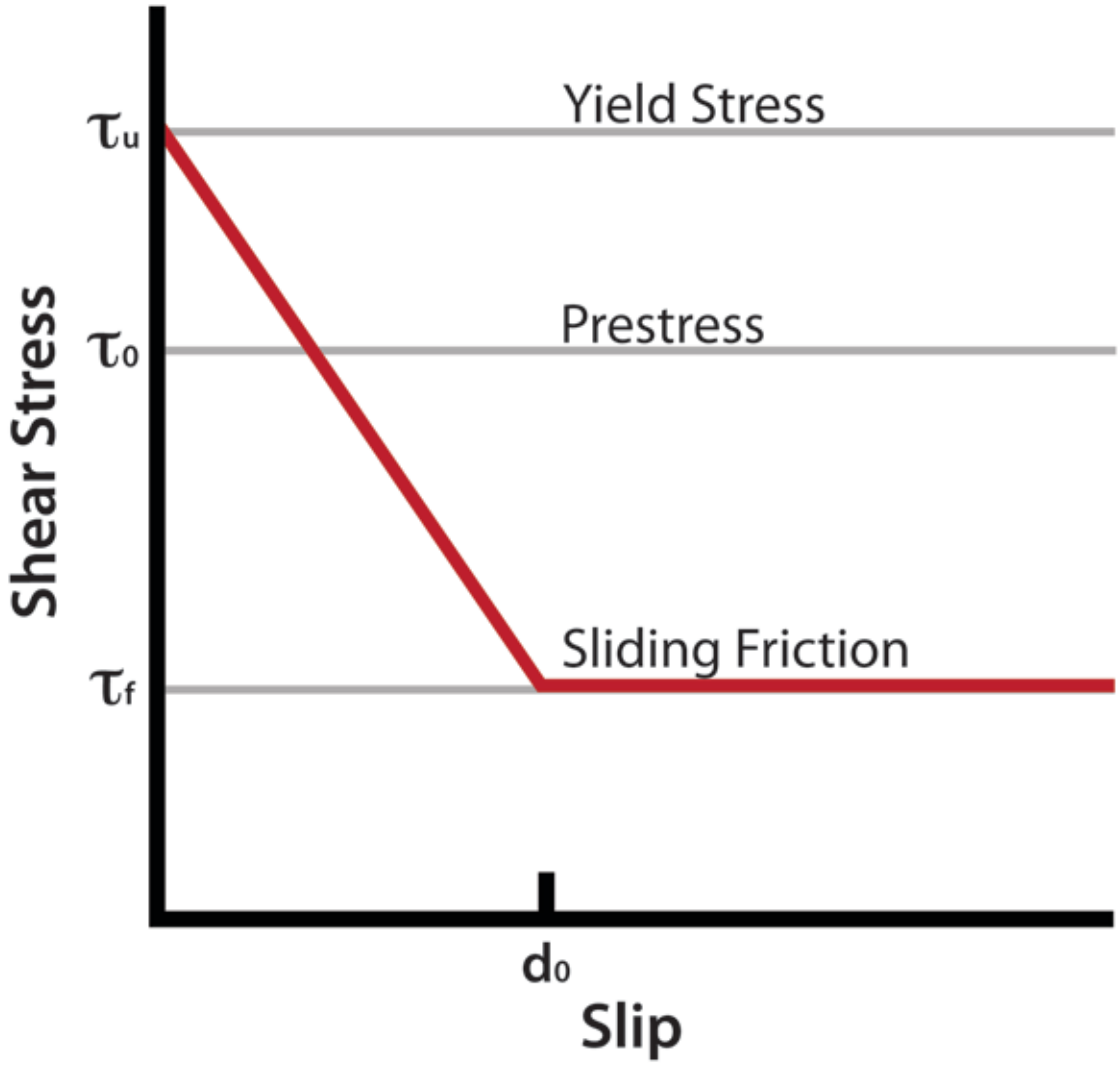

Figure 1.1. Slip-weakening friction, after Day (1982). The red curve represents shear stress on the fault plotted against slip at that point on the fault.

rupture at all, which ultimately means the rupture itself will be less energetic. Thus, a larger d_0 may make it more difficult for rupture to nucleate at all, for it to propagate past the nucleation stage, and for it to re-nucleate on any discontinuous fault strands.

Slip-weakening friction has been used in many dynamic rupture models (e.g., Andrews, 1976a, Day, 1982, and many later studies). In these models, the value of d_0 is generally selected on the basis of somewhat physical arguments or ground motion observations. However, most researchers acknowledge that the uncertainty in d_0 is extremely high, and that the values needed to permit dynamic rupture in simulations are different from the values inferred from laboratory studies. In the present work, we argue that the specific value of d_0 can have a significant effect on the results of a dynamic rupture model, since the manner of fault weakening controls many aspects of the rupture, and since rupture will be more likely to propagate further if the fault weakens faster or over a smaller distance (Day, 1982).

The effect of d_0 size may be particularly pronounced in models of geometrically complex fault systems. Rupture encounters a different static stress state when it turns a bend in the fault, and it must re-nucleate entirely after a discontinuity in the fault trace. In both of these situations, the fault strand after the bend or break must also achieve a critical patch of slip before it can fully rupture. As this critical patch is determined in part by d_0, the value of d_0 in a model may make a significant difference in whether or not rupture will propagate through the modeled geometrical discontinuities. Understanding the ability of rupture to propagate through fault bends and steps is an important issue, since many historic surface ruptures terminate at previously mapped geometrical

discontinuities (Wesnousky, 2008). There have been many past studies on the ability of rupture to propagate across linked and unlinked fault stepovers (e.g., Harris *et al.,* 1991; Harris and Day, 1993; Magistrale and Day, 1999; Oglesby, 2005; Oglesby, 2008; Lozos *et al.*, 2011), but none of these investigate d_0 as a variable parameter that may affect the results. Accurately evaluating and modeling probable rupture behavior of geometrically complex faults is a key part of estimating hazard for those faults. It is useful to know how much one arbitrarily set parameter can affect the results of those models and their resultant hazard analyses.

In the present study, we investigate the effect of d_0 on rupture propagation by conducting suites of dynamic models of disconnected and connected fault stepovers, using several stress states and rupture velocities, and five different values of d_0.

Methods

We used the two-dimensional finite element method (EQdyna2D) to conduct our rupture models (Duan and Oglesby, 2007). EQdyna2D uses a basic slip-weakening friction law, as described in the introduction to this paper. Using slip-weakening, as opposed to any more complex friction laws, allows us to investigate the effects of d_0 directly and independently of other parameters. We chose to conduct this study in two dimensions largely because running the comparable models in 3D would be far more computationally-intensive and time-consuming. The physical and computational input parameters that are not dependent on d_0 are listed in Table 1.1.

Table 1.1. Physical and computational parameters.

Static coefficient of friction	0.75 (subshear) or 0.6 (supershear)
Dynamic coefficient of friction	0.51 (subshear) or 0.3 (supershear)
P-wave velocity	6000 m/s
S-wave velocity	3464 m/s
Density	2700 kg/m^3
Element size	10 m

To investigate the effects of d_0 on rupture propagation at geometrical complexities, we modeled connected and disconnected stepovers on strike-slip faults. Our disconnected stepovers consist of two parallel 15 km segments with 5 km of overlap and variable separation (Figure 1.2, top). Our connected stepovers consist of two parallel 10 km segments connected at a fixed angle by a linking segment of variable length (Figure 1.2, bottom). We chose these fixed angles (35 degrees for extensional, 20 degrees for compressional) because they showed a variety of rupture behaviors based on linking segment length in Lozos *et al.* (2011). These stepover types present different dynamic problems: rupture must actually stop on one fault segment and restart on the next in a disconnected stepover, while in a connected stepover, it has to propagate through a linking fault segment onto which surrounding stresses resolve differently than on the parallel segments. We conducted models of each stepover geometry as both extensional and compressional; this was accomplished by reversing the direction of the regional stress field. We also used different stress fields to induce both supershear and subshear ruptures on all of these geometries. Our "supershear" stresses are those from Lozos *et al.* (2011), and our "subshear stresses" are case D from Harris and Day (1993).

We induced ruptures on all of these geometries and in both stress states using five different values of d_0: 0.05 m, 0.1 m, 0.2 m, 0.4 m, and 0.8 m. For each of these values,

Figure 1.2.

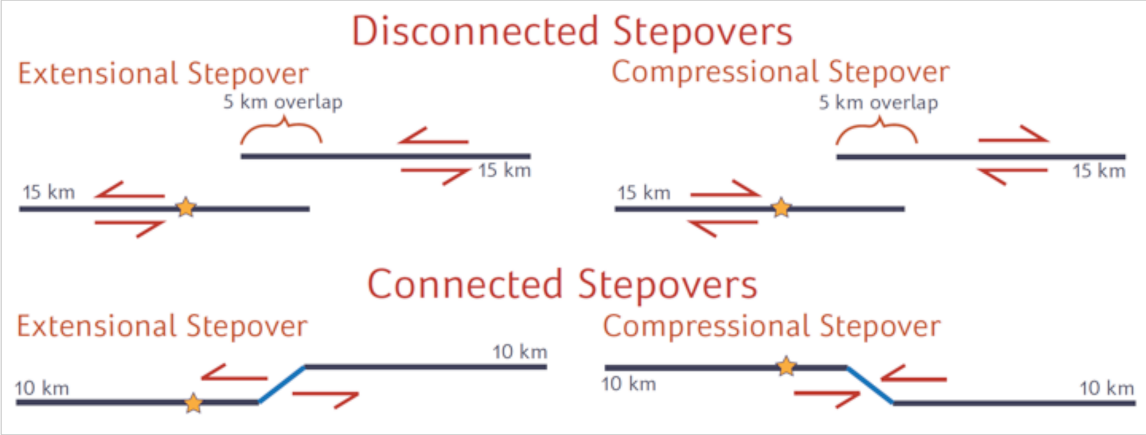

Figure 1.2. Cartoon of fault geometry. Elements of the geometry drawn in black are fixed. Elements in blue (length of the linking segment in the connected case, separation between segments in the disconnected case) are variable. The star marks the location of initial forced nucleation, 3 km from the geometrical discontinuity in both the disconnected and connected cases.

we ran a suite of models, increasing the length of the linking segment (for connected cases) or the separation between the faults (for disconnected cases) until rupture wass no longer able to propagate through the geometrical complexity. We initiated rupture on the first segment artificially; we did so by raising the shear stress above the yield stress (static coefficient of friction multipled by the initial normal stress) at the nucleation point and forcing it to propagate outward at a constant speed for a larger area than the critical patch size required for rupture to sustain itself. For physical reasons the radius of this forced nucleation zone varied depending on which d_0 we use; these radii are listed in Table 1.1. Rupture renucleation on the second fault segment happened naturally. It is there that we observed the effects of d_0 on these rupture processes.

As a check on our d_0 scaling tests, we also conducted a set of models in which we held d_0 constant at 0.2 m and halved or doubled the magnitude of the regional shear and normal stress. We performed these tests for both supershear and subshear ruptures, and

Table 1.2. Forced nucleation zone sizes.

d_0	**Radius of forced nucleation zone**
0.05 m	125 m
0.1 m	250 m
0.2 m	500 m
0.4 m	1000 m
0.8 m	2000 m

on disconnected and connected stepovers. Based on Day's (1982) expression for the critical crack radius necessary for self-sustaining rupture propagation,

$$r_c = \frac{7\pi}{24}\frac{\mu(S+1)d_0}{\Delta\tau}, \quad (1)$$

where μ is the shear modulus, S is the relative fault strength as defined by

$$S = \frac{\tau_{yield} - \tau_{initial}}{\Delta\tau}, \quad (2)$$

and $\Delta\tau$ is the stress drop, the effect on r_c of doubling the regional stresses should be equivalent to cutting d_0 in half, while S (which affects the rupture velocity) remains unchanged. Within each of these stress states, which are listed in Table 1.3, we conducted models with increasingly large linking segments or separation between segments until rupture was no longer able to propagate through the entire fault system.

Table 1.3. Stress cases.

Stress case	**Normal stress**	**Shear stress**
Supershear	100 MPa	45 MPa
Supershear half	50 MPa	22.5 MPa
Supershear double	200 MPa	90 MPa
Subshear	33.3 MPa	20 MPa
Subshear half	16.7 MPa	10 MPa
Subshear double	66.6 MPa	40 MPa

Results

Our models of rupture propagation using different values of d_0 show a set of behaviors that is largely independent of whether the stepover is connected versus disconnected, or extensional versus compressional, or whether the rupture velocity is supershear versus subshear.

We find that there is not a linear correlation between d_0 and the size of geometrical discontinuity through which rupture can propagate. In other words, doubling d_0 does not halve the separation or linking segment length needed to arrest rupture, nor does halving d_0 allow rupture to propagate through geometrical discontinuities that are twice as large. The relationship between d_0 and discontinuity is not even linear.

Figure 1.3.

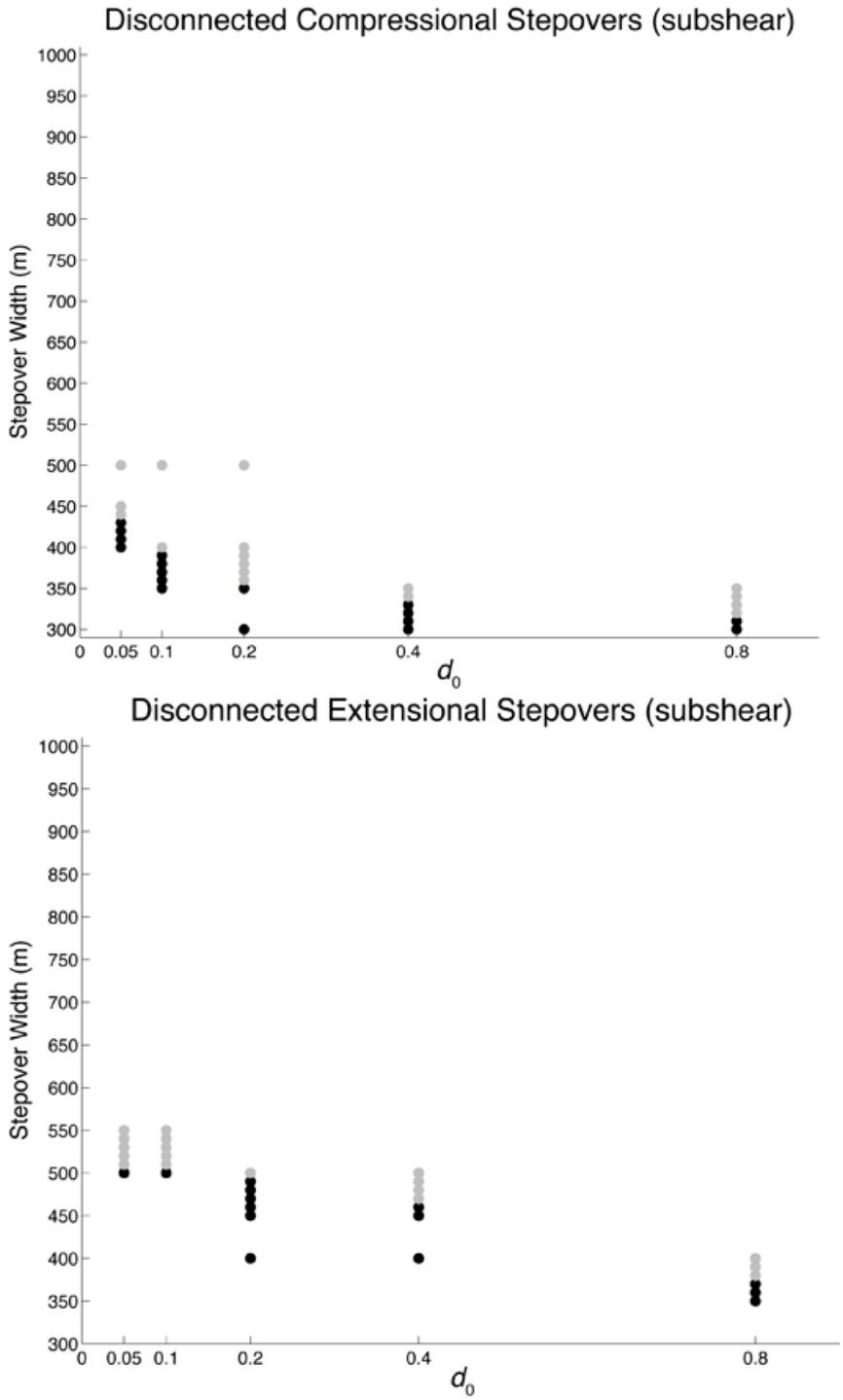

Figure 1.3. Selected results of d_0 scaling tests. Discontinuity size is plotted against d_0. Each dot represents one model. Black means that rupture did propagate through the entire fault system, whereas gray means that rupture stopped at some point along strike. Note that the curve formed by the maximum distance through which rupture can propagate for a given d_0 is not linear in any case.

Figure 1.3, cont'd.

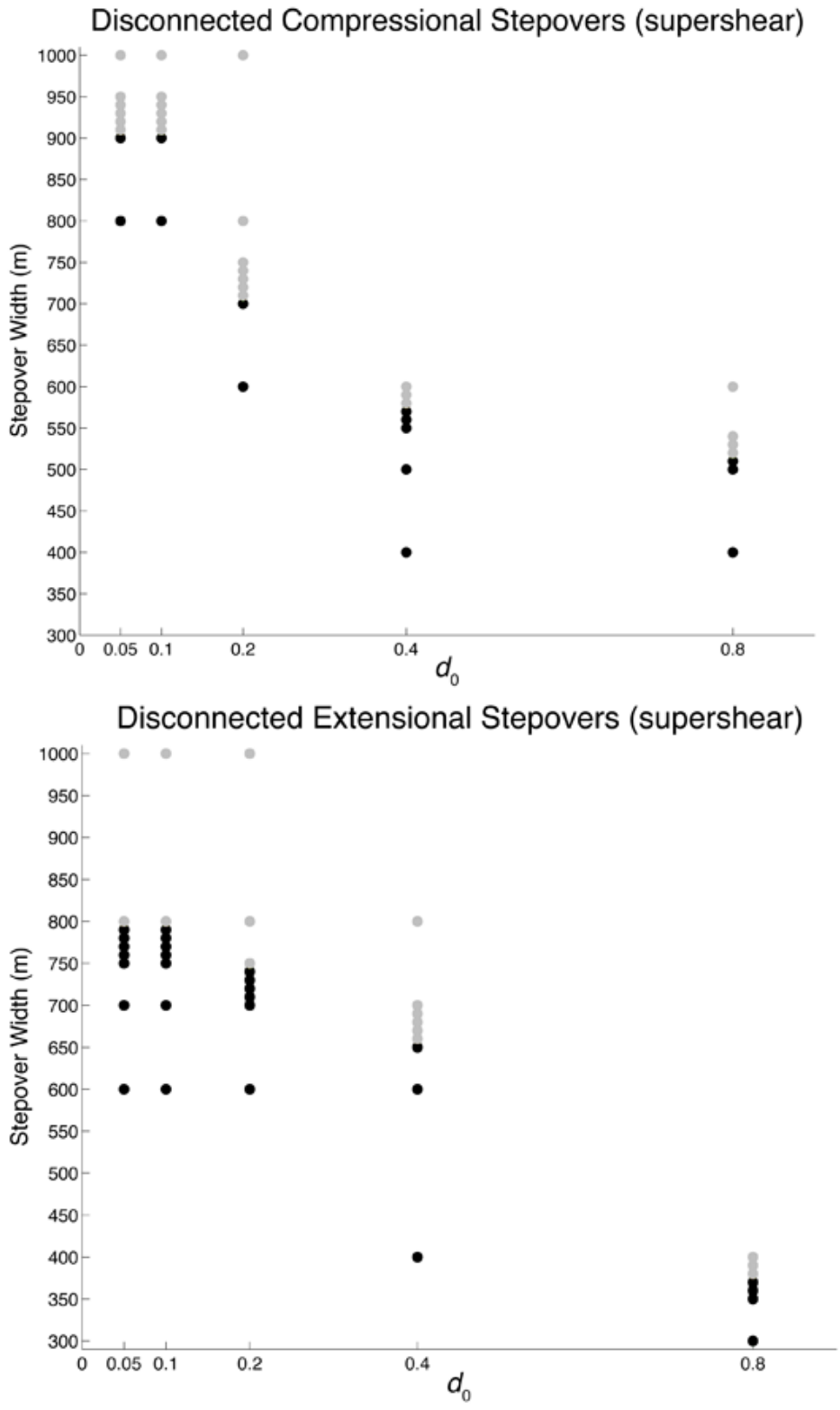

Figure 1.3, cont'd.

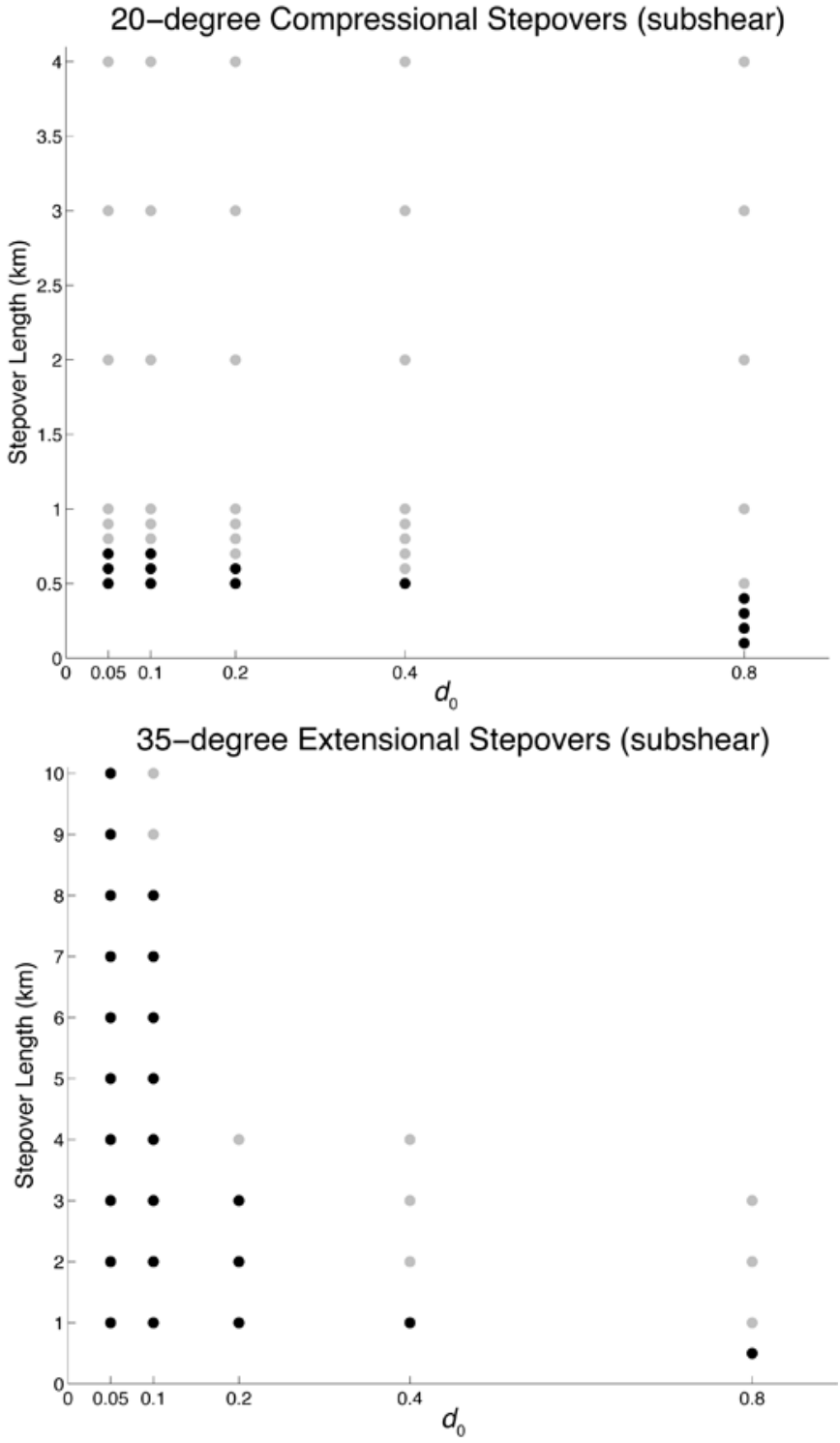

Figure 1.3, cont'd.

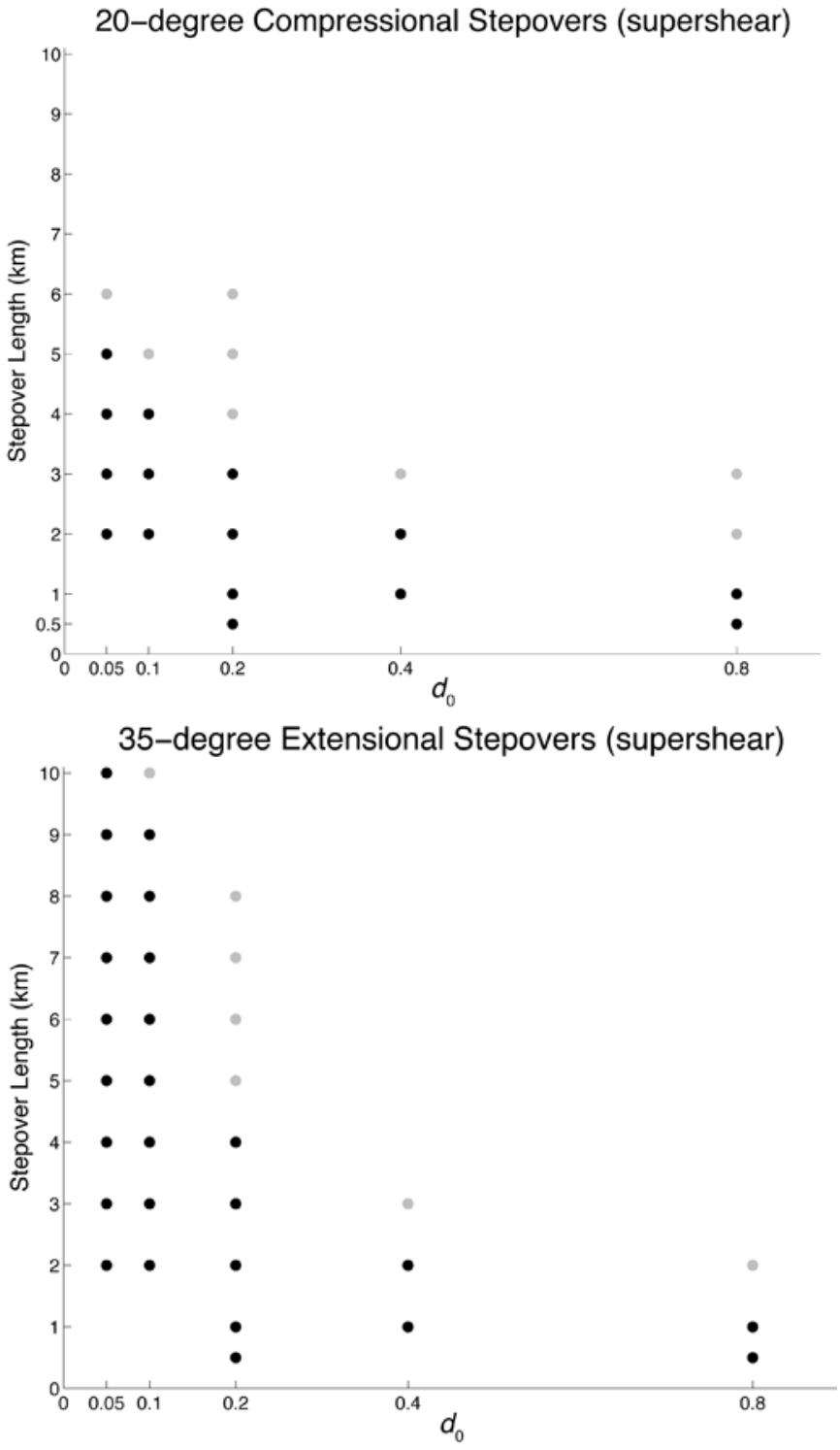

For compressional stepovers, regardless of rupture velocity, the distance through which rupture can propagate as a function of the value of d_0 drops off steeply for small d_0, and then flattens out; for extensional stepovers, this curve decreases slightly for lower d_0 values and drops off more steeply as d_0 becomes larger. Figure 1.3 shows plots of size of maximum geometrical discontinuity size that allows throughgoing rupture versus d_0, for all of the stress states and stepover types we modeled.

Our tests with a fixed d_0 and halved or doubled regional stresses yielded the results consistent with the relationship between d_0 and stress. For disconnected and connected stepovers, extensional and compressional, and with both subshear and supershear rupture velocities, doubling the regional stress produced results equivalent to halving d_0, and vice versa. For any given stepover width in either the subshear or supershear rupture velocity case, the largest difference in jumpable stepover width between d_0 scaling tests and stress scaling tests was only 10 m, which is the size of one element of our mesh, and thus within the level of uncertainty of our modeling method. Figure 1.4 shows the comparison between our d_0 scaling tests and our stress scaling tests, for all stepover geometries and rupture velocities.

Discussion

We find that the non-linear scaling relationship between d_0 and the size of geometrical discontinuity through which rupture can propagate can be interpreted via the pattern of stress change on a neighboring fault segment that results from rupture of the first segment of the stepover. Figure 1.5 is a plot of static stress changes based on the slip

Figure 1.4.

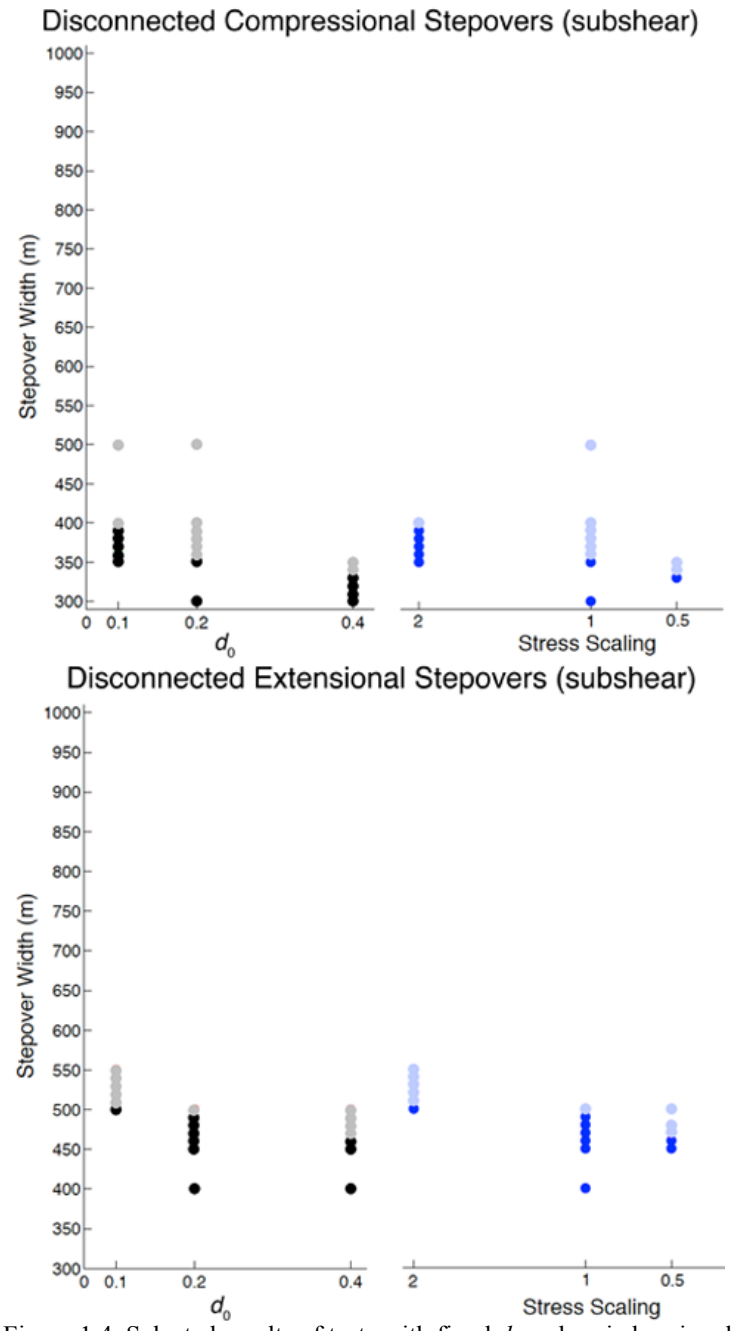

Figure 1.4. Selected results of tests with fixed d_0 and varied regional stress intensity. These plots place the scaled stress results adjacent to the scaled d_0 results. The x-axis values for scaled stresses represent the value by which the stress state from the d_0 scaling tests was multiplied. Each dot represents one model. Black or dark blue dots indicate that rupture did progress through the entire fault system. Gray or light blue dots indicate that rupture stopped at some point along strike. Note that scaling d_0 or scaling the regional stresses has an identical effect on the size of geometrical discontinuity through which rupture can propagate (e.g., halving d_0 is equivalent to doubling the stress amplitude).

Figure 1.4, cont'd.

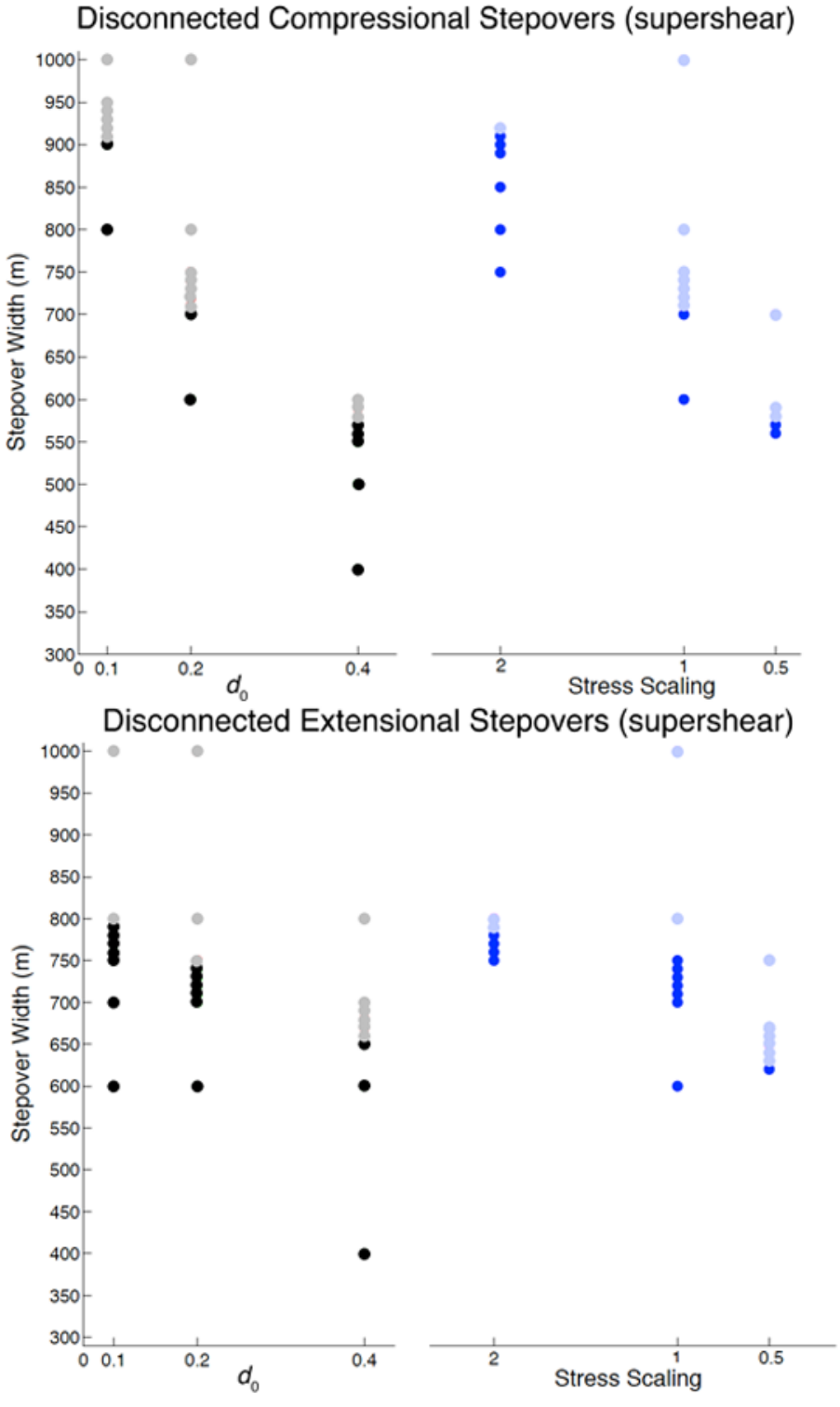

Figure 1.4, cont'd.

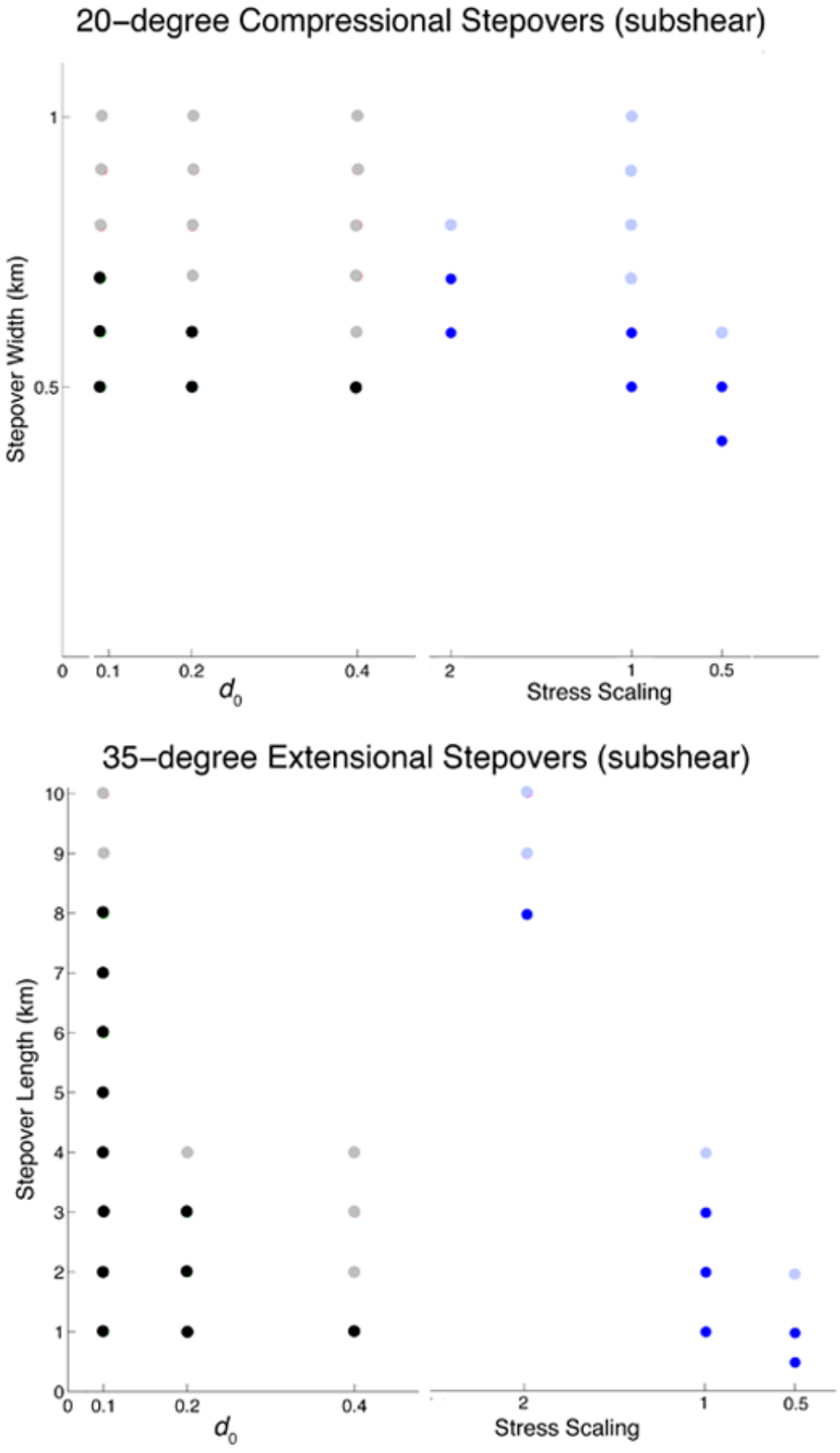

Figure 1.4, cont'd.

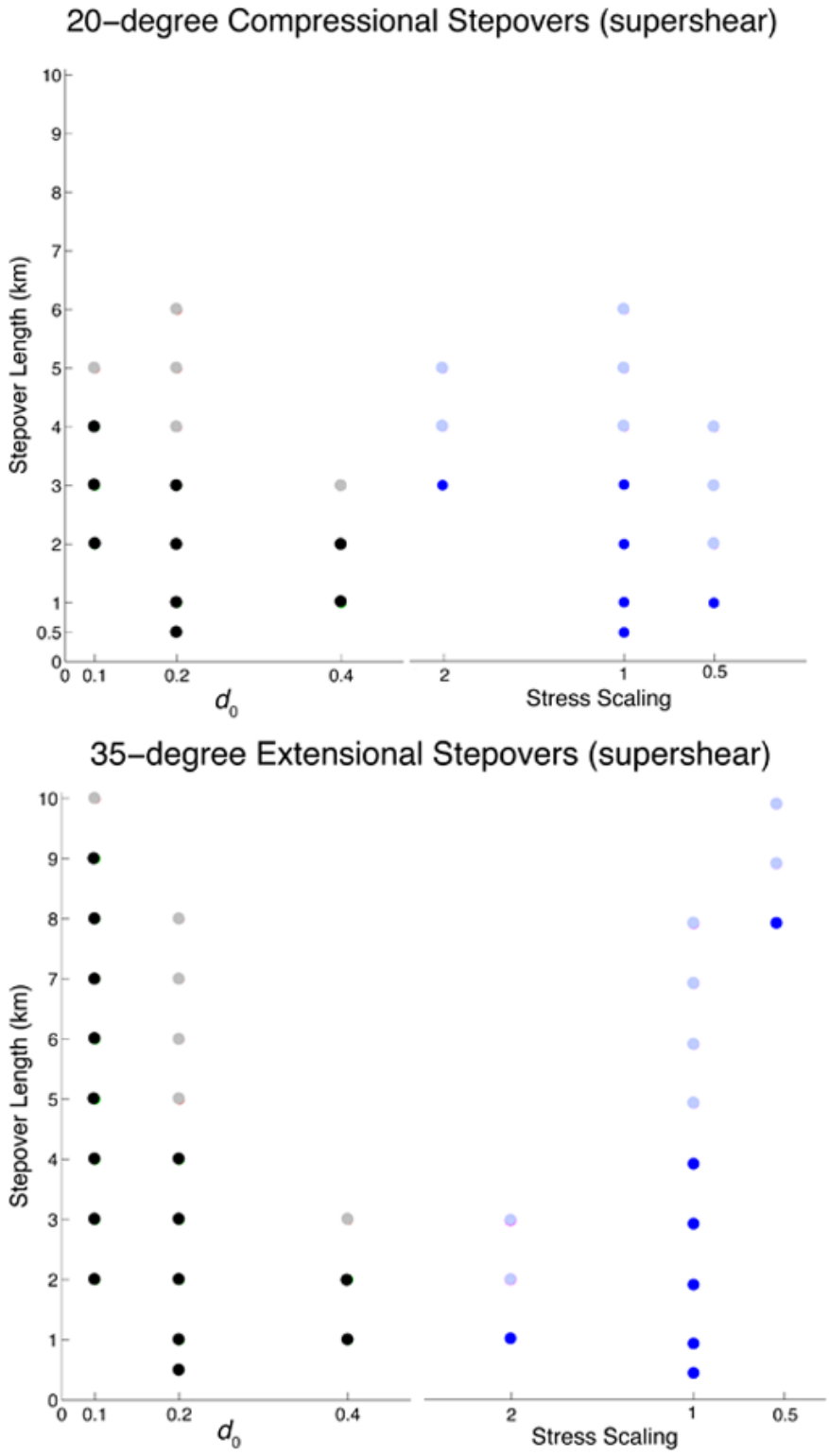

distribution from a rightward-propagating rupture on the right-lateral strike-slip first segment (shown in green) in one of our disconnected supershear models, calculated using Coulomb 3.3 (Toda *et al.*, 2011). Several hypothetical secondary faults are shown in black. The time-dependent dynamic stress field, especially in the near field, would have a similar shape to the static field shown in Figure 1.5 (Harris and Day, 1993). We chose to represent the static field because it is less computationally-intensive to calculate, while still illustrating the overall effect of the stress pattern on jumping rupture.

Figure 1.5 shows only the regions that exceed the Coulomb stress change required for failure (King *et al.*, 1994). For rupture to re-nucleate on a second fault segment, the area of that segment that intersects these failure lobes must be larger than the critical patch size required for self-sustaining rupture, which is dependent on d_0. The larger d_0 is, the larger the area on the second fault that needs to intersect the lobe of increased stress change for rupture to re-nucleate. However, due to the shape and position of these lobes, the area of a fault segment that intersects the lobe does not linearly depend on the width of the stepover. This effect in turn can accounts for the non-linearity of the d_0-maximum ruptureable discontinuity relationship.

The relationship between the area of fault that intersects the lobe of Coulomb failure stress and critical patch size needed to renucleate rupture is a straightforward explanation for our results for disconnected stepovers. The connected cases, however, are more complex. Whether or not rupture can propagate through the entire stepover depends less on rupture stopping and renucleating, and more on its ability to continue across a linking fault segment that may be statically and/or dynamically less favorable for rupture

Figure 1.5.

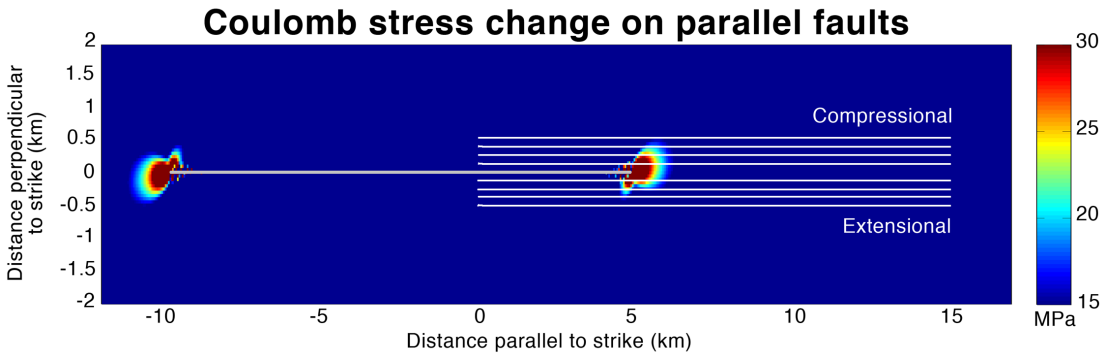

Figure 1.5. Static stress changes above Coulomb failure level, as induced by rupture of a single fault segment (shown in gray) with a tapered slip distribution with a maximum of 4 m of slip, consistent with our supershear disconnected stepover models. The plot is in map view. Several potential secondary fault strands are shown in white. Note that the amount of the secondary fault that intersects the lobe of failure-level Coulomb stress does not vary linearly with distance. This plot was generated using Coulomb 3.3 (Toda *et al.,* 2011).

than the main parallel fault segments. This effect of regional and dynamic stress favorability occurs regardless of d_0. However, on a less-favorably oriented fault segment, more of the rupture energy must go into fracture in order for rupture to propagate through the unfavorable area, effectively raising d_0 and leaving less energy for forward propagation and seismic radiation. In this case, rupture is more likely to stop in the unfavorable area and not progress back to a more favorable part of the fault with a smaller d_0. This effect, in combination with the same Coulomb stress changes that affect the disconnected stepovers, makes the behavior of connected stepovers more difficult to anticipate, while still highlighting the d_0-dependence of the rupture process.

Conclusion

The size of d_0 has a significant effect on rupture propagation through fault stepovers. Increasing d_0 decreases the size of the geometrical discontinuity through which rupture can propagate, but this relationship is not linear. This result holds true for disconnected and connected stepovers, both extensional and compressional, and for both supershear and subshear rupture velocities. The nonlinearity of the relationship between d_0 and the maximum discontinuity through which rupture can propagate is related to the area of the secondary fault that intersects the lobe of stresses increased to failure level, which also changes nonlinearly with distance.

Because the effect of d_0 is so significant, this suggests that the input d_0 value for models of earthquake rupture should be chosen carefully, especially if the modeled faults are geometrically complex. The choice of d_0 in a model of a fault with a stepover may

strongly affect the rupture endpoints predicted by the model, which further emphasizes the importance of understanding what the correct values may be. High-speed friction experiments may be useful to constrain the values of d_0 for natural fault rocks, though much further work will also be necessary to reconcile the apparent difference between experimentally- and observationally-derived values of d_0, as well as the difference between these values and the ones necessary to allow rupture propagation in dynamic models.

References

Andrews, D.J. (1976a). Rupture propagation with finite stress in antiplane strain, *Journal of Geophysical Research* **81**, 3575-3582.

Andrews, D.J. (1976b). Rupture velocity of plane strain shear cracks, *Journal of Geophysical Research* **81**, 5479-5687.

Das, S., and K. Aki (1977). A numerical study of two-dimensional spontaneous rupture propagation, *Geophysical Journal International* **50**, 643-668.

Day, S.M. (1982). Three-dimensional simulation of spontaneous rupture: the effect of nonuniform prestress, *Bulletin of the Seismological Society of America* **72,** 1881-1902.

Dieterich, J.H. (1981). Constitutive properties of faults with simulated gouge, *Geophysical Monograph Series* (J. Handin Festschrift), American Geophysical Union.

Dieterich, J.H., D.W. Barber, G. Conrad and Q.A. Gordon (1978). Preseismic slip in a large scale friction experiment, *Proceedings of the 19th U.S. Rock Mechanics Symposium,* Mackay School of Mines, University of Nevada, Reno.

Duan, B., and D.D. Oglesby (2007). Nonuniform prestress from prior earthquakes and the effect on dynamics on branched fault systems, *Journal of Geophysical Researc*h **112**, B05308, doi 10.1029/2006JB004443.

Harris, R.A., R.J. Archuleta, and S.M. Day (1991). Fault steps and the dynamic rupture process: 2-d numerical simulations of a spontaneously propagating shear fracture, *Geophysical Research Letters* **18,** 893-896.

Harris, R.A., and S.M. Day (1993). Dynamics of fault interaction: parallel strike-slip faults, *Journal of Geophysical Research* **98**, 4461-4472.

Ida, Y. (1972). Cohesive force across the tip of longitudinal-shear crack and Griffith's specific surface energy, *Journal of Geophysical Research* **77**, 3796-3805.

King, G. C. P., R. S. Stein, and J. Lin (1994). Static stress changes and the triggering of earthquakes, *Bulletin of the Seismological Society of America* **84**, 935-953.

Lozos, J.C., D.D. Oglesby, B. Duan, and S.G. Wesnousky (2011). The effects of double fault bends on rupture propagation: a geometrical parameter study, *Bulletin of the Seismological Society of America* **101**, doi: 10.1785/0120100029.

Magistrale, H., and S.M. Day (1999). 3D simulations of multi-segment thrust fault rupture, *Geophysical Research Letters* **26,** 2093-2096.

Oglesby, D.D. (2005). The dynamics of strike-slip stepovers with linking dip-slip faults, *Bulletin of the Seismological Society of America* **95,** 1604-1622.

Oglesby, D.D. (2008). Rupture termination and jump on parallel offset faults, *Bulletin of the Seismological Society of America* **98,** 440-447.

Palmer, A.C., and J.R. Rice (1973). The growth of slip surfaces in the progressive failure of overconsolidated clay, *Proceedings of the Royal Society of London* **A 332**, 527-548.

Toda, S., Stein, R.S., Sevilgen, V., and Lin, J. (2011). Coulomb 3.3 Graphic-rich deformation and stress-change software for earthquake, tectonic, and volcano research and teaching—user guide: U.S. Geological Survey Open-File Report 2011–1060, 63 p., available at http://pubs.usgs.gov/of/2011/1060/.

Wesnousky, S.G. (2008). Displacement and geometrical characteristics of earthquake surface ruptures: issues and implications for seismic-hazard analysis and the process of earthquake rupture, *Bulletin of the Seismological Society of America* **98**, 1609-1632.

Chapter 2: Rupture Propagation and Ground Motion of Strike-Slip Stepovers with Intermediate Fault Segments

Introduction

Natural fault systems are geometrically complex structures, and both geological and geophysical studies indicate that the details of a fault's geometry can have a controlling effect on rupture propagation through that fault. Many modeling studies of fault stepovers (Harris and Day, 1993; Kase and Kuge, 1998; Oglesby, 2008), double bends (Magistrale and Day, 1999; Oglesby, 2005; Lozos *et al*., 2011), and branches (Kame *et al.*, 2003; Duan and Oglesby, 2007) indicate that there is some threshold discontinuity size (i.e. width of separation between faults, or bend/branch angle) that prevents rupture from propagating through the entire fault system. Wesnousky's (2008) study of dozens of historic surface rupture traces corroborates these findings; his analysis shows that 75% of those ruptures have at least one endpoint at a previously mapped geometrical complexity in the fault trace. The stopping point of a rupture strongly influences the distribution of ground motion associated with that rupture, but even in cases where rupture does propagate through bends and stepovers, ground motion is affected by the heterogeneity of the rupture trace (Wald and Heaton, 1994; Brune, 2002; Lozos *et al*., 2013). As such, it is important to further investigate the effects of complex fault geometry on rupture behavior, both in terms of understanding the physics of rupture and in determining shaking hazard associated with such ruptures.

Existing modeling studies of geometrical complexity tend to focus on large-scale breaks and bends in the fault trace. However, many natural faults also include smaller complexities – including short breaks and stepovers, slight bends, and additional fault

strands that are short in comparison to the main trace – in addition to the larger features that have already been well explored in the literature. The San Jacinto Fault in southern California (Figure 2.1) is an excellent example of a fault trace that includes many such features: several large stepovers, with bends and breaks in the individual main traces, and many short parallel strands. The San Gorgonio Pass area of the San Andreas Fault, which is a known barrier to rupture, also includes many of the same types of complexities. Given that large features can control rupture behavior, the effects of small complexities also bear investigation.

In the present study, we focus on stepovers in strike-slip faults. The interaction between the main strands of the stepover produces many types of smaller-scale complexities between the main strands, including extended damage zones, networks of fractures, smaller subsidiary fault strands in a variety of orientations, variations in the strike and dip of each component fault, and flower structures in which all of the component fault segments may join to a single shear zone at depth (Kim *et al.,* 2004; Finzi *et al*., 2009). All of these types of features may affect the ability of rupture to propagate through the stepover. In the current work, we investigate the effect of a smaller fault segment positioned between and parallel to the primary strands of a stepover. This geometrical configuration is motivated by the geometry of the northern San Jacinto Fault, though our somewhat idealized models do not represent that fault zone specifically. We choose to model this geometry in particular because, in a simplistic analysis, the smaller fault segment might be expected to turn the larger stepover into two smaller ones,

Figure 2.1.

Figure 2.1. The Claremont-Casa Loma stepover of the northern San Jacinto Fault, southern California: a real-world example of a stepover with an intermediate fault strand between the primary segments. The rightmost strand is the Claremont, while the leftmost is the Casa Loma. The small fault between the two main strands, in the upper left of the image, is the Farm Road strand (USGS, 2010).

allowing rupture to more easily "stair-step" its way across the gap, and thus aid through-going rupture. We find that the reality is actually much more complicated.

Methods

We conduct all of our models using FaultMod, a 3D finite element code (Barall, 2009), using a slip-weakening Coulomb friction criterion (Ida, 1972; Palmer and Rice, 1973; Andrews, 1976) and a fully elastic medium. The physical and computational inputs for these models are listed in Tables 2.1 and 2.2. In each model, we artificially nucleate the initial rupture by forcing the shear stress above the yield stress (the initial normal stress multiplied by the static coefficient of friction) over a fixed radius larger than the critical patch size required for self-sustaining rupture (Day, 1982). Any secondary rupture nucleations on other fault strands are a naturally calculated result of the physics of the rupture.

Table 2.1. Physical and computational parameters.

P wave velocity	5000 m/s
S wave velocity	3100 m/s
Density	2675 kg/m^3
Static frictional coefficient	0.75
Dynamic frictional coefficient	0.3
D_0	0.4 m
Element size	200 m
Forced nucleation radius	3000 m

All of the models in this study are variations on one basic fault geometry, shown in Figure 2.2: two 50 km long, 16 km deep parallel right lateral strike slip faults, which overlap by 25 km and have 4 km separation between them, with a smaller fault positioned in the stepover region, separated 2 km from either of the primary fault segments. This

Figure 2.2.

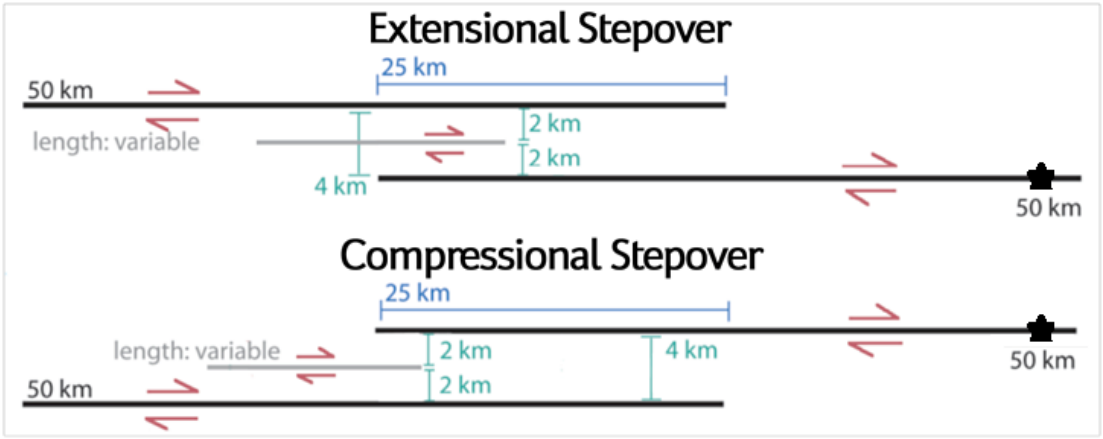

Figure 2.2. Model geometry. The black lines represent the primary fault segments, which are fixed at 50 km length and 16 km basal depth. The gray lines represent the intermediate fault, which is of variable length, and may have a basal depth of 16 km or 8 km. In both the extensional and compressional case, the intermediate fault is centered on the point to which rupture would re-nucleate on the second fault segment, in the absence of the intermediate fault. In the present study, all ruptures have an initial forced nucleation, marked by a star, 3 km from the right end of the right primary segment, at 8 km depth.

geometry can represent either a compressional stepover (left step between the primary segments) or an extensional stepover (right step between the primary segments). The intermediate fault is positioned such that its midpoint is aligned with the point on the second primary fault to which rupture would jump in the absence of the intermediate fault; this position is further along strike outside the stepover region in the compressional case than in the extensional one.

Most of our variables are geometrical in nature. We model fault systems with intermediate segment lengths of 3, 5, 7, 10, and 15 km in order to test the effect of this segment's length on the rupture behavior. We also test two different basal depths for the intermediate segment: 16 km (consistent with the primary segments) and 8 km.

Table 2.2. Stress cases.

Stress case	**Normal stress**	**Shear stress**	**S**
Jumps without segment	16.65 MPa	10 MPa	0.49
No jump without segment (extensional)	17.8 MPa	10.34 MPa	0.6
No jump without segment (compressional)	20.02 MPa	11.01 MPa	0.8

We model these geometries under several different stress states, listed in Table 2.2: one each for compressional and extensional cases in which rupture would jump between the primary segments in the absence of the intermediate fault, and one in which rupture would not jump in the absence of the intermediate fault. These cases help us determine whether the intermediate segment can help shorter ruptures become longer, or arrest ruptures that would have been longer. We chose the values for these initial stresses by varying the fault strength parameter S:

$$S = \frac{\sigma_y - \sigma_0}{\sigma_0 - \sigma_f},$$

where σ_y is the yield stress, σ_0 is initial shear stress, and $\sigma_0 - \sigma_f$ is dynamic stress drop. The lower the value of S, the more energetic the rupture (Das and Aki, 1977). For the case in which rupture would jump anyway in the absence of the intermediate segment, we choose a very low S that produces an easy jump. For the cases in which rupture would not jump in the absence of the intermediate segment, we conducted a suite of models with incremental increases in S of 0.05 until we found the value of S that just barely does not allow rupture to jump. This value of S is different in the extensional case than in the compressional case, which is why the initial stresses for the no-jump case are different between the two stepover types.

Within each of these stress regimes, we conducted models in which the stresses were constant at all depths, and models in which the stresses tapered to 10% of their value at depth within the top 3 km of the fault. We also tested four different nucleation points. Along strike, they 3 km from either end of each primary segment, in order to maximize the effects of rupture directivity. All of these points are 8 km down dip, corresponding to half the seismogenic depth of the fault.

Ground motion is one of the direct outputs of our models. As the grid size used in the models to make them computationally feasible is too large to capture high frequency ground motions, we do not consider our ground motion plots to be quantitative assessments of expected motion from each of our model events. Rather, they are qualitative descriptions of the overall pattern and distribution of ground motion, and of which areas experience comparatively higher or lower particle velocities. The ground motion plots also allow for an easy examination of the extent of rupture along strike.

Results

Different Nucleation Points

Of the four nucleation points we tested, the models most affected by the presence of the intermediate segment were the ones where initial nucleation occurred the farthest away from the intermediate segment, at the right end of the right segment in Figure 2.2. Ruptures that nucleated at either end of the left segment were not affected by the presence of the intermediate segment, likely because the intermediate segment is not within the region of dynamic stress transfer induced by rupture reaching the right end of the left segment. Ruptures that nucleated on the left end of the right segment were affected by the intermediate segment, but because the segment is so close to the region of forced artificial nucleation, it may be responding to the nucleation rather than the dynamic rupture itself, so we cannot consider those results as purely natural behaviors. Thus, the rest of this paper will focus on the models with nucleation on the right end of the right segment.

Compressional Stepovers

The results of our models of compressional stepovers support the idea that the presence of the intermediate segment effectively makes the stepover smaller, and therefore makes it easier for rupture to jump from segment to segment. For the stress state in which rupture would have jumped in the absence of the intermediate segment (Figure 2.3), the segment's presence does not interfere with jumping, and there is a ground motion signature for all three faults. In the stress state in which rupture would not have

Figure 2.3.

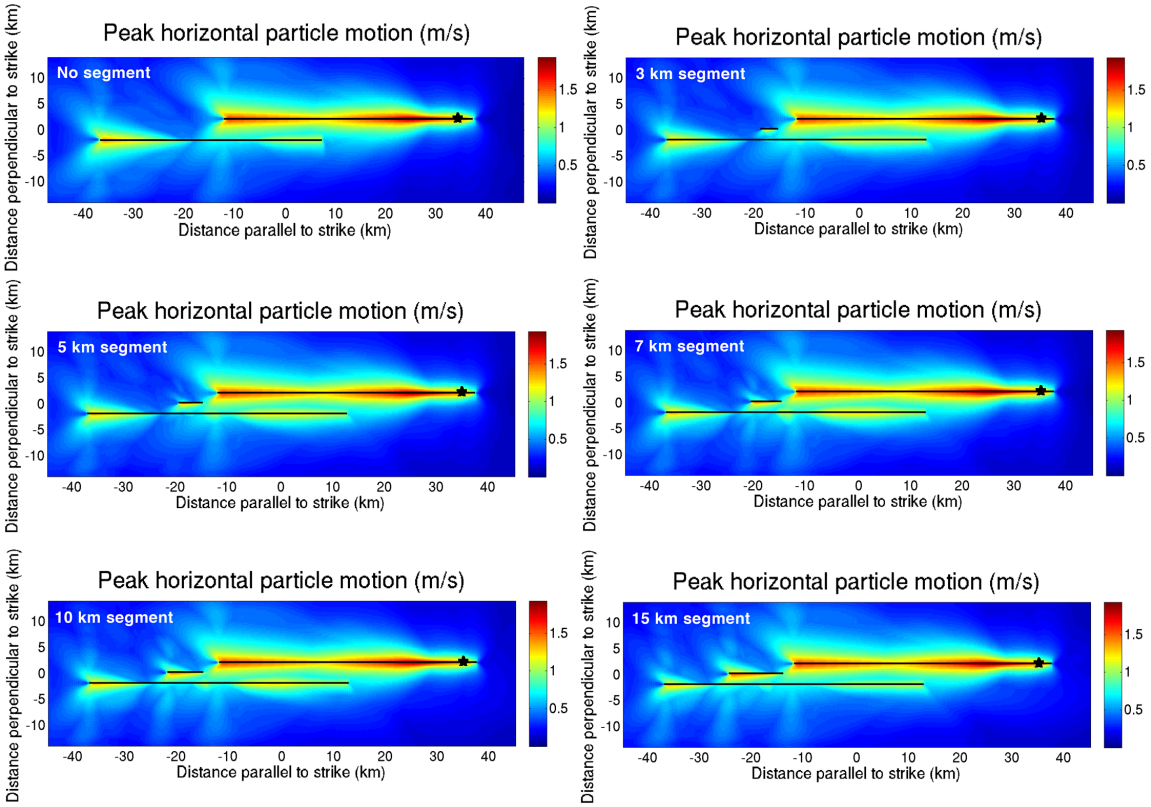

Figure 2.3. Ground motion plots of models of compressional stepovers with intermediate segments of variable length, in a stress state in which rupture is able to jump the stepover in absence of the intermediate segment. The forced nucleation location is marked with a star. Note that the intermediate fault affects the ground motion distribution, but not the ability of rupture to jump.

Figure 2.4.

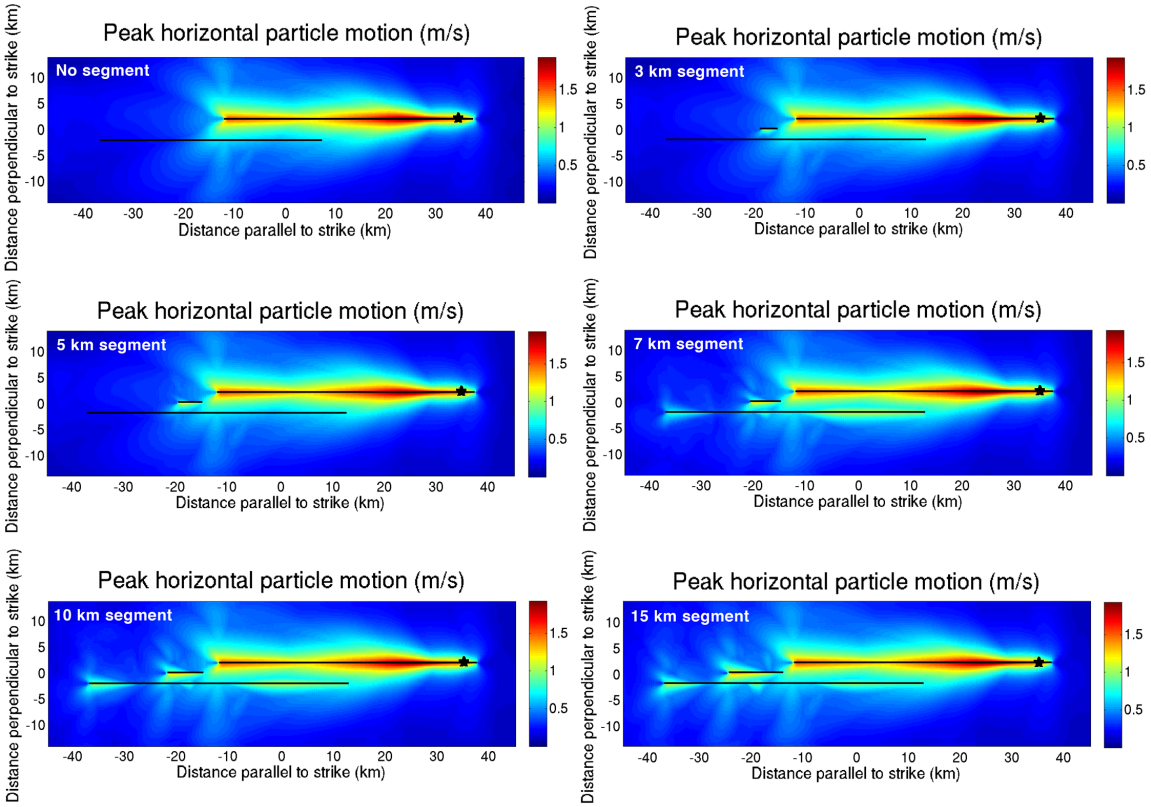

Figure 2.4. Ground motion plots of models of compressional stepovers with intermediate segments of variable length, in a stress state in which rupture is not able to jump the stepover in absence of the intermediate segment. The initial forced nucleation location is marked with a star. If the intermediate fault is long enough, it allows rupture to jump under stress conditions that would have been unfavorable in its absence.

Figure 2.5.

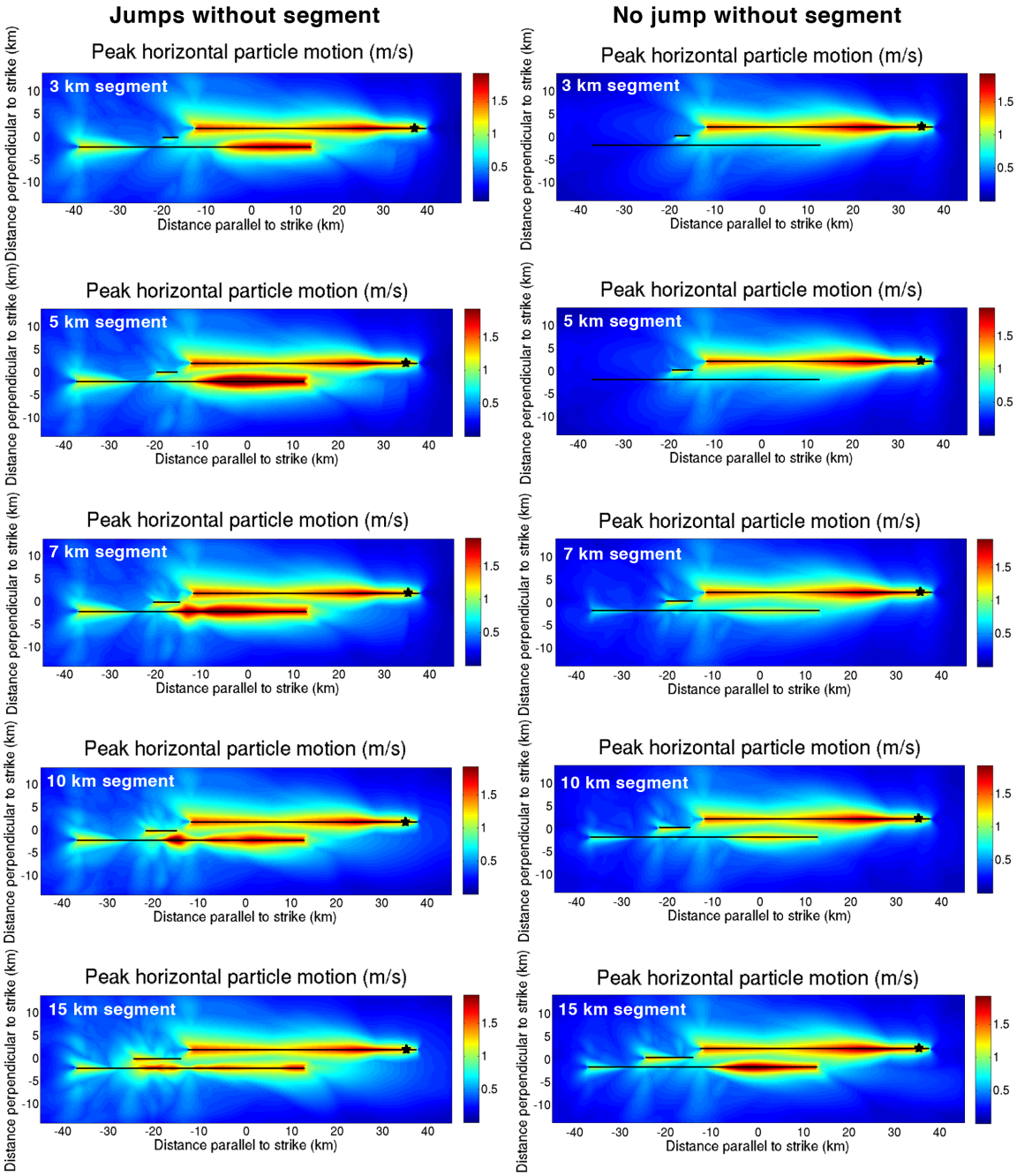

Figure 2.5. Ground motion plots of compressional stepovers with intermediate segments of 8 km basal depth and variable length. The initial forced nucleation point is marked with a star. The shallower basal depth alters the pattern of ground motion when compared to figures 2.4 and 2.5, in which the intermediate fault has a 16 km basal depth, but it does not have a first order effect on rupture's ability to jump, in either stress case.

jumped between the primary segments in the absence of the intermediate fault (Figure 2.4), segments of 7 km and longer do allow rupture to stairstep from the nucleating fault to the intermediate segment to the second primary segment. Hence, the intermediate segment promotes a much longer rupture. Even when the intermediate segment is still too short to allow this sequence of jumping, there is still a jump from the nucleating segment to the intermediate segment. In all of these models, including any length of intermediate segment reduces both the intensity of the ground motion and the area that experiences ground motion when compared to a model with no intermediate segment.

The basal depth of the intermediate segment had no first order effect on the rupture behavior through the compressional fault system. The intensity and distribution of ground motion was affected, as shown in Figure 2.5, but there was no change to whether or not the rupture jumped from segment to segment. Similarly, using depth-dependent stresses on the faults as opposed to homogeneous stresses simply reduced the overall intensity of ground motion, but it did not alter the distribution of highest shaking, nor did it have an effect on whether or not the rupture jumped.

Extensional Stepovers

The results for extensional cases are far more complicated and less systematic than their compressional counterparts. Figure 2.6 shows ground motion plots for the case in which rupture would have jumped in the absence of the intermediate segment. A 3 km long intermediate segment does not affect the jump, but greatly increases the intensity of ground motion (and the area of distribution of the strongest motion) in comparison to a

Figure 2.6.

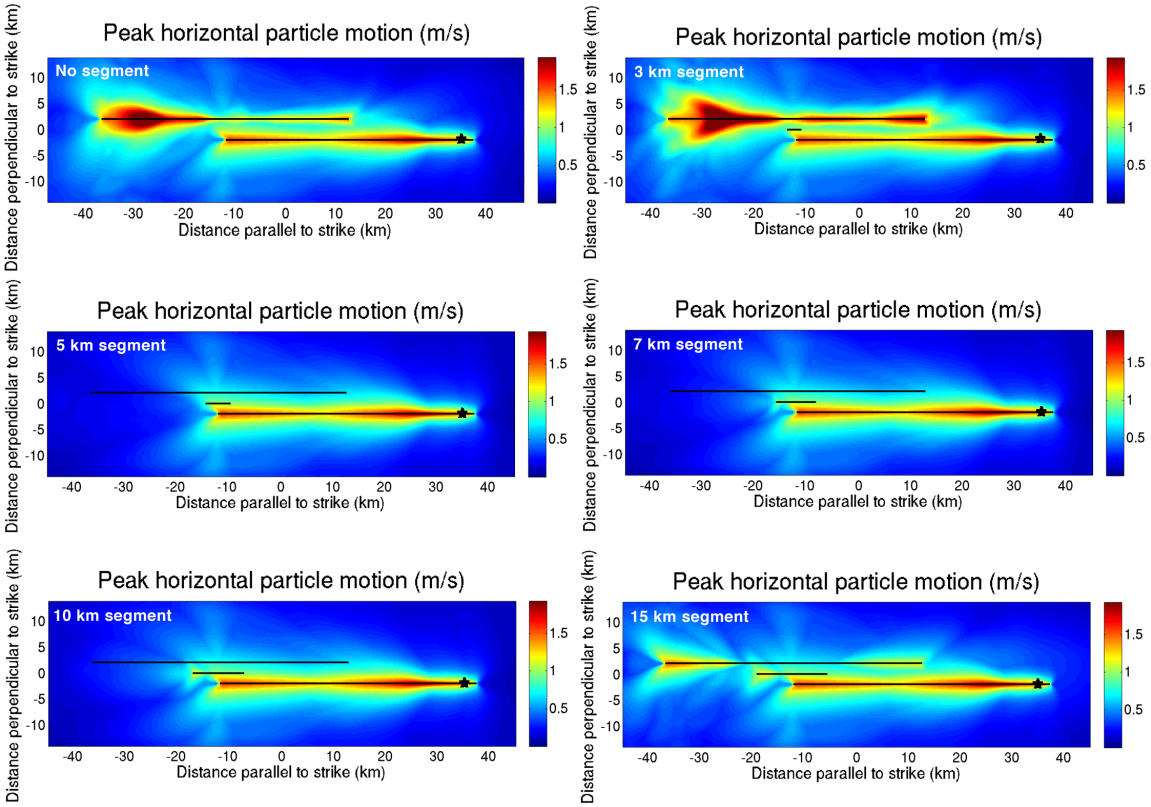

Figure 2.6. Ground motion plots of models of extensional stepovers with intermediate segments of variable length, in a stress state in which rupture is able to jump the stepover in absence of the intermediate segment. The forced nucleation location is marked with a star. A 3 km intermediate fault increases ground motion on the far segment, while intermediate fault lengths of 5, 7, and 10 km allow rupture to jump onto the intermediate fault but not again onto the far fault. At an intermediate fault length of 15 km, rupture is able to jump between all three segments.

fault system with no intermediate segment. However, a 5 km intermediate segment prevents rupture from jumping the stepover; there is not even a ground motion signature on the intermediate segment. For intermediate segments of 7 and 10 km, there is a ground motion signature from the intermediate fault, but rupture does not jump further onto the second primary segment. At 15 km long, the intermediate segment allows rupture to jump onto the second primary segment: a long segment is required in an extensional stepover in order for the rupture to exhibit the sequential jumping that we observed in all of the compressional models.

In the stress state where rupture does not jump in the absence of the intermediate segment (Figure 2.7), adding this segment does not allow rupture to jump to the second primary segment in any case, regardless of length. Rupture does jump onto the intermediate segment, as demonstrated by a ground motion signature on segments of 5 km and longer, but it does not jump a second time.

Also unlike the compressional case, the basal depth of the intermediate segment has a first-order effect on whether or not rupture jumps the extensional stepover, in both stress states (Figure 2.8). In the case where rupture would jump without the intermediate segment, including a segment with a basal depth of only 8 km allows rupture to jump in every case, regardless of the length of the intermediate segment. There is a ground motion signature on all three segments in these cases. In the case where rupture would not have jumped without the intermediate segment, including an 8 km-deep segment does allow rupture to stairstep across all three segments if the intermediate segment is longer than 5 km.

Figure 2.7.

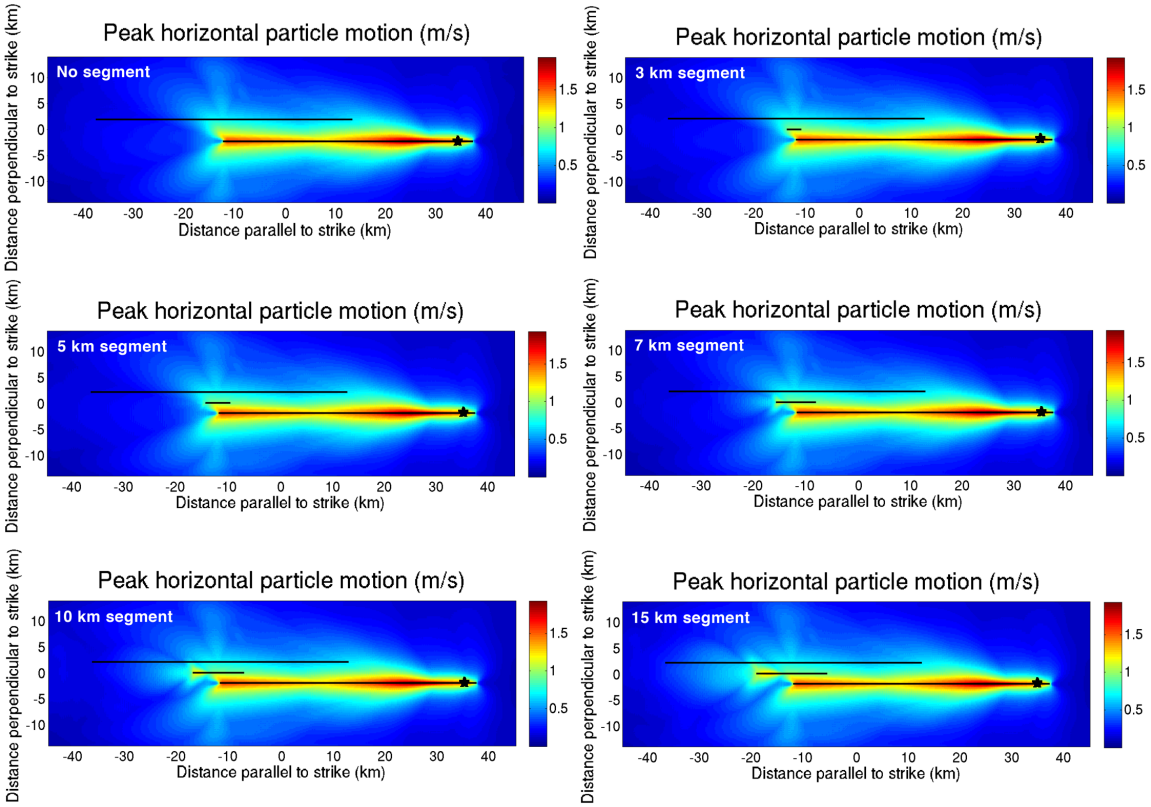

Figure 2.7. Ground motion plots of models of extensional stepovers with intermediate segments of variable length, in a stress state in which rupture is not able to jump the stepover in absence of the intermediate segment. The initial forced nucleation point is marked with a star. Regardless of the length of the intermediate fault, rupture is able to jump to it, but not onto the far primary segment.

Figure 2.8.

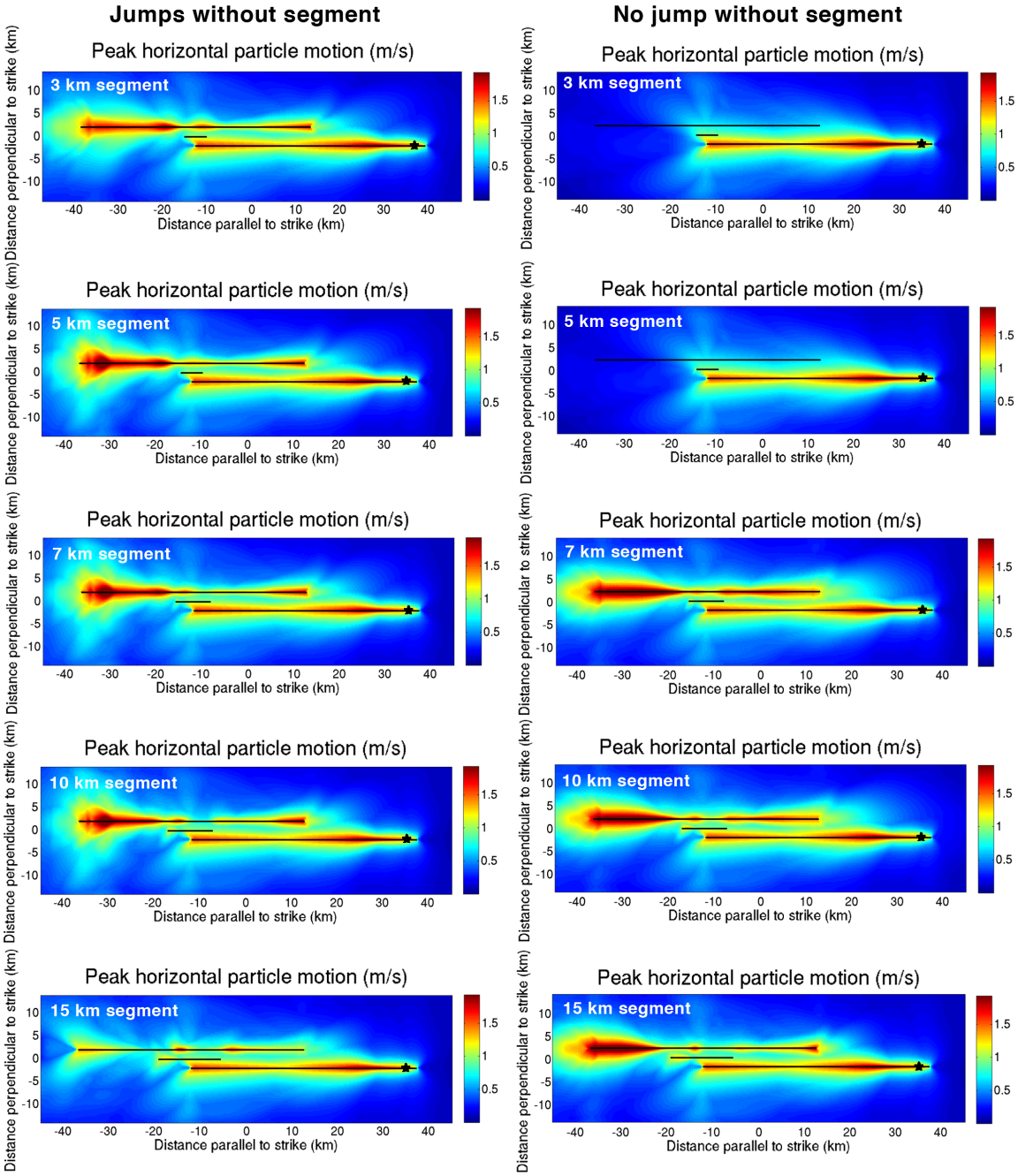

Figure 2.8. Ground motion plots of extensional stepovers with intermediate segments of 8 km basal depth and variable length. The forced nucleation point is marked by a star. In general, the shallower basal depth aids jumping rupture: all intermediate fault lengths lead to rupture jumping between all three segments in the case in which rupture would have jumped in the absence of the intermediate fault, as opposed to the irregular behavior in Figure 2.6. Intermediate segments of 7 km or longer allow jumping rupture in the case that is not favorable for jumping in the absence of the intermediate fault, as opposed to no segment length permitting a jump, as in Figure 2.7.

Whether the stresses on the fault are homogeneous or depth-dependent still does not have a first-order effect on rupture behavior. Whether or not the rupture jumps between all three fault segments is controlled by the many factors and details described above. As in the compressional case, depth-dependent stresses simply reduce the overall intensity of the ground motion associated with the rupture, while keeping the distribution of shaking essentially the same.

Discussion

Across all of our model scenarios, both the ability of rupture to propagate through the entire fault system, and the resulting distribution of ground motion, can be explained by the interaction between rupture directivity and dynamic stress shadowing.

For planar fault segments with homogeneous initial conditions, there is nothing present to disrupt symmetry and directivity of the rupture front. The first disruption of the rupture occurs when it reaches the end of the first primary fault segment. We deliberately positioned the intermediate fault such that it would receive an increase in Coulomb stress as a result of rupture reaching the end of the first primary fault segment, rather than being shadowed by it (Figure 2.9a). This is why the models with a nucleation point 3 km from the right end of the right primary segment are more strongly influenced by the presence of the intermediate segment. With any other nucleation point, rupture passes the intermediate segment before reaching the end of the primary fault, and the lobes of Coulomb stress change that result from rupture reaching the end of the primary fault do not intersect the intermediate fault.

Figure 2.9.

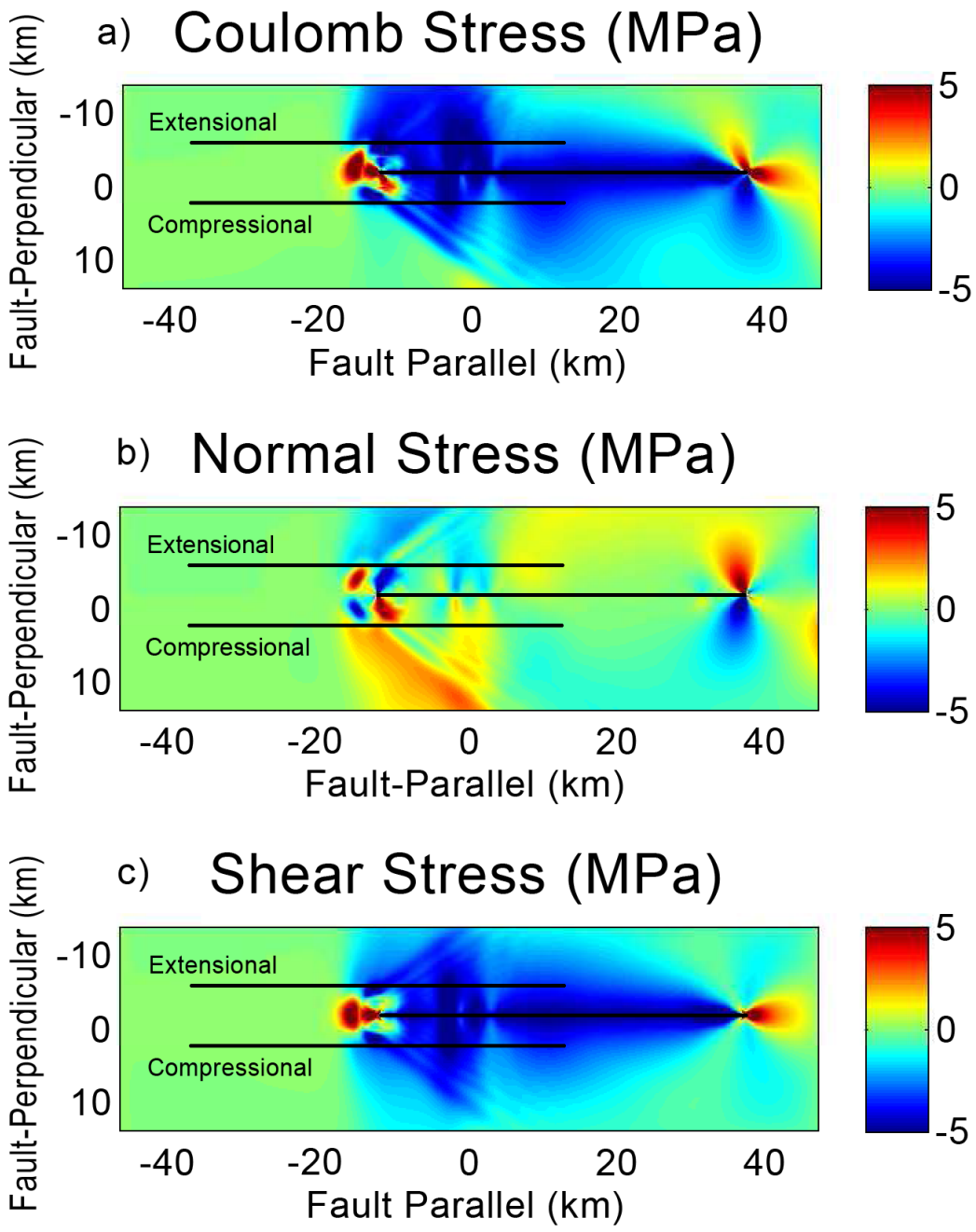

Figure 2.9. Plot of (a) Coulomb, (b) normal, and (c) shear stress changes induced by rupture on a single fault, one second after rupture reaches the end of that fault. The ruptured fault is the center black line; the other black lines represent potential extensional and compressional receiver fault segments. Warm colors correspond with an increase in stress, while cool colors represent a decrease.

The length of the intermediate fault directly controls whether or not rupture on it is able to build up enough directivity to lead to a jump onto the second primary segment. If the intermediate fault is long enough to sustain a continuous, well-localized rupture front, the directivity effect of amplified waves radiating ahead of the rupture front in the direction of rupture is able to produce a large enough change in Coulomb stress on the far primary segment to allow rupture to re-nucleate there. However, if the intermediate fault is not long enough to allow the development of a coherent rupture front, and only sustains patches of unconsolidated slip, there is no amplification effect, and that slip on the intermediate fault does not produce a strong enough increase in Coulomb stress to overcome the stress shadow on the second primary fault produced by rupture on the first one. Figure 2.10 illustrates the difference between these two cases; a 15 km intermediate fault is able to sustain a continuous rupture front (2.10a), while a 3 km intermediate segment is not (2.10b).

Rupture directivity has a strong influence on ground motion intensity, as well as on stress transfer. Ground motion is stronger in the direction of rupture propagation, both along-strike and up-dip, than in the opposite direction. Along-strike directivity effects are straightforward. Longer intermediate faults produce stronger ground motion signatures because the buildup of radiated energy ahead of a rupture front increases with rupture length. Similarly, ruptures that nucleate deeper on the fault have further to propagate before they reach the free surface, and build directivity up-dip as well, which also results in stronger ground motions.

Figure 2.10.

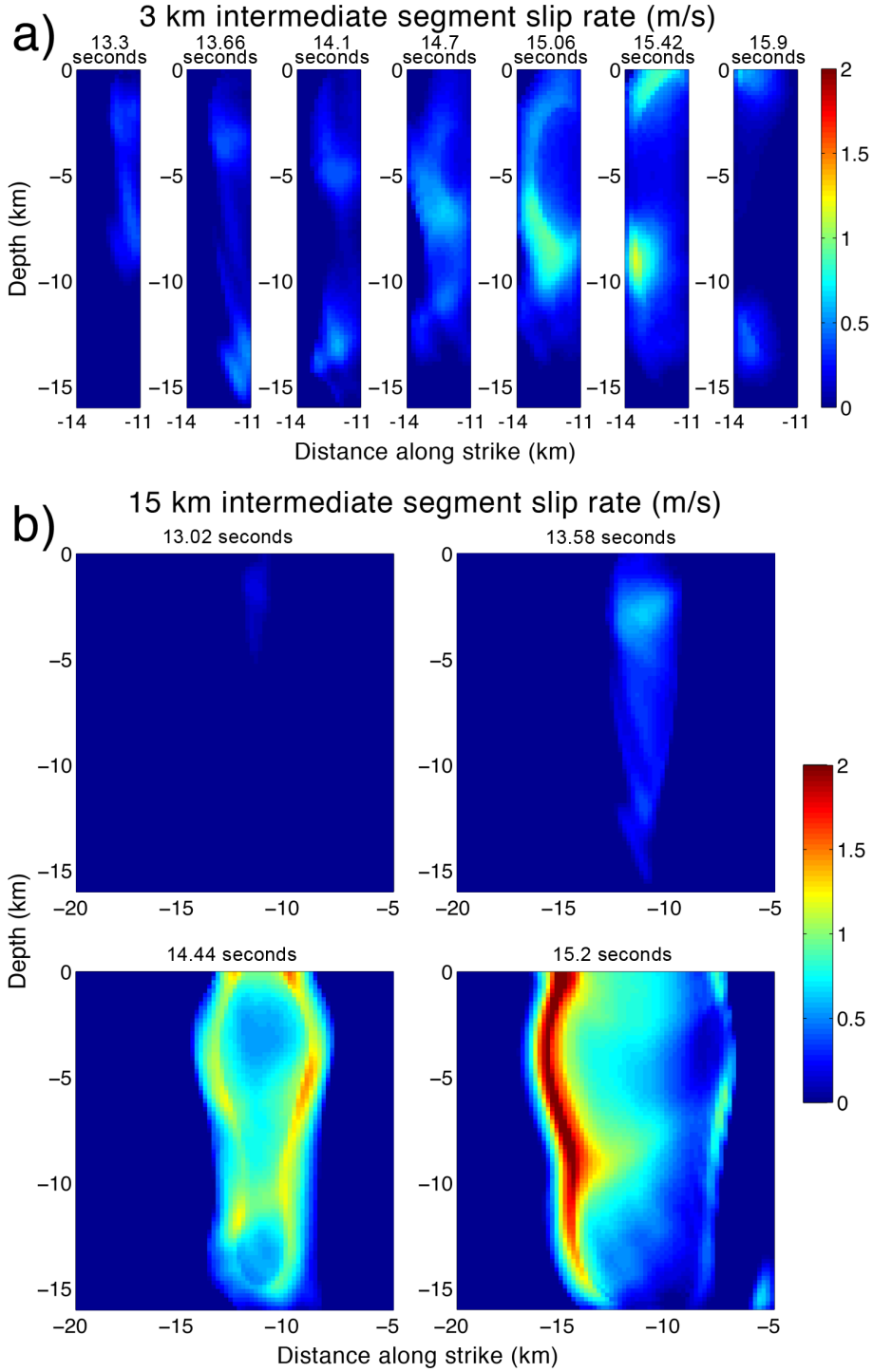

Figure 2.10. Snapshots of slip rate on an intermediate fault segment of 3 km length (a) and 15 km length (b). The 3 km segment experiences patchy slip, but this never coalesces into a coherent rupture front. In contrast, the 15 km segment develops a consolidated rupture front, which is more energetic in the direction away from the stepover itself due to stress shadowing toward the interior of the stepover.

Figure 2.11.

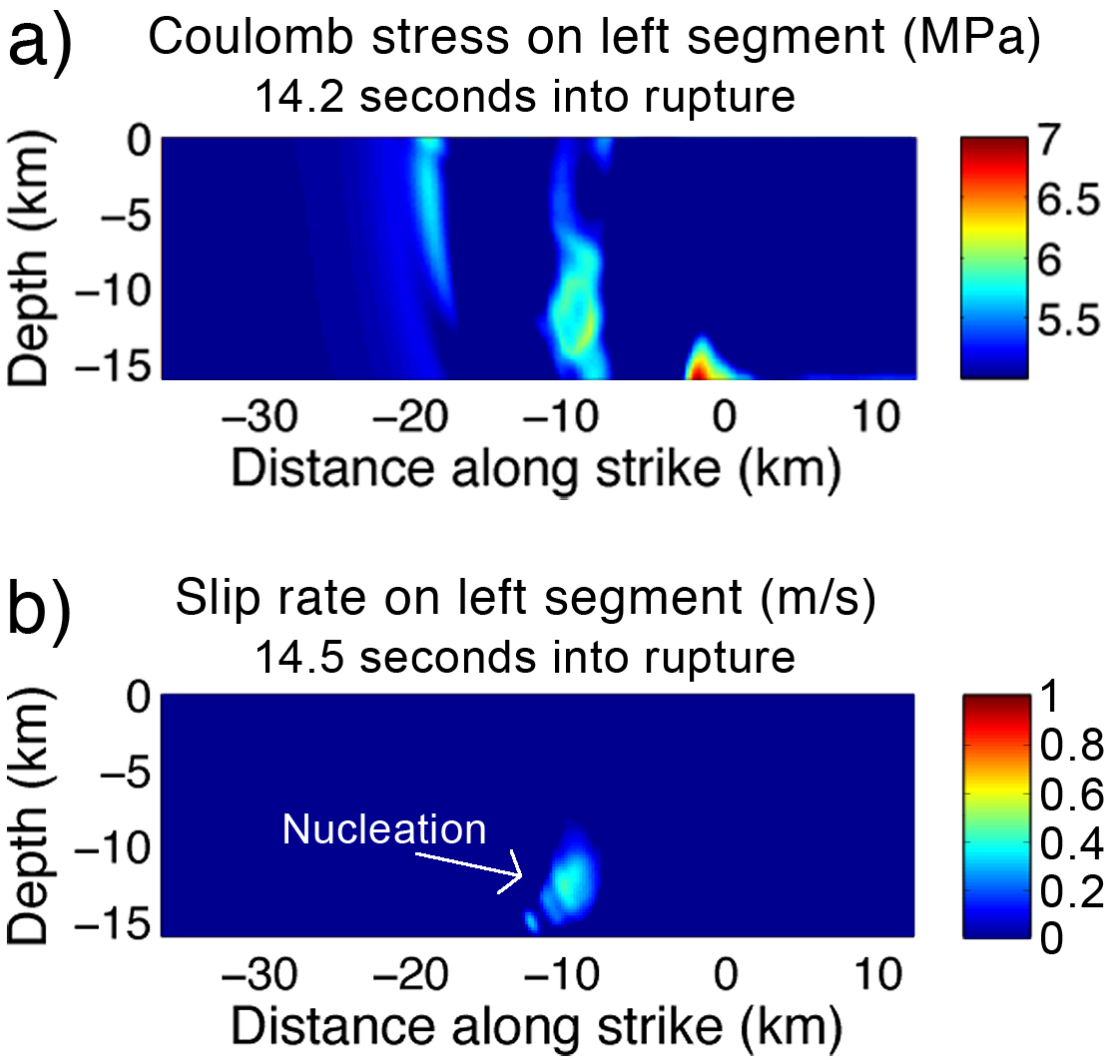

Figure 2.11. Coulomb stress change and rupture re-nucleation on the far primary segment, for a model of an extensional stepover with an intermediate fault of 7 km length and 8 km basal depth. Part A shows the parts of the far primary segment that are experiencing Coulomb stress changes above failure level shortly after rupture terminates on the nucleating segment. Part B shows the slip rate on the far primary segment at the moment of rupture re-nucleation after the jump. Note that the re-nucleation falls within a region of particularly elevated Coulomb stress that is located below the base of the intermediate segment. While this area does not experience the largest Coulomb stress increase of anywhere on the fault, it is a change over a larger area, greater than the critical patch size required for rupture re-nucleation.

These up-dip directivity effects are what produce the differences in rupture behavior and ground motion between the models of different basal depths for the intermediate segment. Rupture on an intermediate fault with a shallower basal depth than the primary segments places the upper part of the second primary segment under a stress shadow, but the lower part into a Coulomb stress increase. This results in rupture re-nucleating deeper on the second primary fault than it would have if the intermediate fault had been the same depth as the primary faults, which in turn results in more up-dip directivity, and therefore stronger ground motion. Figure 2.11 illustrates these effects for an extensional stepover with a 7 km intermediate segment with an 8 km basal depth, in the stress case in which rupture would jump the stepover in the absence of the intermediate fault: 2.11a shows the Coulomb stresses on the far primary segment as a result of rupture on the intermediate segment, and 2.11b shows where on the far primary segment rupture re-nucleates. This increased Coulomb stress at the base of the second primary fault is also why rupture is able to propagate through the entire fault system for more intermediate fault lengths when the intermediate fault has a shallower basal depth; an intermediate fault of the same depth as the primary faults places the full depth of the far primary fault under a stress shadow, making re-nucleation more difficult.

Up-dip directivity effects also explain why models in which the stresses on the fault are tapered toward the surface have the same first-order rupture propagation results as models with homogeneous on-fault stresses, but weaker ground motions. The decreasing stresses toward the surface lead to a reduced energy budget for the rupture,

which weakens the amplification of waves ahead of the rupture front, even though the actual directivity of the rupture front is not broken.

The difference between the more predictable compressional stepover models and the more variable extensional ones is a result of the interaction between the kinematics of the type of stepover and the dynamic stresses that result from rupture through such a system (Figure 2.9b). In a compressional strike-slip stepover, the general slip direction leads to an increase in normal stress between the faults. These conditions are statically unfavorable for rupture, and require a large increase in shear stress to rupture. However, if that shear stress threshold is reached, the resulting rupture has a high dynamic stress drop, which makes it highly energetic. Thus, rupture on even a short intermediate fault may be energetic enough to produce the shear stress changes necessary to re-nucleate rupture on the far intermediate fault. In contrast, the region between the faults in an extensional strike-slip stepover experiences a decrease in normal stress due to the direction of slip. While a fault with lowered normal stress requires less shear stress to initiate rupture, this results in a low dynamic stress drop. This may lead to patches of slip on the intermediate fault, or, if it does produce a consolidated rupture front, it is not as energetic as in the compressional case. This makes it more difficult for stress conditions that would result in rupture on the far primary segment to be met.

Conclusions

We find that the presence of a small intermediate segment between the two primary faults of a strike-slip stepover can have a controlling effect on rupture behavior

through the stepover, as well as the resulting ground motion. However, this effect is far more complex than the intuitive idea that introducing an intermediate fault reduces the width of the stepover and therefore makes the system more conducive to through-going rupture. This effect holds true in compressional stepovers, but in extensional ones, the intermediate segment can serve as either an aid or a barrier to rupture propagation, depending on its length and depth.

These effects are a result of the interaction between dynamic stress shadowing and the buildup of radiated energy ahead of the rupture front in the direction of rupture propagation. In general, if the directivity-induced buildup of energy from rupture on one fault segment produces a large enough Coulomb stress change at the end of the fault to overcome the stress shadow that rupture casts on the other fault segments, then rupture will be able to re-nucleate on that segment. This is why the length of the intermediate fault is a controlling factor: if it is too short, it cannot develop the necessary directivity effects to initiate rupture on the far primary segment.

Our results also concur with past studies, which state that directivity effects also control the intensity of ground motion (Guatteri *et al*., 2003; Guatteri *et al*., 2004; Lozos *et al*., 2013). We find that ground motion becomes stronger with increased along-strike and up-dip directivity alike. We also find that stress shadowing from the intermediate fault can influence where rupture re-nucleates on the far primary segment, which in turn affects the intensity and distribution of the resulting ground motions.

Conventional thought on rupture propagation through stepovers is that it is easier for rupture to jump an extensional stepover than a compressional one of the same width.

Our results contradict this; we find that it is not just an increase or decrease in normal stress that affects the ability of rupture to jump a stepover, but also the dynamic stress drop that results when the fault's yield strength is exceeded.

These results complicate the assessment of rupture behavior and ground motion hazard for geometrically complex fault systems. We show that a single small-scale geometrical complexity in an otherwise simple system is enough to control the extent of rupture and the intensity of shaking. This implies that using simplified models that ignore the many smaller scale complexities that characterize real fault zones may not provide a realistic indication of whether rupture will be able to propagate through those complexities, nor of the ground motion intensities and distribution that may result from those ruptures. Leaving out a small complexity in a fault trace may lead to an artificially high likelihood of through-going rupture in models, and an inaccurate assessment of where the strongest shaking is likely to occur during a given earthquake on that fault.

The high sensitivity to detail in our models – which are still very idealized – suggests that models of specific individual fault systems, incorporating realistic levels of complexity in fault geometry, stress state, and material setting, will be the best way to assess probable rupture and ground motion hazard associated with those faults.

References

Andrews, D. J. (1976). Rupture propagation with finite stress in antiplane strain, *Journal of Geophysical Research* **81,** 3575-3582.

Barall, M. (2009). A grid-doubling technique for calculating dynamic three-dimensional spontaneous rupture on an earthquake fault, *Geophysical Journal International* **178**, 845–859.

Brune, J. N. (2002). Precarious-rock constraints on ground motion from historic and recent earthquakes in southern California, *Bulletin of the Seismological Society of America* **92**, 2602-2611.

Das, S., and K. Aki (1977). A numerical study of two-dimensional spontaneous rupture propagation, *Geophysical Journal of the Royal Astronomical Society* **50,** 643-668.

Duan, B., and D. D. Oglesby (2007). Nonuniform prestress from prior earthquakes and the effect on dynamics of branched fault systems, *Journal of Geophysical Research* **112,** doi:10.1029/2006JB004443.

Finzi, Y., E. H. Hearn, Y. Ben-Zion, and V. Lyakhovsky (2009). Structural properties and deformation patterns of evolving strike-slip faults: numerical simulations incorporating damage rheology, *Pure and Applied Geophysics* **166**, 1537-1573.

Guatteri, M., P. M. Mai, G. C. Beroza, and J. Boatwright (2003). Strong ground-motion prediction from stochastic dynamic source models, *Bulletin of the Seismological Society of America* **93**, 301-313.

Guatteri, M., P. M. Mai, and G. C. Beroza (2004). A pseudo-dynamic approximation to dynamic rupture models for strong ground motion prediction, *Bulletin of the Seismological Society of America* **94**, 2051-2063.

Harris, R. A., and S. M. Day (1993). Dynamics of fault interaction: parallel strike-slip faults, *Journal of Geophysical Research* **98,** 4461-4472.

Ida, Y. (1972). Cohesive force across the tip of a longitudinal shear crack and Griffith's specific surface energy, *Journal of Geophysical Research* **77,** 3796-3805.

Kame, N., J. R. Rice, and R. Dmowska (2003). Effects of pre-stress state and rupture velocity on dynamic fault branching, *Journal of Geophysical Research* **108,** 2265, doi: 10.1029/2002JB002189.

Kase, Y., and K. Kuge (1998). Numerical simulation of spontaneous rupture processes on two non-coplanar faults: the effect of geometry on fault interaction, *Geophysical Journal International* **135**, 911-922.

Kim, Y., D. C. P. Peacock, and D. J. Sanderson (2004). Fault damage zones, *Journal of Structural Geology* **26**, 503-517.

Lozos, J. C., D. D. Oglesby, B. Duan, and S. G. Wesnousky (2011). The effects of fault bends on rupture propagation: a geometrical parameter study, *Bulletin of the Seismological Society of America* **101***,* 385-398.

Lozos, J. C., D. D. Oglesby, and J. N. Brune (2013). The effects of fault stepovers on ground motion, *Bulletin of the Seismological Society of America* **103**, doi: 10.1785/0120120223.

Magistrale, H., and S. M. Day (1999). 3D simulations of multi-segment thrust fault rupture, *Geophysical Research Letters* **26,** 2093-2096.

Oglesby, D. D. (2005). The dynamics of strike-slip step-overs with linking dip-slip faults, *Bulletin of the Seismological Society of America* **95,** 1604-1622.

Oglesby, D. D. (2008). Rupture termination and jump on parallel offset faults, *Bulletin of the Seismological Society of America* **98**, 440-447.

Palmer, A. C., and J. R. Rice (1973). The growth of slip surfaces in the progressive failure of overconsolidated clay, *Proceedings of the Royal Society of London Series A* **332,** 527-548.

U.S. Geological Survey and California Geological Survey (2010). *Quaternary fault and fold database for the United States*.

Wald, D. J., and T. H. Heaton (1994). Spatial and temporal distribution of slip for the 1992 Landers, California earthquake, *Bulletin of the Seismological Society of America* **84**, 668-691.

Wesnousky, S. G. (2008). Displacement and geometrical characteristics of earthquake surface ruptures: issues and implications for seismic-hazard analysis and the process of earthquake rupture, *Bulletin of the Seismological Soceity of America* **98**, 1609-1632.

Chapter 3: Rupture and Ground Motion Models on the Claremont-Casa Loma Stepover of the San Jacinto Fault, Incorporating Complex Velocity Structure, Stresses, and Velocity Structure

Introduction

The San Jacinto Fault (SJF) is a 230 km-long right-lateral strike-slip fault that is one of the major components of the plate boundary in southern California (Figure 3.1). It branches off from the San Andreas Fault in Cajon Pass, and runs sub-parallel to it through to the Imperial Valley. The SJF is a young fault, which has not yet matured into a single primary strand; it is characterized by geometrical complexity. Strand boundaries within the SJF are generally delineated by bends, branches, and stepovers, but the complexity within each strand is such that several different parameterizations exist for the fault zone as a whole (Wesnousky, 1986; WGCEP, 1995; Sanders and Magistrale, 1997; USGS, 2010; Marliyani *et al*., 2013).

The first major complexity along strike from the SJF's endpoint in Cajon Pass is the extensional stepover between the Claremont strand to the northeast and the Casa Loma strand to the southwest (Figure 3.2). The two strands overlap each other for ~25 km along strike, and are separated by a distance of 2.5 to 5 km over that length. Both strands include substantial geometrical complexity within their surface traces, in the form of smaller bends and discontinuities. A shorter intermediate fault strand, known as the Farm Road strand, is positioned at the northern end of the stepover (Park *et al*., 1995). It is separated from the Claremont by 2 km and the Casa Loma by 1 km, and may be as short as 2.4 km (USGS, 2010) or as long as 7 km (Marliyani *et al*., 2013). The dip of all three segments is poorly constrained. Seismic reflection studies suggest that the

Figure 3.1.

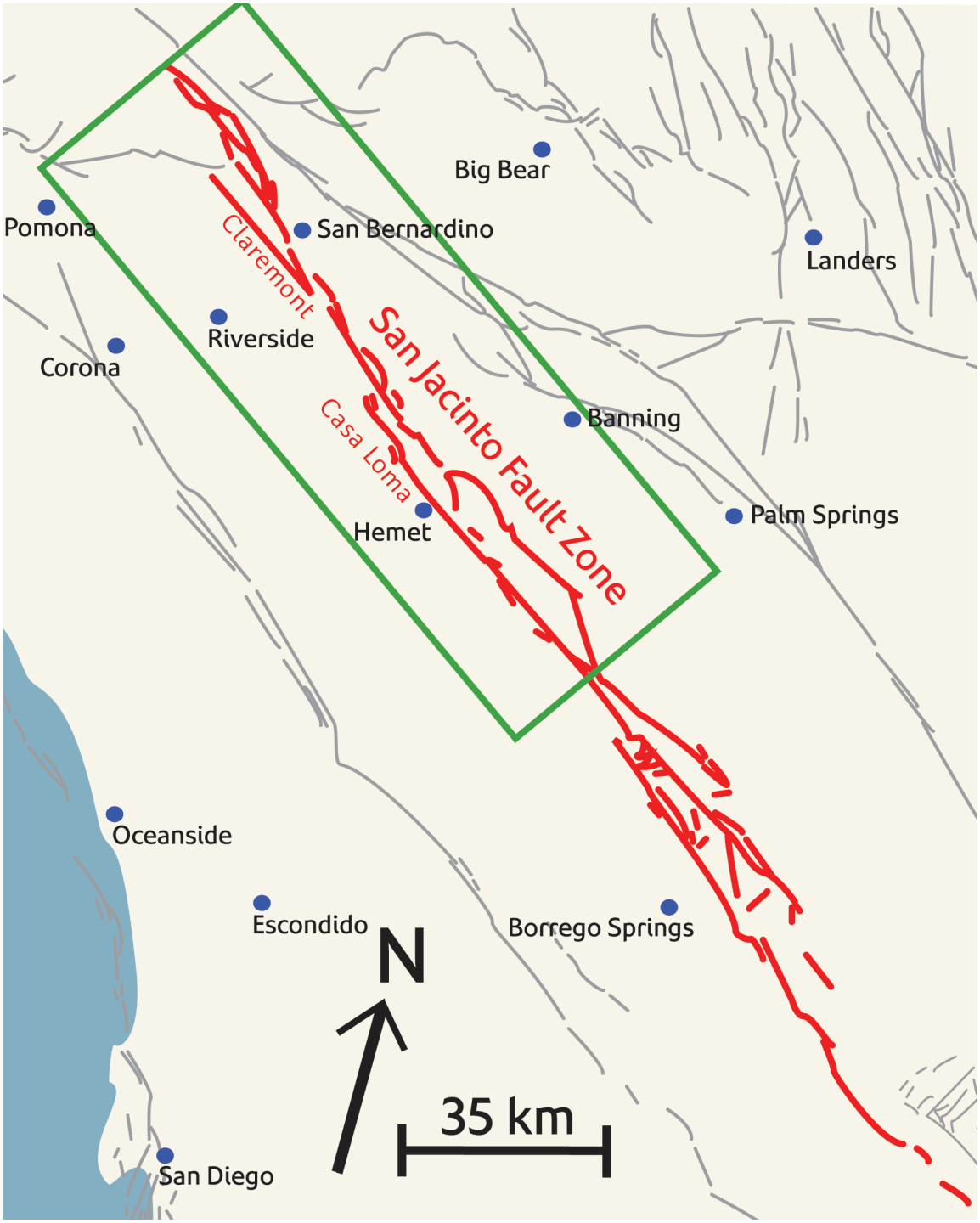

Figure 3.1. Location of the San Jacinto Fault (red) in southern California. The part of the fault zone examined in this study is within the green box. Other Quaternary faults are shown in gray.

Figure 3.2.

Figure 3.2. Close up of the northern San Jacinto Fault Zone. The Claremont-Casa Loma stepover is circled in green. The Claremont strand is the more northeasterly of the two; the Casa Loma is to the southwest. The small fault within the northern end of the stepover is the Farm Road strand.

Claremont and Farm Road strands, and possibly also the Casa Loma, may converge to a flower structure at depth (Park *et al*., 1995), but seismicity data suggests that the dips may be close to vertical (Lin *et al*., 2007). A geologic study by Kendrick and Morton (2012) also suggests that, because the total offset on the SJF (24 km) is equivalent to the overlap length of the Claremont – Casa Loma stepover, the stepover may represent an offset of distinctly separate vertical faults. The Claremont and Casa Loma stands define the edges of the San Jacinto Valley, which is a pull-apart basin with a depth of up to 2.3 km (Park *et al*., 1995).

The Casa Loma – Claremont stepover poses several key questions about the ability of earthquake rupture to negotiate fault zone complexity. The primary question is whether or not a rupture that initiates on the Claremont strand will be able to jump onto the Casa Loma strand, or vice versa. Within this issue is the question of how the smaller scale complexities within those strands may affect rupture propagation, and whether the Farm Road strand is large enough or in an optimal position to sustain its own rupture, or affect propagation on the larger fault strands. Regardless of the extent of the rupture, the question of how complex fault geometry affects ground motion also arises here, and of whether or not that effect is stronger than the effect of the complex velocity structure surrounding the fault. These physical questions also tie directly into questions of seismic hazard in this area, since the northern SJF runs through several cities, including San Bernardino, Moreno Valley, and San Jacinto. Even a moderate rupture on the SJF would have potential to cause considerable damage throughout the densely populated Inland Empire region.

Historical earthquakes and paleoseismology do suggest that there are rupture barriers in the region of the Claremont – Casa Loma stepover. Three M6+ events occurred on the northern SJF, in 1899, 1918, and 1923. The latter event is constrained by damage reports and paleoseismology to have been on the Claremont strand in the vicinity of San Bernardino (Sanders and Kanamori, 1984; Rockwell, 2012). There have been as many different assessments of the locations of the 1899 and 1918 events as there have been studies on the northern SJF. Recent paleoseismology provides strong evidence that 1918 was on the Casa Loma strand, just south of the end of the Claremont strand (Rockwell, 2012), while the location of the smaller 1899 event is still more questionable. Regardless of the exact endpoints of these ruptures, it is evident that the SJF in the vicinity of the Claremont – Casa Loma stepover can fail in a series of smaller events, although the possibility of a larger through-going rupture cannot be ruled out by the data. Dynamic rupture modeling can help assess whether the barriers that lead to this apparent segmentation are geometrical, or are a result of a regional or local stress field, and whether or not a through-going rupture across the stepover is possible.

There is a large and growing, body of work in which dynamic rupture models have been used to investigate the effect of a specific type of geometrical complexity on rupture propagation, including disconnected stepovers between parallel faults (Harris *et al*., 1991; Harris and Day, 1993; Aochi *et al*., 2000; Oglesby, 2008; Lozos *et al*., 2012), parallel faults with another fault linking them at some angle (Magistrale and Day, 1999; Oglesby, 2005; Lozos *et al*., 2011), and fault branches (Kame *et al*., 2003; Duan and Oglesby, 2007). Many of these have results that are directly pertinent to the case of the

northern SJF. Harris and Day's (1993) study of the ability of rupture to jump different stepover widths found that rupture is not likely to jump across an extensional stepover with a separation wider than 4 km, which is narrower than the widest separation between the Claremont and Casa Loma strands. Lozos *et al*.'s (2012) study included an intermediate fault within a stepover, like the Farm Road strand between the Claremont and Casa Loma, found that the length of the intermediate segment can have a controlling effect on whether or not rupture can jump the larger stepover. However, both of these studies, and the others cited above, use fault geometries that are planar aside from the single discontinuity of the type whose effect is being investigated. This type of simplification is crucial to understand primary fault physics, but it may not be adequate to describe the rupture behavior of a realistically-complex fault zone.

In the present study, we investigate the ability of rupture to propagate through the Casa Loma – Claremont stepover of the northern San Jacinto Fault, and the ground motion that results from any ruptures in this area, by constructing dynamic rupture models which incorporate more levels of realistic complexity than in past modeling studies. In particular, we incorporate geometrical complexity within the individual strands of the larger stepover, a regional stress field taken from seismicity studies, and several randomly-generated stochastic stress distributions, and we embed the fault system in an observationally-determined velocity structure for southern California.

Methods

Computational Method

Our dynamic rupture models were conducted using FaultMod (Barall, 2009), a three-dimensional finite element code. We use a slip-weakening Coulomb friction criterion (Ida, 1972; Palmer and Rice, 1973; Andrews, 1976), and a fully-elastic medium. The physical and computational parameters common between all of our models are listed in Table 3.1; however, there is much variability between models, both due to the heterogeneity of initial stress conditions and velocity structure, and due to our choice of stress states. In all cases, we force initial nucleation by raising shear stress on the fault above the yield stress and forcing rupture propagation over a radius larger than the critical patch size required for self-sustaining rupture. Any secondary nucleations on other fault strands occur naturally as a result of the physics of the rupture.

Table 3.1. Physical and computational parameters.

P wave velocity	SCEC Community Velocity Model; minimum clipped to 4157 m/s
S wave velocity	SCEC Community Velocity Model; minimum clipped to 2400 m/s
Density	SCEC Community Velocity Model
μ_{static}	0.6; variable in models with stochastic stresses
$\mu_{dynamic}$	0.2
D_0	0.4 m
Principal stresses	Variable (see Table 3.2)
Stress orientation	N7E
Element size	200 m
Nucleation radius	3000 m

Ground motion is a direct output of FaultMod calculations. However, computational constraints do not allow us to use a small enough mesh size to resolve the high frequency ground motions that pose a hazard to infrastructure. Thus, we apply a

filter to our results such that only frequencies of 1 Hz or less are represented in the ground motion plots in this study. These plots are intended as a qualitative description of the distribution of ground motion, and of which areas experience stronger shaking than others, not a quantitative estimate of what the peak ground motion may be.

Fault Geometry

Our model encompasses the area from the end of the SJF in Cajon Pass to the known seismic gap in Anza, for a model fault length of 106.8 km. We take our fault geometry from the USGS Quaternary Fault Database (USGS, 2010). In this parameterization, the Claremont strand is 75.6 km long, the Casa Loma strand is 55 km long, and the Farm Road strand is 2.4 km long. All three strands have a basal depth of 16 km. The USGS Quaternary Fault Database consists of surface traces only, and our models extend that surface complexity at depth. Many of the smaller bends and discontinuities in the surface trace may smooth out into a more planar surface at depth, but as there is no high resolution data for the SJF at depth, we choose to use the surface trace. Extension of the complex surface geometry to depth results in a highly heterogeneous pattern of stresses (discussed at length below) for the whole seismogenic thickness of the fault, which may induce more barriers and potential endpoints than a smoother fault would. Thus, we consider this geometry to be an end member case for extreme geometrical complexity, opposite from the planar approximations used in many modeling studies of real world faults.

We give all three fault strands a vertical dip. This is how the SJF is represented in the SCEC Community Fault Model (Plesch *et al*., 2007), which is corroborated by seismicity (Lin *et al*., 2007) and geology (Kendrick and Morton, 2012). Incorporating variation in dip would lead to further heterogeneity in the stress state of the fault, but because complexity down-dip is not as well understood as the complexity of the surface trace, we have elected to focus on along-strike complexity and keep the down-dip geometry more simplified. We also do not currently have the capability to make a mesh representing the type of flower structure inferred in reflection data (Park *et al*., 1995). Representing the SJF as a flower structure rather than a true stepover would turn the problem into that of a branch fault, in which rupture selects the more favorable branch, rather than needing to re-nucleate. This is a fundamentally different problem, which we chose not to address because many types of observational data suggest that the Claremont and Casa Loma strands are fully disconnected.

Our fault mesh is generated within FaultMod itself, and is shown in Figure 3.3. The complex geometry is constructed based on a series of latitude-longitude waypoints, with spline curves extrapolated between them. The waypoints used to construct this mesh are listed in Appendix 3.1.

Velocity Structure

Our models incorporate the SCEC Community Velocity Model (Magistrale *et al*., 2000), rather than embedding the faults in a homogeneous or simplified material setting. However, the element size required for our models to be computationally feasible is large

Figure 3.3.

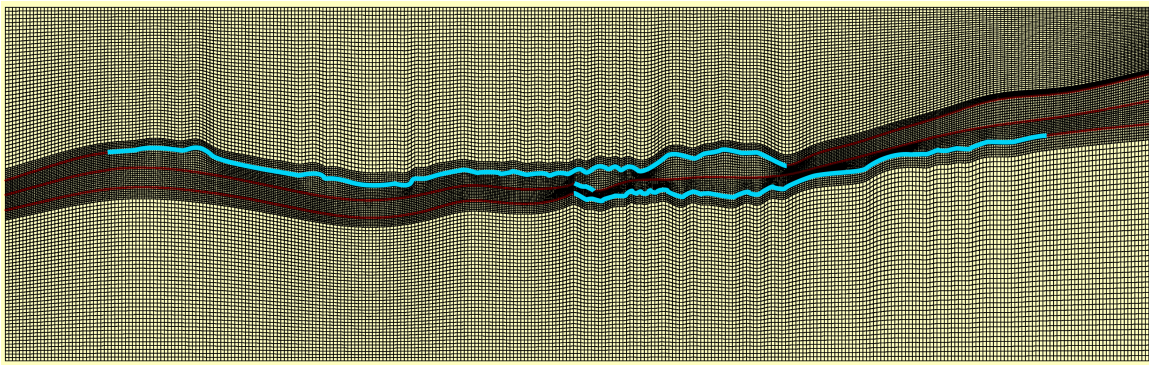

Figure 3.3. FaultMod mesh of the northern San Jacinto Fault, with a model geometry based on the USGS Quaternary Faults Database. The Claremont strand is the topmost strand in this figure. The parts of the fault system that are permitted to rupture are marked in blue. The larger elements on the outside of the figure are 400 m square, and the smaller ones surrounding the fault are 200 m square.

enough that we would not be able to resolve high frequency ground motions produced in the lowest velocity regions of the model. In order to ensure that we are resolving ground motions up to 1 Hz, we clip the minimum P and S wave velocities to the values listed in Table 1. This results in a smoothing of some of the details of the velocity structure, particularly in the case of boundaries between sedimentary rock and unconsolidated sediment. A hybrid dynamic and kinematic modeling procedure would be necessary to resolve ground motions from the full range of velocities in the CVM, given our current computational constraints.

Constant Traction Models

The default way in which FaultMod assigns stresses to a fault is to apply specified shear and normal stress values everywhere along the trace, resulting in constant traction, dynamic stress drop, and fault strength S,

$$S = \frac{\sigma_y - \sigma_0}{\sigma_0 - \sigma_f},$$

where σ_y is yield stress, σ_0 is initial shear stress, and $\sigma_0 - \sigma_f$ is dynamic stress drop, with a lower S value resulting in a more energetic rupture (Das and Aki, 1977). We conducted a series of constant traction models using a constant stress drop of 5.5 MPa, a constant S of 0.6. The forced nucleation points in these models were 8 km down-dip, representing half the seismogenic thickness of the fault, at 3 km along strike from the northeast end of the Claremont strand and 3 km along strike from the southwest end of the Casa Loma strand, in order to maximize directivity toward the stepover. We conducted constant

traction models with the faults embedded in a homogeneous half space in which V_p = 5000 m/s, V_s = 3100 m/s, and r = 2675 kg/m^3, and embedded in the complex material setting of the SCEC CVM.

Regional Stresses

We modified FaultMod to allow it to apply a homogeneous regional stress field to the fault system, resulting in different values for shear and normal stress depending on the orientation of each part of the fault. In order to do this, we calculate the stress tensor for a chosen stress drop and fault strength S for a 45-degree northwest-striking fault, the overall orientation of the SJF. This tensor is then resolved individually onto each node of the fault.

Table 3.2. Model stress states.

$\sigma_{vertical}$	$\sigma_{north\text{-}south}$	$\sigma_{east\text{-}west}$	**Stress Drop**	**S**
20 MPa	28.5 MPa	8.5 MPa	5.5 MPa	0.5
20 MPa	29.45 MPa	9.05 MPa	5.5 MPa	0.55
20 MPa	30.05 MPa	9.5 MPa	5.5 MPa	0.6
20 MPa	53.25 MPa	17.3 MPa	9.5 MPa	0.65
25 MPa	54.9 MPa	18.3 MPa	9.5 MPa	0.7
25 MPa	56.1 MPa	19.1 MPa	9.5 MPa	0.75
20 MPa	42.2 MPa	10.2 MPa	9.5 MPa	0.25

We use a seismicity-based regional stress field in which the maximum horizontal compressive stress is oriented N7E (Hardebeck and Hauksson, 2001) in most of our models. We also ran several tests in which we kept the same magnitude of principal stresses as in the N7E models, but rotated their orientation 10 degrees in either direction in order to test the effect of overall stress orientation on rupture extent. We conducted

models with two different input dynamic stress drops, as resolved on a 45-degree NW-striking planar fault: 5.5 MPa, which falls in the middle of the range of average stress drops inferred for continental strike-slip faults (Kanamori and Anderson, 1975; Kanamori and Brodsky, 2004), and 9.5 MPa, which is the inferred stress drop of the M6.5 1968 Borrego Mountain earthquake, the most recent historic event on the San Jacinto Fault (Burdick and Mellman, 1976). Within each stress drop case, we varied S to gauge the effect of fault strength on rupture extent. Our different stress cases are described in Table 3.2. While this paper refers to these cases by their input stress drop and S, note that both stress drop and S become highly heterogeneous along strike as a result of the complex fault geometry.

Figure 3.4 depicts the regional stress field as resolved as shear stress onto all three of our model fault segments. While this example is for a case with a stress drop of 5.5 MPa and an S of 0.6, the overall pattern of zones of high and low stress and strength is consistent between cases; the only variability is in magnitude. Because the geometry is consistent between the surface and the base of the fault, the stress field produces strong horizontal variation in the stress field, but no vertical variation. In order to compensate for decreasing confining stresses toward the surface, on top of this stress field, we taper the shear and normal stresses to 1% of their initial value over the top 3 km of the fault; this is done separately from the initial stress field generation, which is why this effect does not appear in Figure 3.4. We also clip the minimum shear stress at zero, to avoid the unrealistic case of the fault locally becoming left lateral.

Figure 3.4.

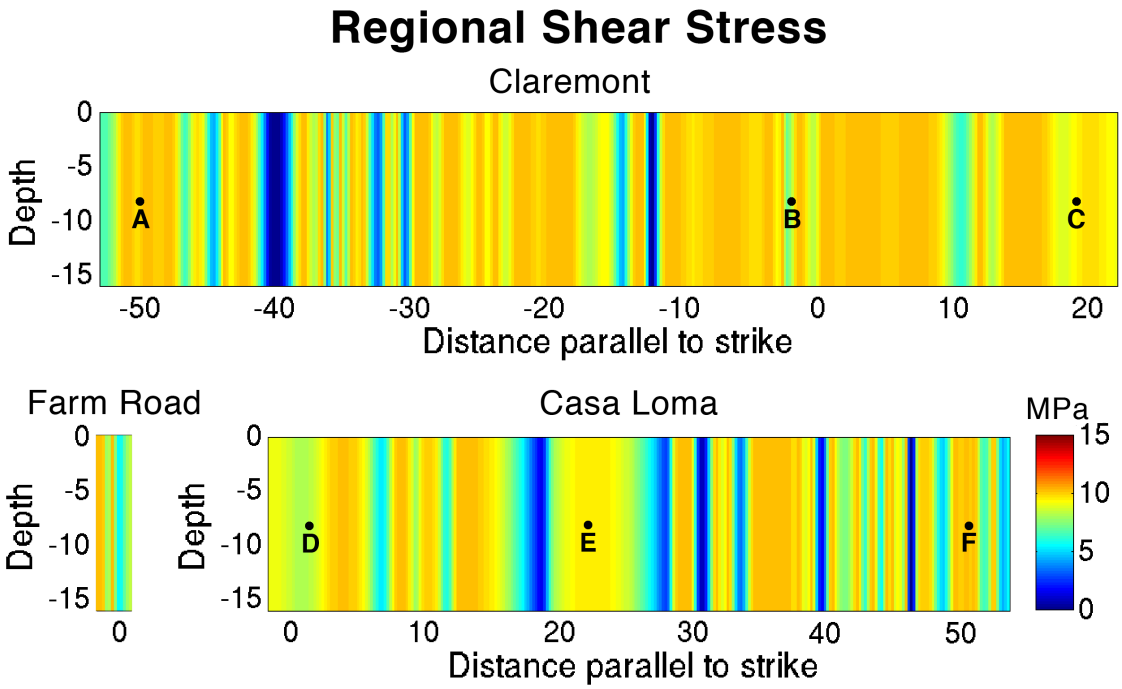

Figure 3.4. Shear stress distribution resulting from a regional stress orientation of N7E resolving on the northern San Jacinto Fault geometry shown in Figure 3.3. The lettered points indicate different locations in which we forced initial rupture nucleation. This figure was made using an input stress drop of 5.5 MPa and an input S of 0.6. Different input values produce different shear stress magnitudes, but the overall pattern of high and low stress areas remains the same regardless of input values.

The lettered dots in Figure 3.4 are points we used for the initial forced nucleation. Points A, C, D, and F are all 3 km from the end of their respective fault segments, and were chosen to maximize directivity effects. Points B and E align with the end of the stepover itself; past models of extensional stepovers show that, within an event, rupture jumps on to the portion of the second segment that is directly opposite the end of the first segment (Harris and Day, 1993), which means these are also plausible locations for nucleation for a second event following an initial rupture that did not jump the discontinuity.

Stochastic Stresses

To account for stress variations that may not be geometrically induced or on a regional scale, we also conducted models that combine the regional stress field described above with several different randomized stochastic stress distributions. We generate these stress fields using the method of Andrews and Barall (2011), which creates a random self-similar shear stress distribution based on a specified fault size, frictional parameters, normal stress, and four random number seeds. We used the same input frictional parameters as in the FaultMod models, listed in Table 3.1, and our input normal stress was the average normal stress from the regional stress field for a given S and stress drop. The random number seeds for our four realizations are listed in Appendix 3.2. In order to insure that the smallest stochastic variability was at the scale of a single element and not inherently larger, we generated our stochastic stresses at a grid size of 60 m, then stretched everything out as we combined it with the regional stress field; 60 m

Figure 3.5.

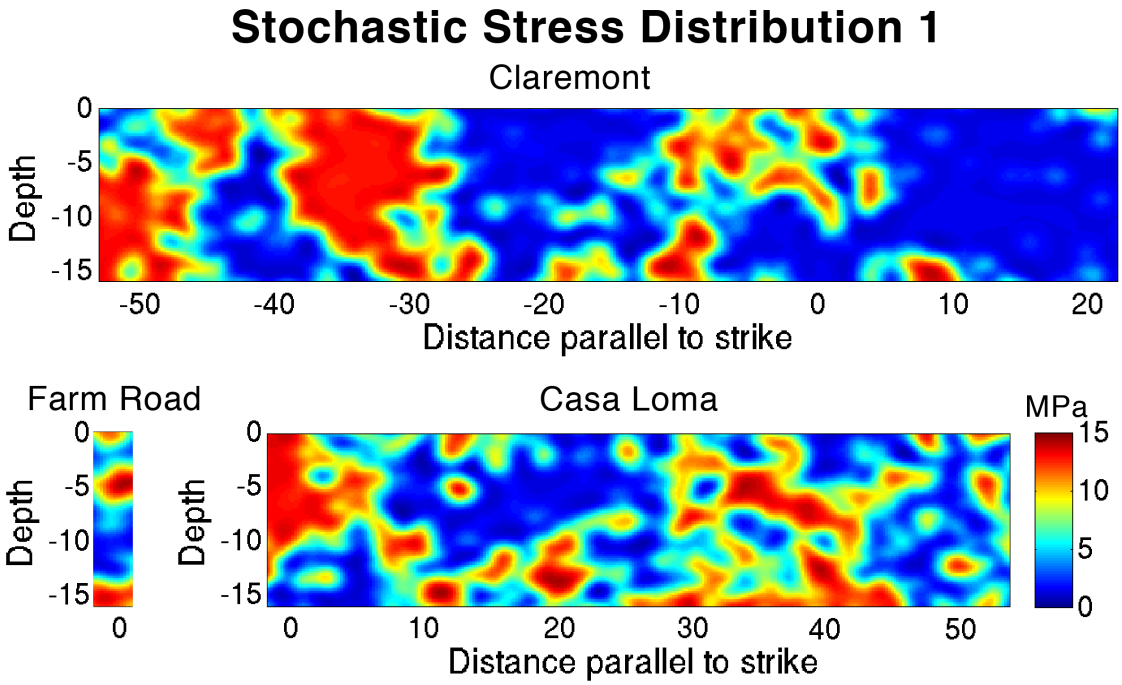

Figure 3.5. Example stochastic shear stress distribution. This plot was generated using an input stress drop of 5.5 MPa, an input S of 0.6, and random number seed set 1 (see Appendix 3.1). The distribution of stresses is controlled by the random number seeds, and the intensity by the input stresses; for this set of random numbers, different initial stresses produce a distribution that is identical in pattern and different only in magnitude.

Figure 3.6.

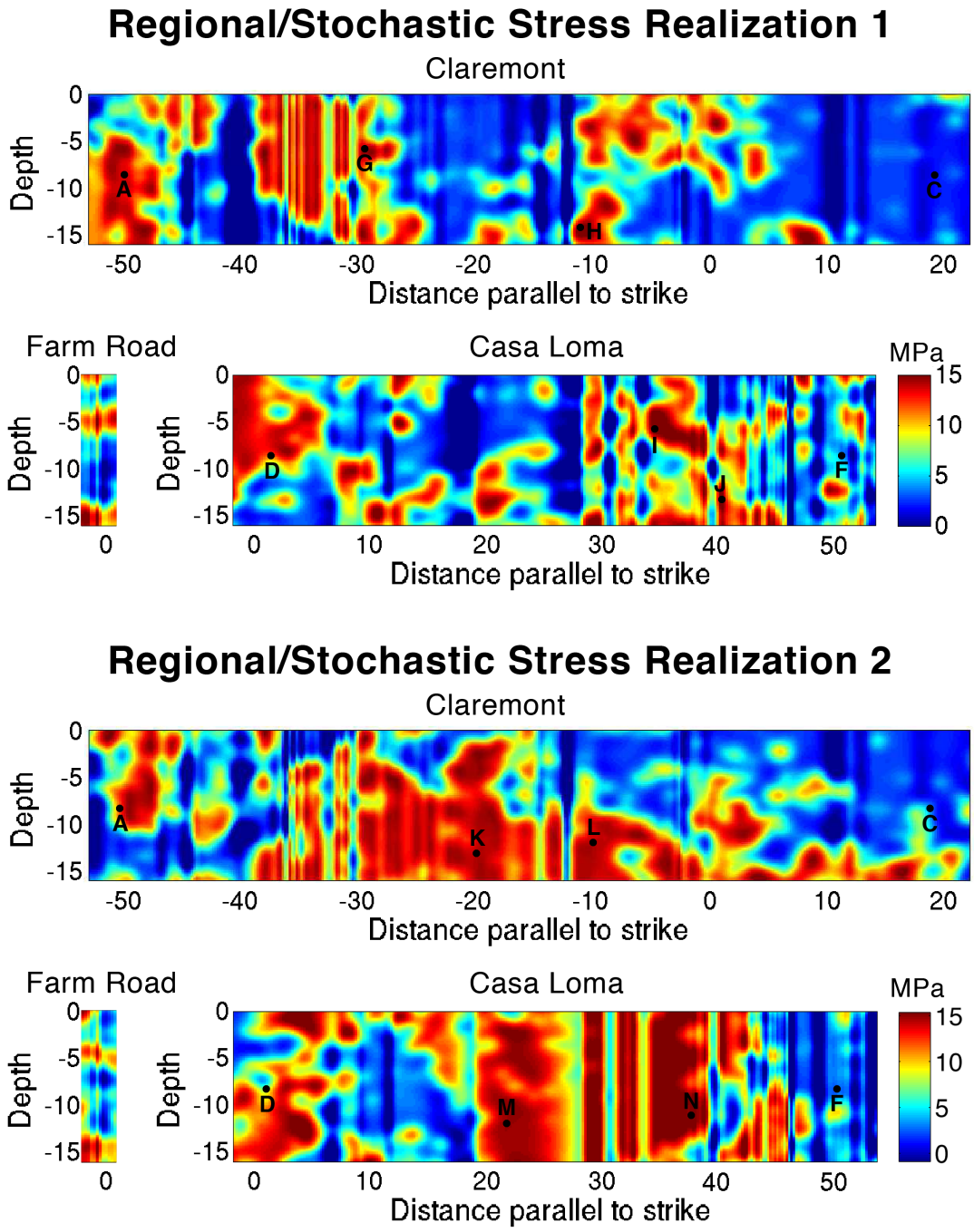

Figure 3.6. Full shear stress realizations, combining the regional stress field (Figure 3.4) with four different stochastic shear stress distributions. The lettered dots represent different forced nucleation sites. These plots are for an input stress drop of 5.5 MPa and an input S of 0.6; different initial values do not affect the shape of the distribution, only the magnitude of the stresses.

Figure 3.6, continued.

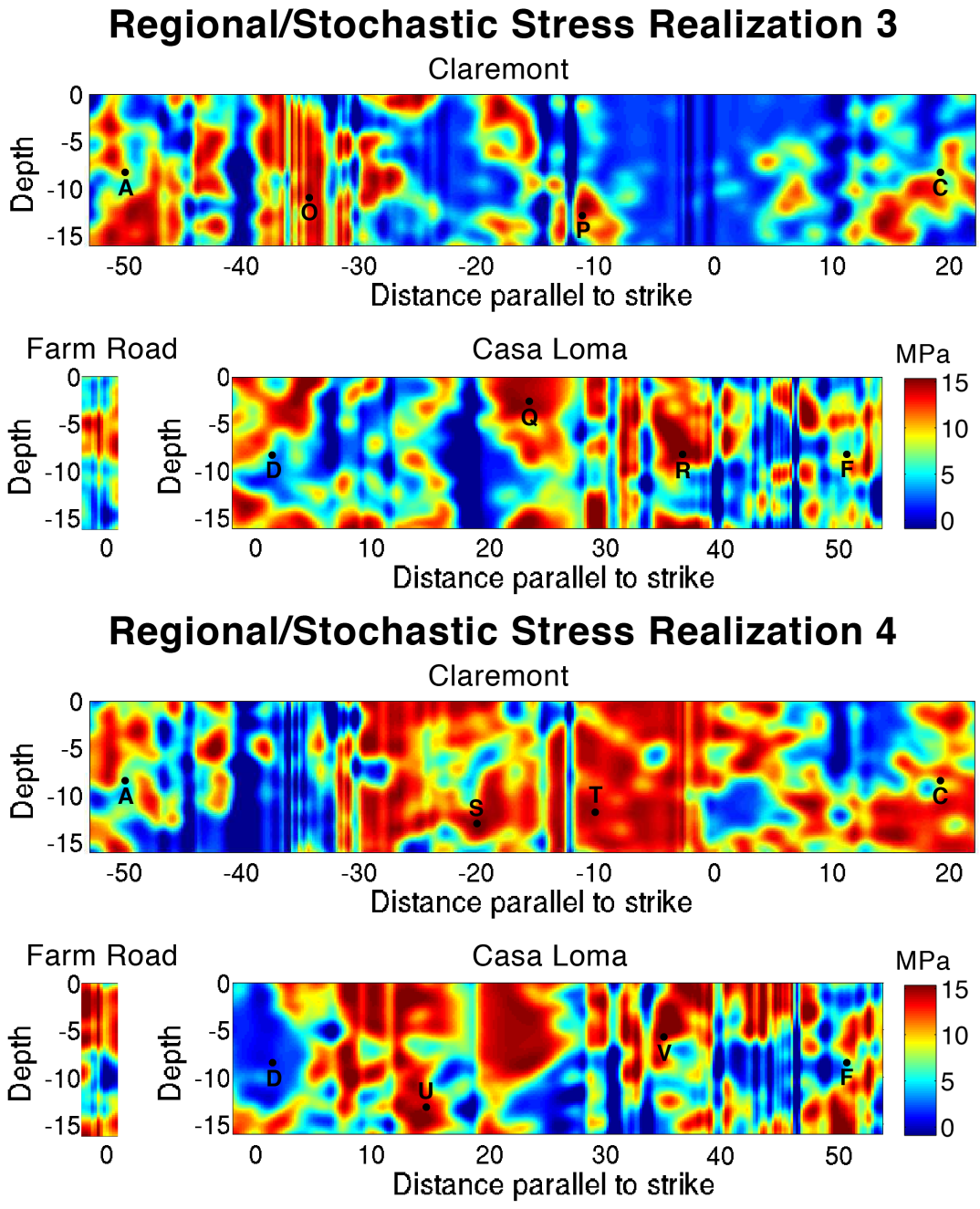

Figure 3.6. continued. More full shear stress realizations, combining a regional stress field with a stochastic shear stress distribution.

complexities in the stochastic stress output become 200 m complexities in the FaultMod stress field input. Andrews and Barall's (2011) code is set up to generate a stress distribution that concentrates stochastic asperities at the center of the fault, and has homogeneous stresses around the edges. Because we wanted the stochastic stresses to cover our entire faults, we generated distributions that were three times the size of our faults in terms of both strike and dip, then clipped out the middle third to apply to our models. Figure 3.5 is an example stochastic stress distribution, with average normal stress taken from the regional stress field in Figure 3.4.

Table 3.3. Forced nucleation locations.

Nucleation Point	Realization	Along-Strike Coordinate	Down-Dip Coordinate
A	All	-50.4 km Claremont	-8 km
B	Regional	-1.6 km Claremont	-8 km
C	Regional	19.2 km Claremont	-8 km
D	Regional	1.4 km Casa Loma	-8 km
E	Regional	22.2 km Casa Loma	-8 km
F	All	50.4 km Casa Loma	-8 km
G	1	-29 km Claremont	-6 km
H	1	-11 km Claremont	-13 km
I	1	34 km Casa Loma	-6 km
J	1	41 km Casa Loma	-13 km
K	2	-20 km Claremont	-13 km
L	2	-10 km Claremont	-12 km
M	2	22 km Casa Loma	-12 km
N	2	37 km Casa Loma	-11 km
O	3	-34 km Claremont	-11 km
P	3	14 km Claremont	-13 km
Q	3	23 km Casa Loma	-3 km
R	3	37 km Casa Loma	-8 km
S	4	-20 km Claremont	-13 km
T	4	-10 km Claremont	-12 km
U	4	14 km Casa Loma	-13 km
V	4	35 km Casa Loma	-6 km

To combine the regional stress field with the stochastic stress distribution, first we subtracted the average shear stress of the entire regional stress field from the stochastic stress value for each element, then added the residual stress for each element to the initial regional stress value at that element:

$$\tau_{combined} = \left[\tau_{stochastic} - mean(\tau_{regional})\right] + \tau_{regional}$$

Figure 3.6 shows the four combined regional and stochastic stress realizations that we used in this study, with Realization 1 corresponding to the combination of Figure 3.4 and Figure 3.5. The lettered dots in Figure 3.6 represent different nucleation points. A and F correspond with the points in Figure 3.4 that were chosen to maximize directivity, but all of the other points were chosen to correspond with large areas of high stress, which are more realistic natural nucleation points. Table 3.3 describes the along-strike and down-dip locations for all of these nucleation points.

As in the models that incorporate the regional stress field alone, we taper the stresses to 1% of their initial value over the top 3 km of the fault, and we set the minimum shear stress to be zero in order to prevent the fault from becoming locally left lateral. In addition, we cap the maximum shear stress to be 90% of the yield stress, in order to avoid spontaneous nucleations at localized points of high stress.

Results

Constant Traction Models

For constant traction models in which the fault system is embedded in a homogeneous half space, rupture is only able to jump between the Claremont and Casa

Loma strands of the SJF and propagate through the whole system if rupture nucleates on the Claremont strand. Rupture does not jump if the initial forced nucleation is on the Casa Loma strand. Figure 3.7 shows ground motion plots for these models. Despite the constant traction, the ground motion distribution is highly asymmetrical about the bends in the fault, with lobes of strongest motion occurring at the end of each relatively planar section of the fault, right before the next bend. This suggests that geometry in and of itself can affect rupture behavior, even when divorced from the issue of how regional stresses resolve upon that geometry.

The constant traction model can also illustrate the effect of the velocity structure. The models in Figure 3.8 use the same geometry and stresses as in Figure 3.7, but are placed within a heterogeneous material setting taken from the SCEC Community Velocity Model. The extent of rupture is no different for nucleation on the Casa Loma strand, but the Claremont nucleation no longer results in rupture jumping from the Claremont onto the Casa Loma. The asymmetrical ground motion around the bends in the fault remains, but the intensity and specific pattern of ground motion differ between Figure 3.7 and Figure 3.8. Including the velocity structure in the models produces stronger ground motions in low-seismic-velocity areas such as the San Jacinto Valley (around Hemet and San Jacinto), the San Bernardino Basin (around San Bernardino and Redlands), and into San Gorgonio Pass (around Banning and Yucaipa).

Figure 3.7.

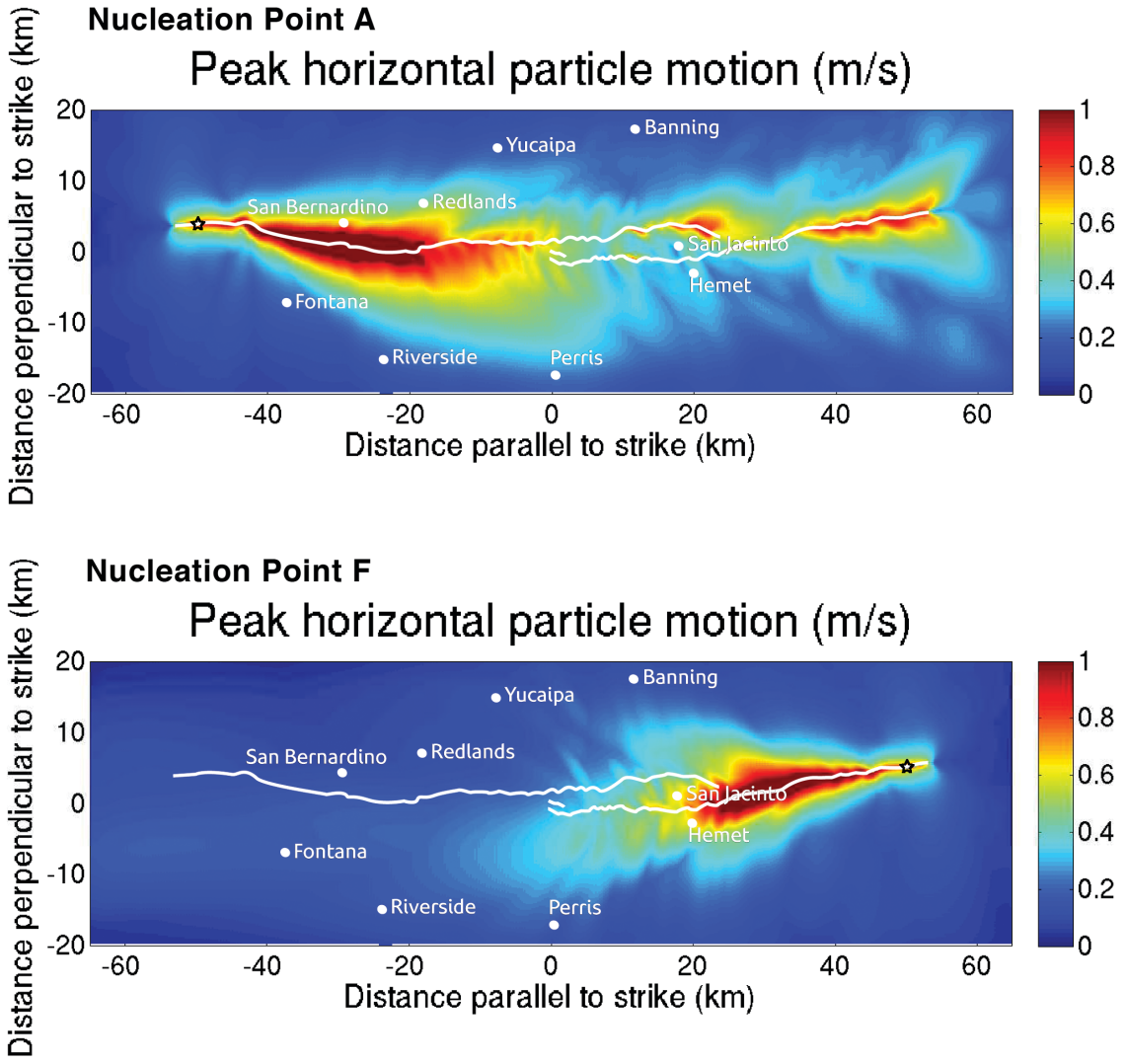

Figure 3.7. Ground motion plots for ruptures on the complex San Jacinto Fault model geometry (white lines), with constant traction and constant S, embedded in a homogeneous material setting. The initial nucleation points are marked with stars. Even with homogeneous initial stresses and material properties, the ground motion pattern is highly asymmetrical.

Figure 3.8.

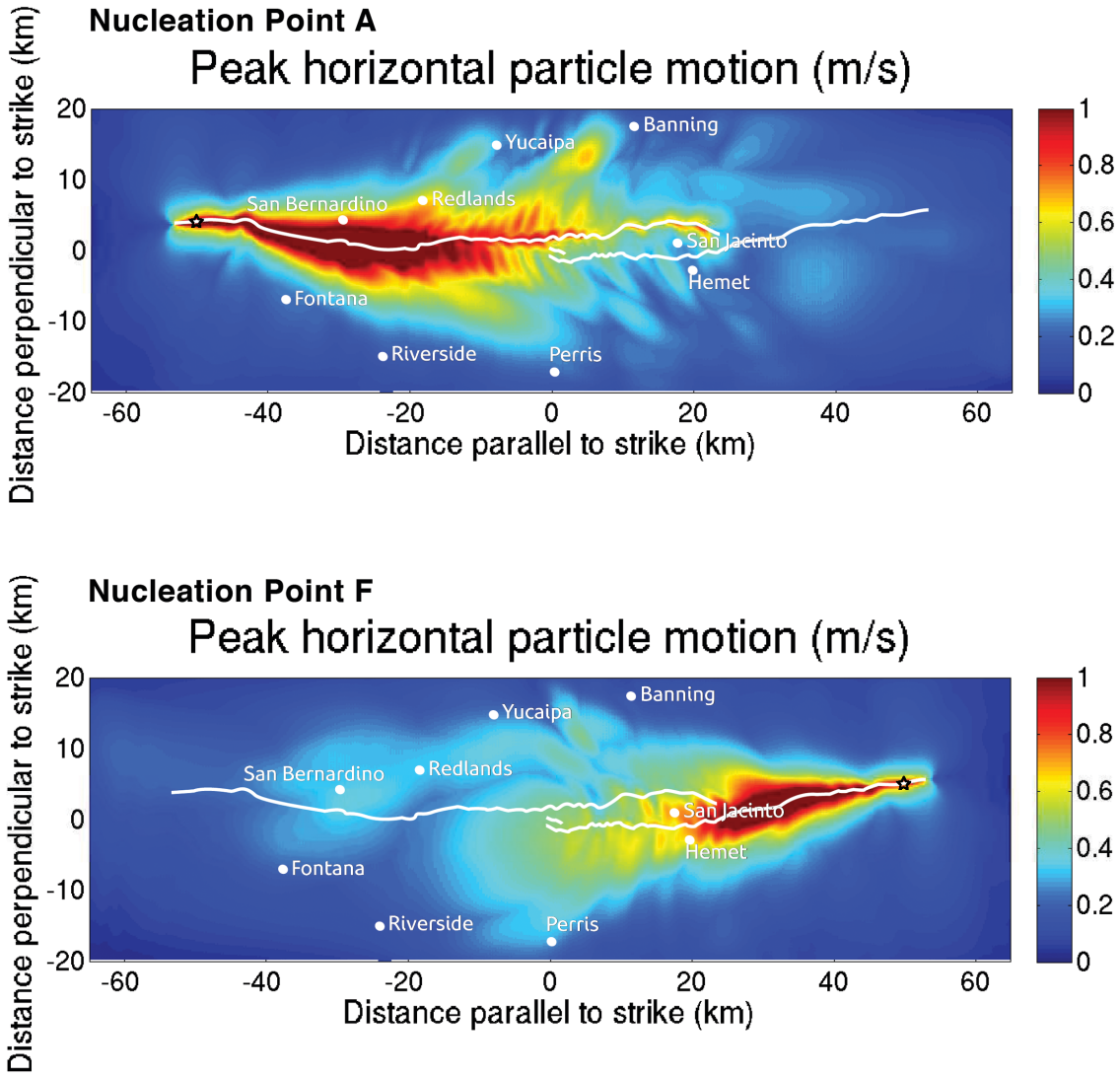

Figure 3.8. Ground motion plots for ruptures on the complex San Jacinto Fault model geometry (white lines), with constant traction, embedded in a heterogeneous material setting taken from the SCEC Community Velocity Model. The initial nucleation points are marked with stars. Note that rupture is no longer able to jump from the Claremont strand onto the Casa Loma strand. Also note that ground motions in San Jacinto, Hemet, Redlands, Banning, and Yucaipa are stronger in these models than models in which the faults are surrounded by homogeneous materials (Figure 3.7).

Regional Stress Field Models

Placing the fault system within a regional stress field immediately imposes limits on the extent of rupture, as well as setting some bounds on the strength of the fault. Figure 3.9 shows a set of models with an input dynamic stress drop of 5.5 MPa and different choices of input S, with forced nucleation at points A and F from Figure 3.4. Regardless of the forced nucleation location, a spontaneous nucleation occurs at a high stress area on the northern Claremont strand. That this occurs suggests both that this might be a likely nucleation point for a future event, and that the strength of the fault must be higher than in this model or else this event might have already occurred. Regardless of the spontaneous nucleation, rupture does not even reach the end of either the Claremont or the Casa Loma strand in these models, let alone jump the stepover. A model we conducted in which there was no forced nucleation and only the spontaneous one had the same result. In order to prevent the spontaneous nucleation, we had to raise the input S to 0.6. These models are shown in the bottom row of Figure 3.9. In this case, rupture nucleating at point A is able to propagate through most, but not all, of the Claremont strand, while rupture nucleating at point F barely propagates beyond the forced nucleation radius on the Casa Loma strand. The smaller scale geometrical complexities halt the rupture before it even reaches the stepover.

The regional stress field models with a dynamic stress drop of 9.5 MPa, shown in Figure 3.10, include many of the same effects. Spontaneous nucleation occurs on the northern Claremont strand unless the input S value is 0.7 or greater. In all cases, regardless of spontaneous nucleation, rupture with forced nucleation at point A is not able

Figure 3.9.

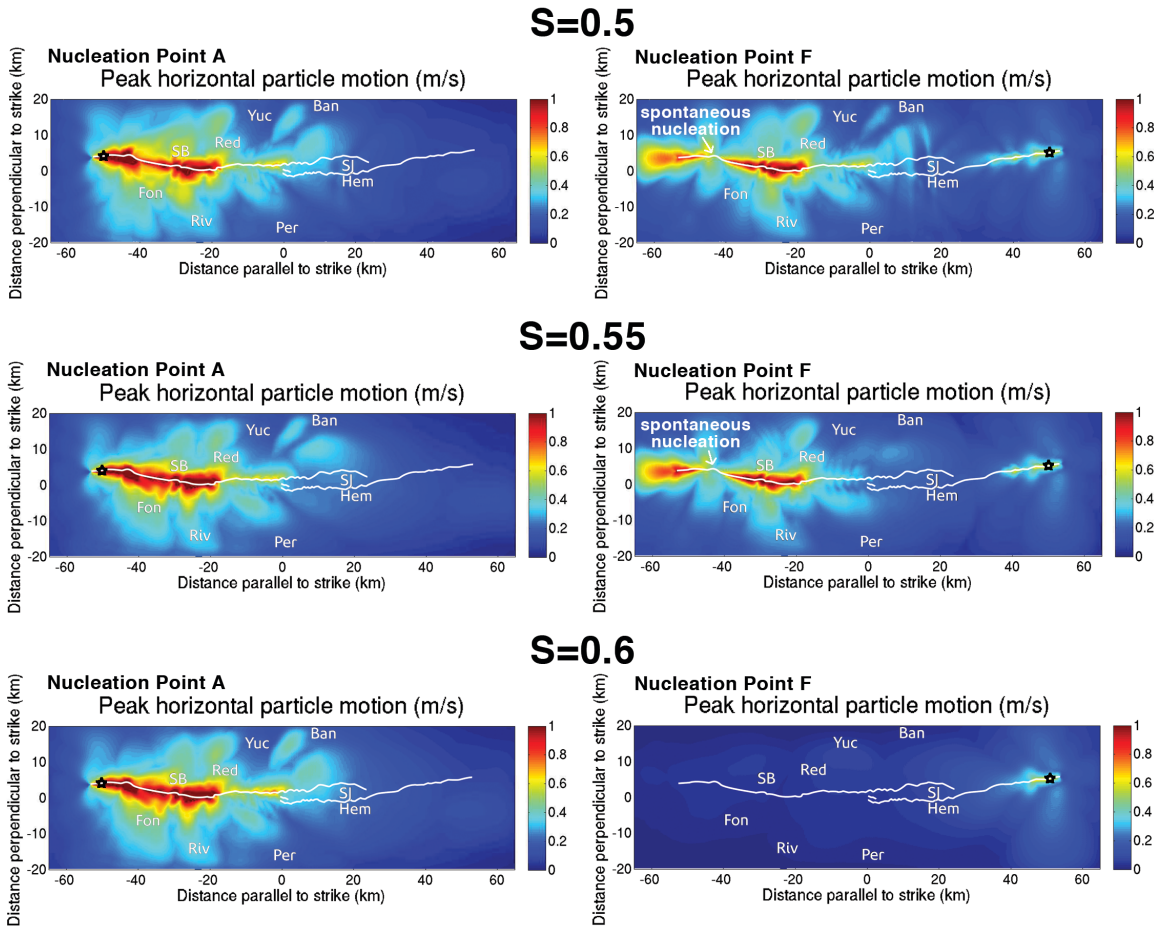

Figure 3.9. Ground motion plots for ruptures on the northern San Jacinto Fault, incorporating a regional stress orientation of N7E, an input stress drop of 5.5 MPa, variable input S, and a complex material setting taken from the SCEC Community Velocity Model. The fault is shown in white, the nucleation point is marked with a star, and the letters mark nearby cities (SB = San Bernardino; Fon = Fontana; Red = Redlands; Riv = Riverside; Yuc = Yucaipa; Per = Perris; Ban = Banning; SJ = San Jacinto; Hem = Hemet). Note that rupture does not jump the stepover in any of these models, and that the input S must be greater than 5.5 in order to prevent a spontaneous nucleation on the northern Claremont strand.

Figure 3.10.

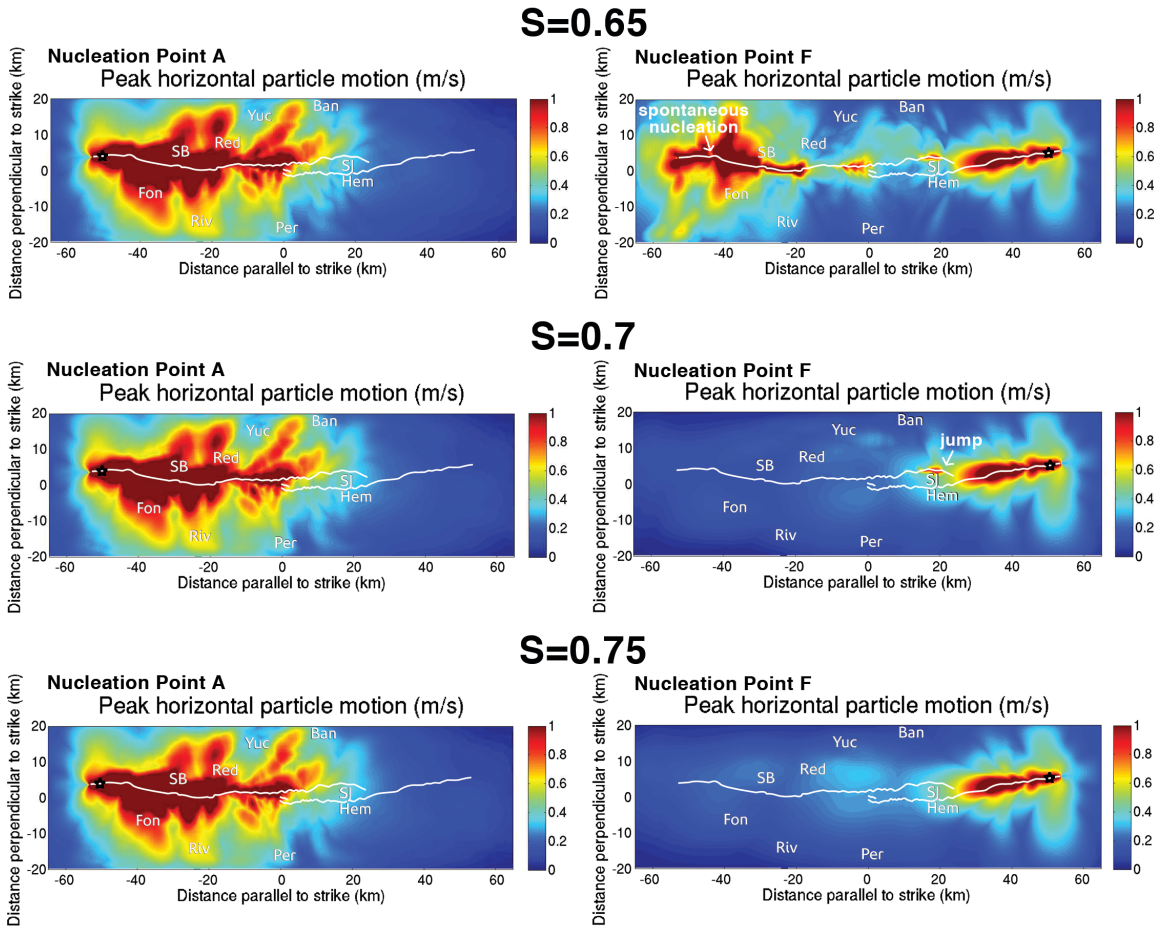

Figure 3.10. Ground motion plots for ruptures on the northern San Jacinto Fault, incorporating a regional stress orientation of N7E, an input stress drop of 9.5 MPa, variable input S, and a complex material setting taken from the SCEC Community Velocity Model. The fault is shown in white, the initial nucleation point is marked with a star, and the letters mark nearby cities (SB = San Bernardino; Fon = Fontana; Red = Redlands; Riv = Riverside; Yuc = Yucaipa; Per = Perris; Ban = Banning; SJ = San Jacinto; Hem = Hemet). The primary difference between these models and the ones with a 5.5 MPa stress drop (Figure 3.9) is in the intensity and distribution of the strongest ground motion. Rupture extent on the Claremont strand is no longer than in the lower stress drop cases, and rupture extent on the Casa Loma strand is only slightly longer. Note that the Casa Loma nucleation model with an S of 0.7 does result in rupture jumping onto the Claremont strand, but the resulting rupture does not propagate very far along strike.

to propagate through the entire Claremont strand. Ruptures with forced nucleation at point F do not propagate very far along the Casa Loma strand, though for input values of S that are less than 0.7, rupture on the Casa Loma still produces enough of a stress change to initiate rupture on the southern end of the Claremont strand. This northward-propagating rupture does not progress very far along strike, however. When we raise the input S to 0.75, this jump no longer occurs. Aside from this jump, however, the overall rupture extent is not very different between the 5.5 MPa and 9.5 MPa stress drop cases. The difference in these cases manifests more strongly in the intensity of the resulting ground motion.

Using the lowest input S that did not result in a spontaneous nucleation for each stress drop – 0.6 for the 5.5 MPa stress drop and 0.7 for the 9.5 MPa stress drop – we conducted models with forced nucleations at points B, C, D, and F from Figure 3.4, to determine whether the nucleation location affected the ability of rupture to jump the stepover. Figure 3.11 shows several of the results from these tests. As with nucleation on either end of the entire fault system, none of these nucleation points produced a jump from segment to segment. A geometrical barrier toward the southern end of the Claremont strand controls the extent of all ruptures nucleating on that strand. Ruptures starting at point B, at the center of the Claremont, propagate bilaterally to Cajon Pass to the north and the persistent barrier to the south, while ruptures nucleating at point C, the far southern end of the Claremont, do not propagate beyond the barrier. Nucleation anywhere on the Casa Loma strand tends to produce shorter ruptures than on the Claremont; none of the nucleaction points on this strand result in rupture propagation

Figure 3.11.

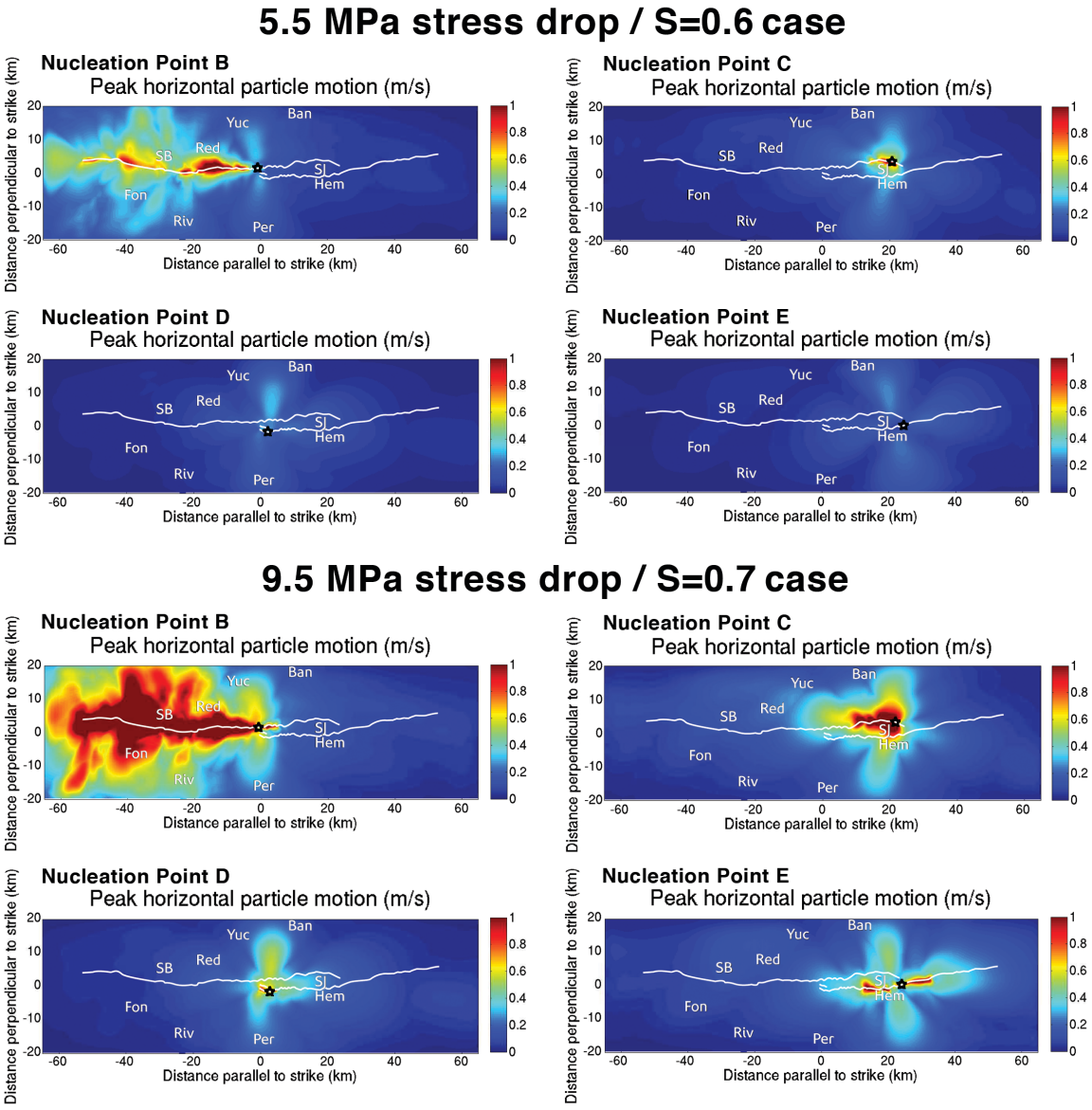

Figure 3.11. Ground motion plots for ruptures on the northern San Jacinto Fault, with nucleation at points B, C, D, and E (Figure 3.4), indicated by black stars. The fault is shown in white, and the letters mark nearby cities (SB = San Bernardino; Fon = Fontana; Red = Redlands; Riv = Riverside; Yuc = Yucaipa; Per = Perris; Ban = Banning; SJ = San Jacinto; Hem = Hemet). With the exception of nucleation point B, at the center of the Claremont strand, these models result in shorter ruptures than nucleation at points A or F do. The primary difference between the 5.5 MPa and 9.5 MPa stress drop cases is in the intensity and distribution of strong motion, not in the along-strike extent of rupture.

through more than 20 km of the fault. For all but one of the nucleation points on either strand, the stress drop had no effect on the extent of the rupture, the exception being point E, which produced no propagation beyond the forced nucleation in the 5.5 MPa stress drop case, and resulted in a 20 km bilateral rupture in the 9.5 MPa stress drop case. In the other models, the primary difference between the 5.5 MPa and 9.5 MPa stress drop cases is that the latter produce a wider distribution of stronger ground motion over the length of the rupture.

We also conducted a series of models in which we rotated the orientation maximum horizontal compressive stress 10 degrees in either direction from N7E, corresponding with one standard deviation away from that mean value (Hardebeck and Hauksson, 2001), while keeping the magnitudes of the principal stresses the same as in the N7E case. In these cases, we focused on nucleation points A and E. We used the principal stress magnitudes that would correspond to the 5.5 MPa stress drop 0.6 S case and the 9.5 MPa stress drop 0.7 S case, as resolved on a 45-degree NW-striking planar fault. However, changing the angle of the regional stress field changes how the stresses resolve on the fault, regardless of complexity. This results in a different effective input S and dynamic stress drop, as taken from the planar fault, and a different complex pattern of S and stress drop once the planar fault values are resolved onto the complex fault geometry. These models are shown in Figure 3.12.

Rotating the orientation of the maximum horizontal stress to N17E resulted in shorter rupture lengths with less intense ground motions than in the N7E case, for both nucleation locations and both stress cases. However, a maximum horizontal stress of

Figure 3.12.

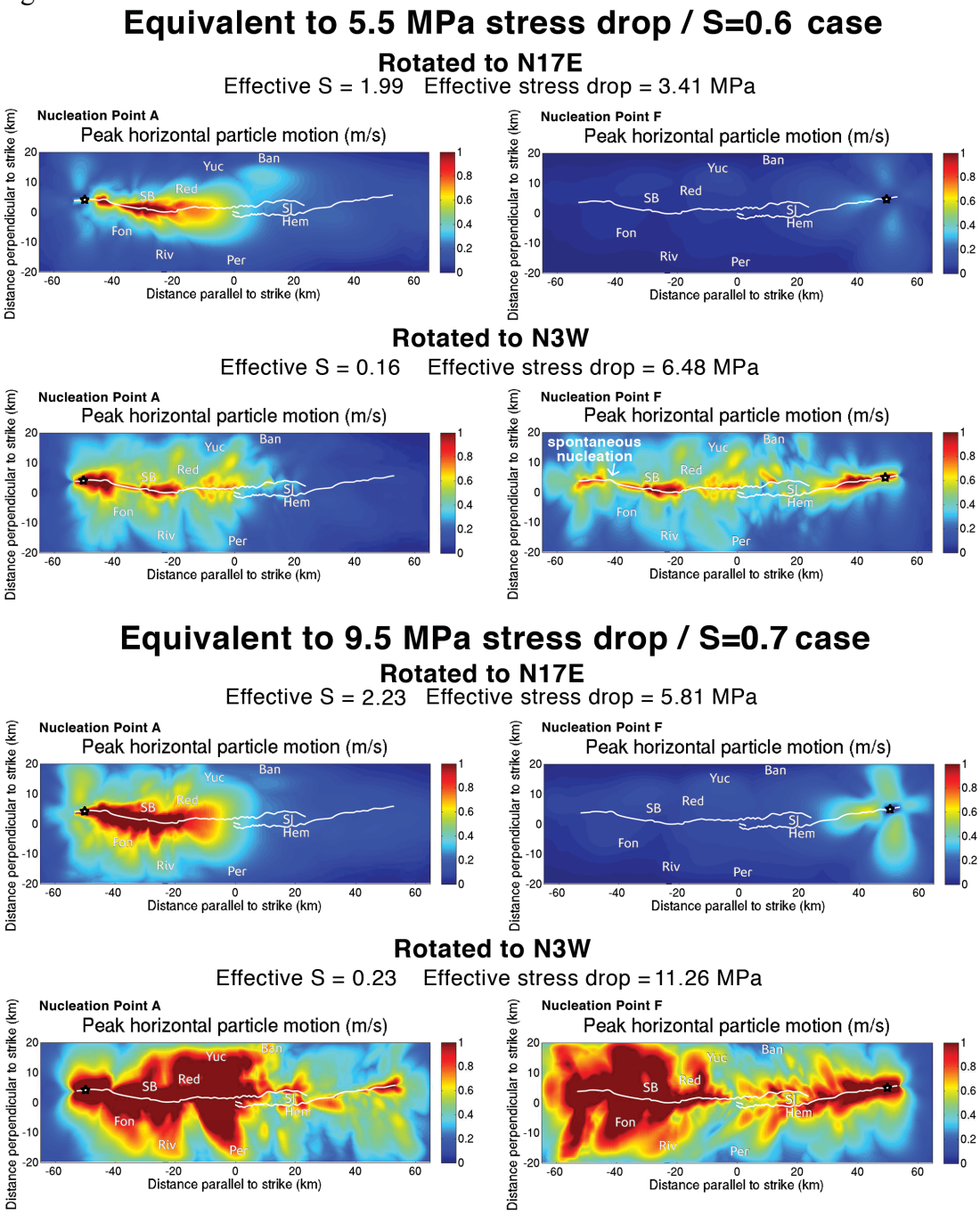

Figure 3.12. Ground motion plots for ruptures on the northern San Jacinto Fault, with the regional stress field rotated to N17E and N3W. The fault is shown in white, the nucleation point is marked by a star, and the letters mark nearby cities (SB = San Bernardino; Fon = Fontana; Red = Redlands; Riv = Riverside; Yuc = Yucaipa; Per = Perris; Ban = Banning; SJ = San Jacinto; Hem = Hemet). A N17E orientation produces shorter ruptures with weaker ground motion compared to the inferred real orientation N7E. An orientation of N3W produces stronger ground motion and longer ruptures when compared to N7E, and produces jumping rupture in higher input stress drop models.

N3W results in ruptures that are much more energetic than in the N7E case. For the 5.5 MPa stress drop case, the spontaneous nucleation on the northern Claremont strand returned, and the resulting rupture propagated through the entire Claremont strand, regardless of nucleation point. In the 9.5 MPa stress case, nucleation on the Claremont and the Casa Loma alike produced jumping rupture that propagated through the entire fault system and resulted in very high ground motions.

Stochastic Stresses

We initially approached nucleation in the models with a combined regional and stochastic stress field in the same way as all the previous models: forcing nucleation at the northern end of the Claremont (point A) or the southern end of the Casa Loma (point F) in order to maximize energy building up ahead of the rupture front in the direction of rupture, and therefore maximize the chances of rupture jumping from one fault strand to the other. This quickly proved to not be an effective method: even with an input stress drop of 9.5 MPa and an S value of 0.25 – which would result in extremely energetic supershear rupture propagation on a homogeneous planar fault – rupture did not propagate far beyond the forced nucleation zone. However, the difference between the four stress realizations is still evident in the ground motion signatures for these models. The models in Figure 3.13 have the same regional stress field, material setting, and forced nucleation point, but the differences between the stochastic realizations is enough to produce very different behaviors even in models that failed to develop self-sustaining rupture.

Figure 3.13.

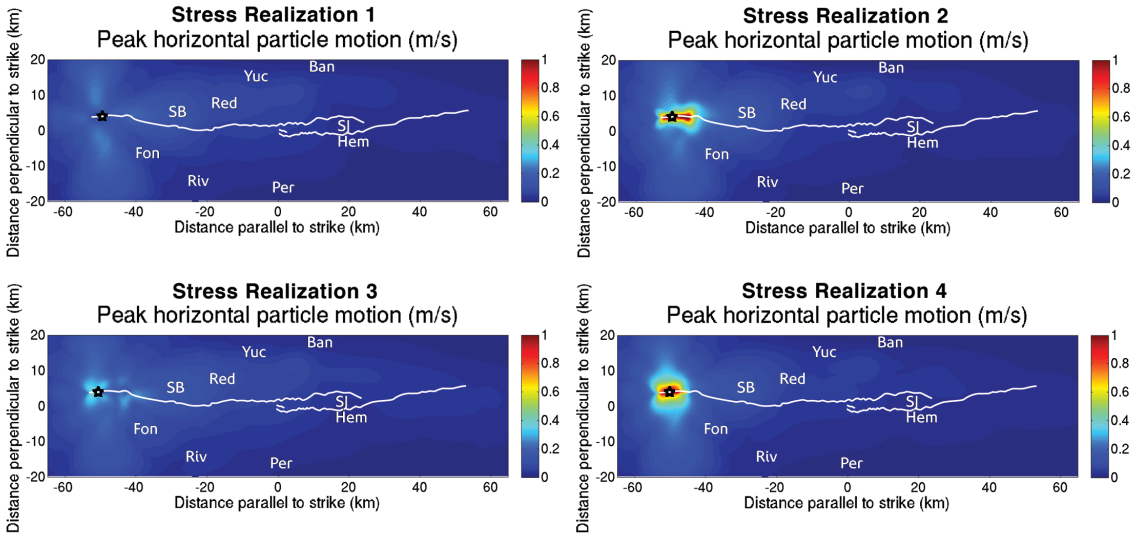

Figure 3.13. Ruptures initiated at nucleation point A, indicated by a black star, in all four stochastic/regional stress realizations (Figure 3.6), with an input stress drop of 9.5 MPa and an input S of 0.25. The fault is shown in white, and the letters mark nearby cities (SB = San Bernardino; Fon = Fontana; Red = Redlands; Riv = Riverside; Yuc = Yucaipa; Per = Perris; Ban = Banning; SJ = San Jacinto; Hem = Hemet). Despite the high stress drop and low S, rupture does not propagate far past the forced nucleation zone in any of these models. However, the resulting ground motion pattern even from these failed nucleations still highlights the differences between the four stress realizations.

Given the complexity of the regional/stochastic stress realizations, we decided to approach these models by choosing points of particularly high shear stress within a large area of elevated shear stress as forced nucleation sites. This is a more realistic approach to nucleation, as the yield stress of a fault is most likely to be exceeded at local high points of shear stress. The resulting suite of models produced longer and more complex ruptures, and allowed us to resume using the same 5.5 MPa stress drop/0.6 S and 9.5 MPa stress drop/0.7 S cases as in the rest of this study. Figure 3.14 shows ground motion distributions for a selection of models with different stress realizations and nucleation points. The different regional/stochastic stress realizations produce a wide range of rupture lengths and ground motion intensities. Whether the Claremont or the Casa Loma sustains longer ruptures varies from realization to realization, and the persistent geometrical barrier on the Claremont from the regional stress field models is capable of being overridden if it falls within a region of high stress from the stochastic field. While most of these models still result in rupture that remains on the fault strand on which it nucleated, one did produce jumping rupture; that model, which used stress realization 4, had a forced nucleation on the Claremont strand. As in the models with a regional stress field only, the input stress drop for these models affected ground motion intensity far more than it affected the extent of rupture.

Discussion

Constant Traction Models

The asymmetrical ground motion distribution in the constant traction models is a result of rupture directivity and dynamic stress changes. As rupture propagates through a

Figure 3.14.

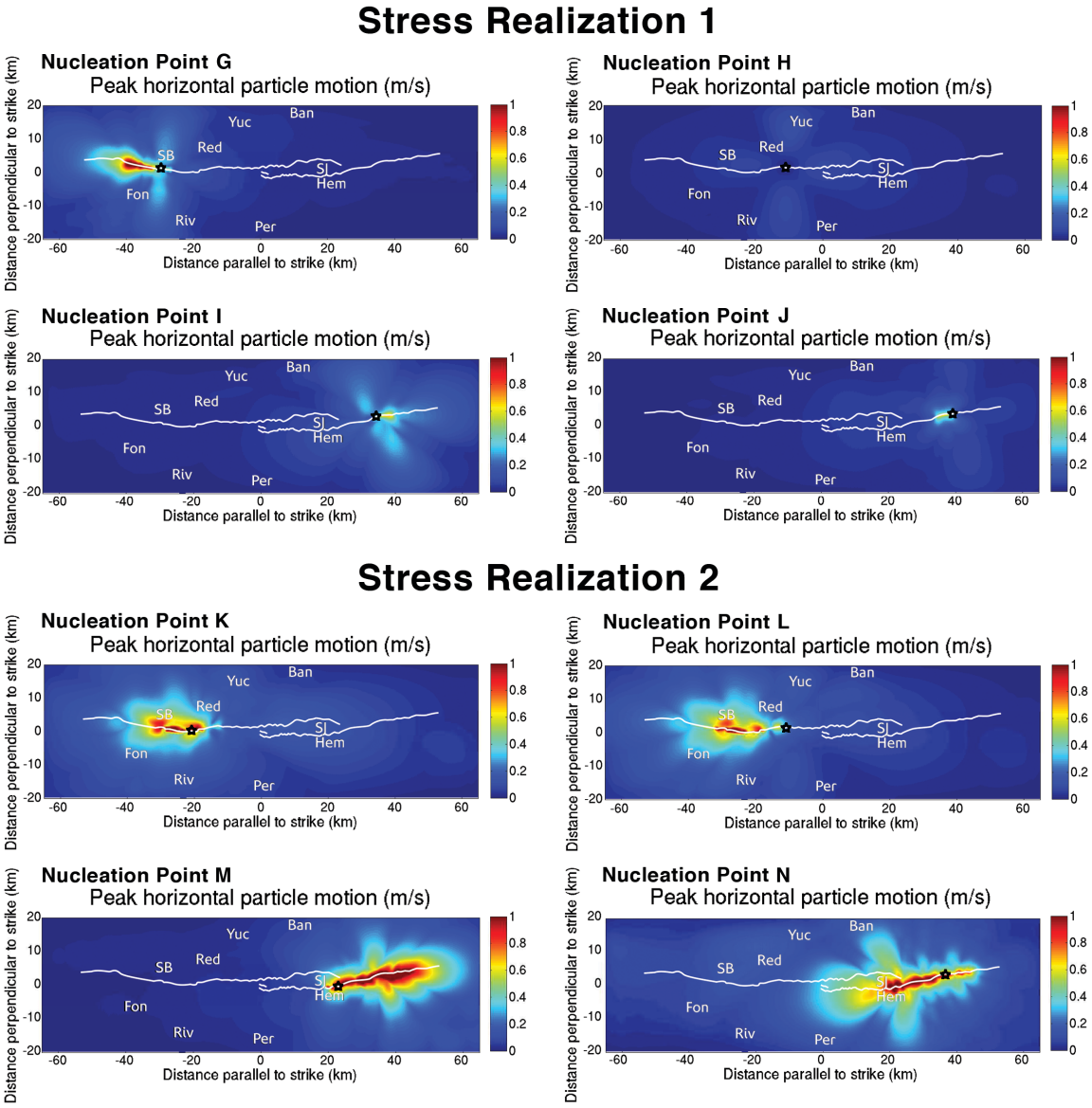

Figure 3.14. Ground motion plots for models incorporating four different combined regional and stochastic stress fields. The location of the initial forced nucleation in each model coincides with a local zone of high shear stress, and is indicated by a black star. Each stress realization, and its associated nucleation points, is shown in Figure 3.6. The fault is shown in white, and the black letters mark nearby cities (SB = San Bernardino; Fon = Fontana; Red = Redlands; Riv = Riverside; Yuc = Yucaipa; Per = Perris; Ban = Banning; SJ = San Jacinto; Hem = Hemet).

Figure 3.14, continued.

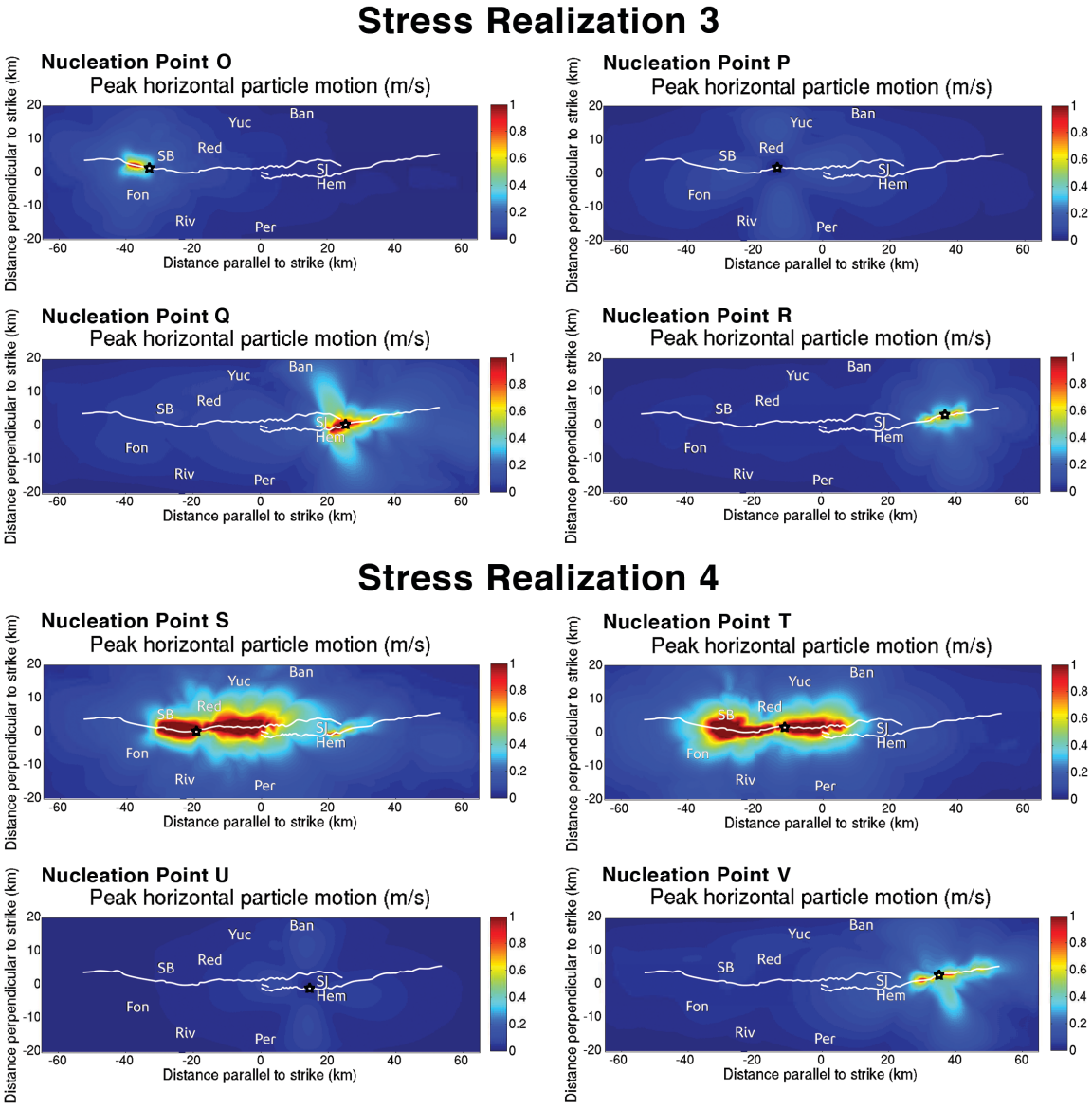

Figure 3.14, continued. More ground motion plots for models incorporating combined regional and stochastic stress fields, and nucleation points optimized to coincide with local highs in shear stress. Note that rupture jumps from the Claremont strand onto the Casa Loma strand when initial forced nucleation occurs at point S.

relatively straight section of a fault, amplified waves ahead of the rupture front result in a buildup of energy that allows the rupture front to become more energetic. This results in increasingly strong ground motion the further rupture propagates through that straight fault section. However, as soon as rupture reaches a bend or break in the fault, directivity is broken, and the effect must build up again as rupture propagates through the next segment. Previous dynamic modeling studies on stepovers with planar segments (e.g. Lozos *et al.*, 2013) have shown this same directivity effect. This effect explains why the weakest ground motions in the constant traction models occur right after rupture has turned a bend in the fault trace, and the strongest motions occur right before the next bend. Previous dynamic models of more simplified non-planar faults (e.g. Oglesby and Mai, 2012) have produced similar ground motion patterns.

The series of breaks in directivity that comes with rupture along a non-planar fault also results in dynamic stress changes that may place the next section of the fault in either a region of stress increase or stress shadow, depending on its orientation, thus imposing heterogeneous stresses further along strike even if the initial stress state was homogeneous. This effect makes certain parts of the fault more or less favorable for rupture than others, which is why ground motion intensity on a given section of the fault in Figures 3.7 and 3.8 does not simply scale with the length of that segment, as it would if directivity were the only effect at work.

The fact that non-planar fault geometry with constant traction can still result in such heterogeneous rupture propagation and ground motion is cautionary against using a variable along strike stress field on a planar fault as a proxy for how a regional stress

field resolves on a non-planar fault. While the energy of the rupture front would still be very heterogeneous in such a model, there would be no break in the direction of the rupture, and therefore nothing to interrupt the buildup of waves ahead of the rupture front. Also, the area ahead of the rupture front on a planar fault is always in a region of increased dynamic stresses; the possibility of the next part of the fault falling within a region of stress shadow is lost when there is no geometrical complexity.

The fact that the incorporation of the complex velocity structure into the constant traction models results in rupture no longer being able to jump from the Claremont strand onto the Casa Loma strand, as it is able to do in a homogeneous material setting, emphasizes the importance of including a realistic velocity structures in models of real faults. The inability of rupture to jump in the model with the velocity structure is a result of the rupture front losing energy as it negotiates sharp contrasts in material properties.

Regional Stress Field Models

While we have used the input stress drop and fault strength S to describe the stress cases we use in our models, the actual shear and normal stresses on the fault are modulated by the geometry, and are therefore at least as heterogeneous as the geometry itself. Figure 3.15 shows the actual local fault strength S over the entire fault system; though the input S is 0.6 in this case, the actual distribution of S is quite heterogeneous. As on a planar fault, the parts of the fault system with lower values of S sustain more energetic rupture, while higher values of S are more likely to slow or stop rupture propagation. The part of the northern Claremont strand that nucleated spontaneously at

Figure 3.15.

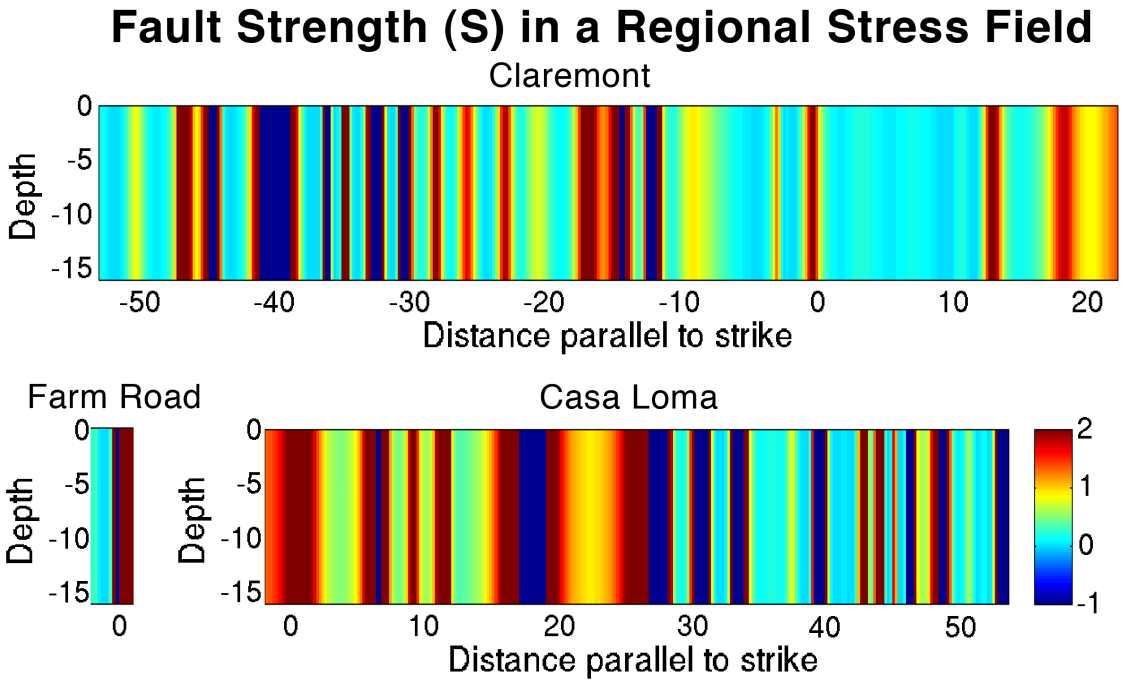

Figure 3.15. Fault strength parameter S for a N7E-oriented regional stress field with an input stress drop of 5.5 MPa and an input S of 0.6. Different input values of S and stress drop would produce different effective S values, but not a different pattern of relative high S to relative low S. Note that the actual S value on most parts of the fault is not equal to the input S value. The Claremont strand has less variation in S overall than the Casa Loma strand does, and that the bands of particularly high or particularly low S are wider on the Casa Loma than on the Claremont.

low input S corresponds with a wide zone of very low S. Similarly, the persistent geometrical barrier toward the southern end of the Claremont strand is a result of rupture losing energy in the high S region at -18 km along strike, and being unable, in this depleted energy state, to propagate past a second high S region at 0 km along strike.

Areas of high fault strength pose barriers to rupture, but the size of the high S region can have more of an effect on its ability to stop rupture than the actual value of S. For a narrow high strength patch, a rupture front may be energetic enough to simply fracture through the unfavorable area, or dynamic stress changes from rupture leading up to that point may be strong enough to re-nucleate on the other side of the barrier, jumping over it as if it were effectively a break in the fault trace. Directivity also affects rupture's ability to negotiate a barrier: the more energy that has built up ahead of the rupture front, the more energy can go into fracturing through an unfavorable barrier, or, failing that, the stronger the stress change that results from rupture hitting the barrier, which increases the likelihood of rupture jumping over the barrier altogether. The forced nucleation points which are closer to high S regions (for example, the southern end of the Claremont, or any of our Casa Loma nucleation points) result in shorter ruptures because the rupture front cannot build up enough directivity to negotiate the barriers.

In our models, the Claremont strand is more favorable for longer rupture than the Casa Loma strand is. This is partly because the Claremont has larger areas of lower local S than the Casa Loma strand does. The Claremont has fewer geometrical complexities along its length than the Casa Loma does, which means there are fewer places in which a bend in the trace can result in a local high-S zone. The Casa Loma has more barriers, and

therefore more potential rupture endpoints, as well as more limits on how much of a directivity effect any rupture on the Casa Loma can build up.

A rupture with a higher stress drop is a more energetic rupture. However, choosing a higher input stress drop versus a lower one, or a higher or lower input S, does not change the relative strength along the fault. Regardless of the actual value of S, or of shear or normal stress, barriers are still relatively high strength compared to the rest of the fault, and particularly favorable areas are still relatively low strength. This is why the higher stress drop cases did not, for the most part, produce longer ruptures than the lower stress drop cases. The few cases in which it did, such as in the nucleation point at the center of the Casa Loma strand, were a result of there being enough fracture energy for the rupture to propagate through narrower barriers; these ruptures still terminated at larger areas of higher S. In all of the high stress drop models, the stronger ground motion compared to the lower stress drop models at the same nucleation points is a result of there being more available energy budget for seismic radiation.

The results for the rotated stress field models are directly related to the issue of relative strength and energy budget as well. Rotating the maximum horizontal compressive stress a small amount in either direction does not significantly change the relative strength distribution across the fault; barriers and particularly favorable zones remain in the same places as in the N7E case. However, this rotation, with the same magnitude of stresses, does change the effective input S and stress drop. The N17E models produce shorter ruptures with weaker ground motions because the 5.5 MPa stress drop/S=0.6 case becomes a 3.47 MPa stress drop/S=1.88 case, and the 9.5 MPa stress

drop/S=0.7 case becomes 5.8 MPa stress drop/S=2.23. The overall fault strength is higher, and there is less energy budget overall. Conversely, the N3W models produce jumping rupture with extreme ground motions because 5.5 MPa stress drop/S=0.6 case becomes a 6.5 MPa stress drop/S=0.11 case, and the 9.5 MPa stress drop/S=0.7 case becomes 11.26 MPa stress drop/S=0.23. The entire fault system is more favorable for rupture under these conditions, and the rupture fronts are energetic enough to fracture through or jump over most of the higher strength barriers.

This interpretation initially may appear to contradict our result that the choice of input S and stress drop does not have a large effect on rupture extent. However, past work on the correlation between dynamic weakening and initial stresses suggests that doubling the initial stresses and halving the critical weakening distance are equivalent, and vice versa (see Chapter 1). Thus, a high input stress drop effectively reduces the critical weakening distance of the fault, regardless of the model input critical weakening distance. This coupled with a very low fault strength results in an energetic rupture front that does not need to re-budget much energy into fracture when it encounters a high-strength barrier. Similarly, a low input stress drop and a high input S leads to an effectively larger critical weakening distance, a less energetic rupture front, and more energy expended on fracture than on seismic radiation. These effects are not readily apparent in the N7E models because our input S values for both input stress drop cases are close to one another. The extremely high and extremely low input S values that occur as a result of rotating the stress field allow this effect to have more of a controlling role in the extent of the rupture.

Stochastic Stress Models

The models in which we combine stochastic stress field with the regional stress field result in more complex rupture behaviors and ground motion distributions, because the down-dip homogeneity of stresses in the models with only a regional stress field is broken, in addition to the along-strike heterogeneity being made more complicated. Rupture behavior in these models is still controlled by the distribution of low strength/high favorability areas and the ability of a rupture to build up enough energy to fracture through or jump over a high-strength barrier. However, the irregular shape and distribution of these barriers and asperities, coupled with the geometrical complexity of the fault trace, makes it considerably more difficult for a consistent directivity effect to develop, and also greatly complicates the pattern of dynamic stress transfer that occurs when rupture reaches a bend or barrier.

In general the relatively high strength areas of the fault are larger in the combined regional/stochastic stress field models, and they tend to surround the high shear stress/low strength asperities. This is a sharp contrast to the regional stress field models, in which the high strength barriers are narrow features that are surrounded by lower stress regions. This results in the extents of ruptures being confined by the extent of the high shear stress/low strength stress patches in which they nucleate. The reason our arbitrary forced nucleation points at the end of either fault segment did not produce extensive rupture (Figure 3.13) is that in all four stress realizations, that point did not lie in or near a large region of high stress. Forced nucleation in a low shear stress/high strength area did not result in a self-sustaining rupture at all, while forced nucleation in a smaller area of

high shear stress/low strength resulted in rupture that died upon reaching the ends of the patch. These results are corroborated by inversions of real earthquakes conducted by Mai et al. (2005), which suggest that nucleation tends to occur within or near a zone of high slip, and therefore also high stress or low strength.

As in the regional stress field models, rupture is able to propagate through or around a localized high strength area if the rupture front is energetic enough or the high strength patch is small enough. The stochastic distributions also bring up the question of rupture's ability to propagate through a narrow zone of low fault strength surrounded by larger areas that are not favorable for rupture. We find that, the narrower the low strength area, or the longer the distance it spans between larger asperities, the more likely it is to arrest rupture before it can reach the next large asperity. Thus, stress distributions with more large asperities that are more closely connected (realizations 2 and 4) are able to sustain longer ruptures than realizations where the asperities are smaller and more widely distributed (realizations 1 and 3). Furthermore, in order for rupture to jump the stepover, both the end of the first fault segment and the area aligned with that endpoint on the next segment must be high shear stress/low strength areas.

Ground motion distributions in the stochastic/regional stress realization models are also more variable and irregular than in the models incorporating only a regional stress field. This is explainable by the interaction between directivity and geometrical spreading. Ground motion is strongest in the direction of rupture propagation, both along strike and up dip. The strongest shaking would result from nucleation in at the lower edge of an asperity, since that allows for the most directivity to develop in both spatial

dimensions. If that asperity were to be located near the base of the fault, however, much of the energy would attenuate and spread before reaching the surface, resulting in weaker intensities at the surface than if the asperity were closer to the top of the fault.

Conclusions

There are many types of complexity in real fault zones, and all of these factors contribute to rupture behavior and ground motion intensity and distribution. Complicated fault geometry alone leads to a complex interaction of directivity and dynamic stress transfer effects. A regional stress field resolved onto that geometry produces a static pre-rupture stress distribution that is highly heterogeneous along strike. Incorporating random distributions of high shear stress asperities, as are inferred to exist on real faults by way of inversions of real earthquakes, makes the distribution of high and low strength areas on the fault even more heterogeneous. When all of these effects are combined into a single model, the effect of any one factor is less evident in the results when compared to a model that isolates that factor, but leaving out any of these details produces very different results from models that include it. We therefore suggest that it is crucial to include as many levels of realistic complexity as is computationally feasible when one is constructing models to investigate the behavior of a specific real-world fault.

The distribution of stresses on the fault, and how strong or weak different parts of the fault are relative to each other, are the controlling factor in rupture behavior, regardless of which levels of model complexity are used in producing that stress state. Sustained rupture propagation is promoted within large areas of high shear stress or low

fault strength, and in areas with fewer breaks in directivity. Rupture is able to propagate through a higher strength area if it is energetic enough to fracture through that area while still retaining enough energy for propagation and radiation of seismic energy, or if the stress changes induced by rupture stopping at the high strength area are strong enough to cause rupture to re-nucleate on the other side of the barrier, much like what determines whether or not rupture can jump across a stepover in the fault trace. For a given input fault strength, a higher stress drop results primarily in stronger ground motion, since there is more energy budget for seismic radiation, though it may result in rupture propagation through some smaller barriers. For a given input stress drop, lower values of input fault strength produce longer ruptures.

Pertaining to the northern San Jacinto Fault specifically, we find that the Claremont strand is more favorable for longer ruptures than the Casa Loma strand. This is due in part to the fact that a maximum horizontal compressive stress orientation of N7E produces lower S values on the Claremont than on the Casa Loma, and also because the Claremont has less geometrical complexity, and therefore fewer potential barriers, along its trace than the Casa Loma does. With or without a stochastic stress distribution combined with the regional stress field, very few of our models produce jumping rupture from the Claremont onto the Casa Loma or vice versa, and even fewer produce an end-to-end rupture on either strand of the fault. The tendency of our models to produce shorter ruptures, even when nucleation is forced at the most favorable points within the largest asperities, is consistent with the SJF's historical behavior. We cannot say whether the barriers that stopped rupture in historic northern SJF events are purely geometrical or are

a result of other features of the stress distribution on the fault, because we do not know the real world distribution and shape of its non-geometrical asperities. More detailed analysis of seismicity would be useful both for determining the geometry of asperities, and of the fault itself at depth, and could lead to production of even more realistic models of the SJF.

The historical and model tendency for the San Jacinto Fault to produce shorter ruptures is a good thing from a hazard standpoint, as fewer communities would be severely affected by such a rupture than one that propagated through an entire segment or across the stepover. However, neither our models nor paleoseismology can rule out the possibility of jumping rupture altogether. Furthermore, all of the longest ruptures our models produce involve the northern part of the Claremont strand, which runs through the most densely populated parts of the Inland Empire, and which is surrounded by the soft sediments of the San Bernardino Basin. Thus, even with its tendency to produce short ruptures, the northern San Jacinto Fault still poses a significant hazard to its surrounding region. Our continued work on the northern SJF involves conducting higher resolution models that are able to encompass the full frequency range of ground motions that would result from a number of scenario ruptures. These models will serve the dual purpose of describing shaking hazard from possible future events, and of comparison with the locations of precariously balanced rocks near the fault trace to help constrain possible extents of historic events.

References

Andrews, D. J. (1976). Rupture propagation with finite stress in antiplane strain, *Journal of Geophysical Research* **81,** 3575-3582.

Andrews, D. J., and M. Barall (2011). Specifying initial stress for dynamic heterogeneous earthquake source models, *Bulletin of the Seismological Society of America* **101**, 2408-2417.

Barall, M. (2009). A grid-doubling technique for calculating dynamic three-dimensional spontaneous rupture on an earthquake fault, *Geophysical Journal International* **178**, 845–859.

Burdick, L. J., and G. R. Mellman (1976). Inversion of the body waves from the Borrego Mountain earthquake to the source mechanism, *Bulletin of the Seismological Society of America* **66**, 1485-1499.

Aochi, H., and E. Fukuyama (2002). Three-dimensional nonplanar simulation of the 1992 Landers earthquake, *Journal of Geophysical Research* **107,** doi:10.1029/2001JB001456.

Das, S., and K. Aki (1977). A numerical study of two-dimensional spontaneous rupture propagation, *Geophysical Journal of the Royal Astronomical Society* **50,** 643-668.

Duan, B., and D. D. Oglesby (2007). Nonuniform prestress from prior earthquakes and the effect on dynamics on branched fault systems, *Journal of Geophysical Research* **112**, B05308, doi:10.1029/2006JB004443.

Hardebeck, J.L., and E. Hauksson (2001). Crustal stress field in southern California and its implications for fault mechanics, *Journal of Geophysical Research* **106**, 21859-21882.

Harris, R. A., R. J. Archuleta, and S. M. Day (1991). Fault steps and the dynamic rupture process - 2-D numerical simulations of a spontaneously propagating shear fracture, *Geophysical Research Letters* **18,** 893-896.

Harris, R. A., and S. M. Day (1993). Dynamics of fault interaction: parallel strike-slip faults, *Journal of Geophysical Research* **98,** 4461-4472.

Ida, Y. (1972). Cohesive force across the tip of a longitudinal shear crack and Griffith's specific surface energy, *Journal of Geophysical Research* **77,** 3796-3805.

Kame, N., J. R. Rice, and R. Dmowska (2003). Effects of pre-stress state and rupture velocity on dynamic fault branching, *Journal of Geophysical Research* **108,** 2265, doi: 10.1029/2002JB002189.

Kanamori, H., and D. L. Anderson (1975). Theoretical basis of some empirical relations in seismology, *Bulletin of the Seismological Society of America* **65**, 1073-1095.

Kanamori, H., and E. E. Brodsky (2004). The physics of earthquakes, *Reports on Progress in Physics* **67**, doi:10.1088/0034-4885/67/8/R03.

Kendrick, K. J., and D. M. Morton (2012). "Geomorphic evidence for structural evolution of the northern San Jacinto fault zone in the San Timoteo badlands." Seismological Society of America Annual Meeting, Town and Country Resort and Convention Center, San Diego, California. Conference presentation.

Lin, G., P. M. Shearer, and E. Hauksson (2007). Applying a three-dimensional velocity model, waveform cross correlation, and cluster analysis to locate southern California seismicity from 1981 to 2005, *Journal of Geophysical Research* **112**, doi: 10.1029/2007JB004986.

Lozos, J. C., D. D. Oglesby, B. Duan, and S. G. Wesnousky (2011). The effects of fault bends on rupture propagation: a geometrical parameter study, *Bulletin of the Seismological Society of America* **101***,* 385-398.

Lozos, J. C., D. D. Oglesby, J. N. Brune, and K. B. Olsen (2012). Small intermediate fault segments can either aid or hinder rupture propagation at stepovers, *Geophysical Research Letters* **39**, doi: 10.1029/2012GL053005.

Lozos, J. C., D. D. Oglesby, and J. N. Brune (2013). The effects of fault stepovers on ground motion, *Bulletin of the Seismological Society of America* **103,** 1922-1934.

Mai, P. M., P. Spudich, and J. Boatwright (2005). Hypocenter locations in finite-source rupture models, *Bulletin of the Seismological Society of America* **95**, 965-980.

Magistrale, H., and S. M. Day (1999). 3D simulations of multi-segment thrust fault rupture, *Geophysical Research Letters* **26,** 2093-2096.

Magistrale, H., S. Day, R. Clayton, and R. Graves (2000). The SCEC southern California reference three-dimensional seismic velocity model version 2, *Bulletin Seismological Society of America* **90 (6B),** S65-S76.

Marliyani, G. I., T. K. Rockwell, N. W. Onderodonk, and S. F. McGill (2013). Straightening of the northern San Jacinto Fault, California, as seet in the fault-

structure evolution of the San Jacinto Valley stepover, *Bulletin of the Seismological Society of America* **103**, doi: 10.1785/0120120232.

Oglesby, D. D. (2005). The dynamics of strike-slip step-overs with linking dip-slip faults, *Bulletin of the Seismological Society of America* **95,** 1604-1622.

Oglesby, D. D. (2008). Rupture termination and jump on parallel offset faults, *Bulletin of the Seismological Society of America* **98**, 440-447.

Oglesby, D. D., and P. M. Mai (2012). Fault geometry, rupture dynamics and ground motion from potential earthquakes on the North Anatolian Fault under the Sea of Marmara, *Geophysical Journal International* **188**, 1071-1087.

Palmer, A. C., and J. R. Rice (1973). The growth of slip surfaces in the progressive failure of overconsolidated clay, *Proceedings of the Royal Society of London Series A* **332,** 527-548.

Park, S.K., D. Pendergraft, W.J. Stephenson, K.M. Shedlock, T.C. Lee (1995). Delineation of intrabasin structure in a dilational jog of the San Jacinto fault zone, southern California, *Journal of Geophysical Research* **100***,* 691-702.

Plesch, A., J.H. Shaw, C. Benson, W.A. Bryant, S. Carena, M. Cooke, J. Dolan, G. Fuis, E. Gath, L. Grant, E. Hauksson, T. Jordan, M. Kamerling, M. Legg, S. Lindvall, H. Magistrale, C. Nicholson, N. Niemi, M. Oskin, S. Perry, G. Planansky, T. Rockwell, P. Shearer, C. Sorlien, M. P. Süss, J. Suppe, J. Treiman, and R. Yeats (2007). Community fault model (CFM) for Southern California, *Bulletin of the Seismological Society of America* **97***,* 1793-1802.

Rockwell, T. (2012). "Summary of paleoseismic observations along the San Jacinto fault." Seismological Society of America Annual Meeting, Town and Country Hotel, San Diego, CA. Conference presentation.

Sanders, C.O., and H. Kanamori (1994). A seismotectonic analysis of the Anza seismic gap, San Jacinto fault zone, southern California, *Journal of Geophysical Research* **89**, 5873-5890.

Sanders, C., and H. Magistrale (1997). Segmentation of the northern San Jacinto fault zone, southern California, *Journal of Geophysical Research* **102**, 27453-27467.

U.S. Geological Survey and California Geological Survey (2010). *Quaternary fault and fold database for the United States*.

Wesnousky, S.G. (1986). Earthquakes, quaternary faults, and seismic hazard in California, *Journal of Geophysical Research* **91**, 12587-12632.

Working Group on California Earthquake Probabilities (1995). Seismic hazard in southern California: probable earthquakes, 1994 to 2024, *Bulletin of the Seismological Society of America* **85**, 379-439, 1995.

Appendix 3.1: Latitude-longitude waypoints used to construct the FaultMod mesh.

Claremont strand

-116.529143 33.556412
-116.612420 33.604587
-116.670275 33.645500
-116.731177 33.673697
-116.785222 33.699087
-116.830620 33.719681
-116.876391 33.740978
-116.904567 33.753991
-116.912993 33.776661
-116.919902 33.785203
-116.926957 33.790822
-116.944432 33.809905
-116.952590 33.813522
-116.962714 33.820253
-116.975808 33.825508
-116.979175 33.830463
-117.002590 33.846635
-117.010724 33.847300
-117.034231 33.858692
-117.040213 33.867612
-117.047406 33.870852
-117.047797 33.873282
-117.055049 33.878535
-117.060956 33.886348
-117.071070 33.891066
-117.080395 33.895781
-117.081228 33.898131
-117.085621 33.902155
-117.092588 33.903998
-117.103646 33.913886
-117.113527 33.920308
-117.118446 33.926175
-117.133942 33.938049
-117.138321 33.945025
-117.151891 33.954808
-117.156392 33.959751
-117.171747 33.973130
-117.181536 33.984532
-117.197717 33.994401
-117.212511 34.002875
-117.217082 34.004191

-117.224723 34.008939
-117.232797 34.014388
-117.236826 34.014644
-117.251526 34.024697
-117.262396 34.033508
-117.271850 34.041030
-117.280446 34.049215
-117.291263 34.063282
-117.302150 34.076466
-117.305797 34.079158
-117.308040 34.084803
-117.319417 34.096382
-117.321037 34.097247
-117.337406 34.114904
-117.349530 34.128836
-117.360286 34.143162
-117.374751 34.161217
-117.382968 34.175630
-117.389361 34.193964
-117.402840 34.203080
-117.417004 34.217688
-117.431399 34.230675
-117.442329 34.237411
-117.459104 34.249554
-117.551802 34.298086

Farm Road strand
-116.540860 33.531514
-116.628480 33.584975
-116.720971 33.645348
-116.809908 33.691944
-116.872002 33.724043
-116.913077 33.746348
-116.958335 33.782260
-116.986239 33.806526
-117.019290 33.831444
-117.048953 33.855000
-117.069549 33.864359
-117.086183 33.873148
-117.089056 33.877544
-117.090721 33.882638
-117.096317 33.890012
-117.096839 33.892036
-117.102792 33.895681

-117.111308 33.899800
-117.127907 33.911504
-117.156089 33.935816
-117.190452 33.970023
-117.222066 33.988991
-117.287719 34.031640
-117.356236 34.109142
-117.403521 34.169090
-117.475043 34.237469
-117.565533 34.287022

Casa Loma strand
-116.569887 33.521799
-116.653421 33.579923
-116.668666 33.589493
-116.691178 33.602568
-116.722322 33.625275
-116.732249 33.629015
-116.746053 33.639758
-116.749146 33.641325
-116.763556 33.651815
-116.773424 33.656200
-116.776242 33.658754
-116.831105 33.689429
-116.834729 33.690030
-116.844206 33.693907
-116.917615 33.735351
-116.922928 33.736691
-116.937036 33.748500
-116.944967 33.749726
-116.953888 33.753608
-116.959026 33.761708
-116.972690 33.766583
-116.983020 33.776216
-116.989964 33.784254
-116.994558 33.789347
-116.999989 33.793945
-117.003699 33.800529
-117.005174 33.802122
-117.017888 33.805698
-117.020181 33.807588
-117.030704 33.826225
-117.036578 33.828811
-117.040082 33.832081

-117.047818 33.835664
-117.052005 33.840761
-117.053403 33.841225
-117.057481 33.847575
-117.063094 33.847714
-117.066965 33.849257
-117.077529 33.857202
-117.090858 33.862625
-117.097045 33.870110
-117.102691 33.875480
-117.107193 33.887161
-117.114811 33.890504
-117.125373 33.894589
-117.145971 33.906189
-117.175369 33.931773
-117.209545 33.963156
-117.241849 33.979773
-117.306826 34.022436
-117.375185 34.102058
-117.427524 34.164381
-117.492980 34.224314
-117.577747 34.274078

Appendix 3.2: Random number seeds for stochastic stress distributions.

Realization 1

Fault	**Seed 1**	**Seed 2**	**Seed 3**	**Seed 4**
Claremont	5555	6666	7777	8888
Farm Road	5678	6785	7856	8567
Casa Loma	8888	7777	6666	5555

Realization 2

Fault	**Seed 1**	**Seed 2**	**Seed 3**	**Seed 4**
Claremont	1812	1899	1918	1923
Farm Road	1800	1812	1899	1918
Casa Loma	1800	1899	1918	1968

Realization 3

Fault	**Seed 1**	**Seed 2**	**Seed 3**	**Seed 4**
Claremont	4444	3333	2222	1111
Farm Road	4321	3214	2143	1432
Casa Loma	1111	2222	3333	4444

Realization 4

Fault	**Seed 1**	**Seed 2**	**Seed 3**	**Seed 4**
Claremont	1857	1887	1984	1910
Farm Road	1883	1984	1888	1910
Casa Loma	1984	1988	1910	1926

Chapter 4: Three-Dimensional Dynamic Rupture Models on Partially-Creeping Strike-Slip Faults

Introduction

The coseismic rupture behavior of partially-creeping faults – faults that sustain both non-episodic, measurable surface creep, and large-scale dynamic rupture – is not currently well understood. It is, however, an important question of fault dynamics, both from the standpoint of how rupture negotiates fault complexity and what controls the endpoints of those ruptures, and from the standpoint of the seismic hazard associated with such faults. The Hayward Fault, in the San Francisco Bay Area, California, is the archetypal example of a hazardous partially-creeping fault, since it has a surface creep rate of 3 to 8 mm/yr (Lienkaemper *et al*., 2001; McFarland *et al*., 2009), it experiences large surface-displacing earthquakes on average every 160 years (Lienkaemper and Williams, 2008), the most recent of which was in 1868. Furthermore, risk associated with a rupture on the Hayward is great, since it is located under a population center of over 7 million people.

The 1868 Hayward earthquake exemplifies the general questions posed by partially-creeping faults. Up to 1.9 meters of surface displacement were measured in the wake of the earthquake (Yu and Segall, 1996), but it cannot be determined whether all of this displacement was coseismic rupture, or whether it occurred in the immediate postseismic period. The along-strike extent of slip in 1868 did not extend along the entire Hayward Fault (Yu and Segall, 1996; Boatwright and Bundock, 2008), but it is not clear whether the rupture stopped where it did as a result of the rupture front encountering patches of creep, or whether this was a result of geometrical or stress complexities. The

1868 earthquake was pre-instrumental, so no seismic inversions can be conducted to look into these questions. However, dynamic modeling of ruptures on partially-creeping faults can be used to investigate the questions of whether or not coseismic rupture can propagate through a creeping zone on a fault, and of the effect of the distribution of creeping and locked parts of a fault on the endpoints of rupture, in a more generalized way.

Dynamic rupture models are frequently used to investigate the effects of complex fault geometry and stress state on rupture behavior and termination (Harris and Day, 1993; Magistrale and Day, 1999; Kame *et al*., 2003; Oglesby, 2005; Lozos *et al*., 2011a; Andrews and Barall, 2011; Gilchrist *et al*., 2012). Dynamic modeling has also been used to investigate how different individual frictional and weakening parameters affect rupture behavior (Lozos *et al*., 2011b; Ryan, 2012), and to attempt to recreate the rupture behavior of instrumentally-observed events in which rupture may have propagated a rate-strengthening part of of a fault to a zone of the fault normally characterized by rate-strengthening behavior (Barbot *et al.*, 2012; Noda and Lapusta, 2013; Kozdon and Dunham, 2013). Dynamic rupture propagation into a rate-strengthening zone has also been observed in foam block models (Day *et al*., 2008). However, to our knowledge, there exists only one forward dynamic modeling study that investigates the effect of rate-strengthening regions within a predominantly rate-weakening fault (Ryan *et al*., 2013), and no such studies for strike-slip faults specifically.

In the present study, we conduct a series of dynamic rupture models for two different simplified cases of a partially-creeping strike-slip fault: one in which a patch of

surface creep is embedded near the surface in a predominantly locked fault, and one in which a locked patch is embedded at the base of a predominantly creeping fault.

Methods

We use FaultMod (Barall, 2009), a 3D finite element code, to conduct dynamic rupture models of partially-creeping planar strike-slip faults embedded in a homogeneous fully elastic half space. These models represent a single coseismic rupture, and do not incorporate the physics of the process of aseismic creep, only the effects of creeping zones on coseismic rupture propagation.

We implement rate-state friction, specifically a modified Dieterich-Ruina aging law (Dieterich, 1978; Ruina, 1983): $\tau = a\sigma_d \text{arcsinh}[\frac{V}{2V_0}\exp(\frac{f_0 + \psi}{a})]$,

where state variable ψ is defined as $\frac{d\psi}{dt} = -\frac{bV_0}{L}(\exp(-\frac{\psi_{ss}}{b}) - \exp(-\frac{\psi}{b}))$,

ψ_{ss} is the state variable at steady state, V is the slip rate, V_0 is a reference velocity, f_0 is a reference friction coefficient, τ is shear stress, σ_d is time-dependent normal stress, and a and b are dimensionless direct effect parameters. It is the difference between a and b that controls the overall frictional behavior of the fault. If b-a is positive, the steady-state friction on the fault weakens as the slip rate increases, allowing for normal dynamic rupture, while a negative b-a means that the fault strengthens with increased slip rate, thus promoting aseismic creep and disfavoring coseismic rupture. Therefore, we parameterize locked sections of the fault with rate-weakening properties, while creep is modeled as rate-strengthening. We use two different creep parameterizations: one with

stronger rate-strengthening properties, which should be more resistant to coseismic rupture, and one with weaker rate-strengthening. In all of our models, we force nucleation within the rate-weakening zones by raising the shear stress above the yield stress and forcing rupture to propagate over a fixed radius that is larger than the critical patch size needed for self-sustaining rupture propagation. Our physical and computational parameters are listed in Table 4.1.

Table 4.1. Physical and Computational Parameters

Shear stress	75 MPa
Normal stress	120 MPa
a (rate weakening)	0.008
a (rate strengthening)	0.016 (strong) or 0.014 (weak)
b	0.012
f_0	0.6
V_0	1 x 10^{-6} m/s
D_c	0.02015 m
ψ_{init}	0.135524
P wave velocity	6000 m/s
S wave velocity	3464 m/s
Density	2670 kg/m^3
Element size	200 m
Nucleation radius	3000 m
Nucleation shear stress	100 MPa

The geometry for our models of a creeping patch embedded within a locked fault is shown in Figure 4.1. We place a semi-circular rate-strengthening patch at the top center of the fault, as a representation of a fault with measurable surface creep. In the primary set of models, we test creeping patch radii of 4, 6, 8, 10, and 12 km, while keeping the other fault dimensions fixed, and keeping the nucleation at 3 km from the left edge of the fault and 8 km from the base of the fault. In order to test for horizontal directivity effects, we also conducted a set of models in which we extended the length of the fault as we

Figure 4.1.

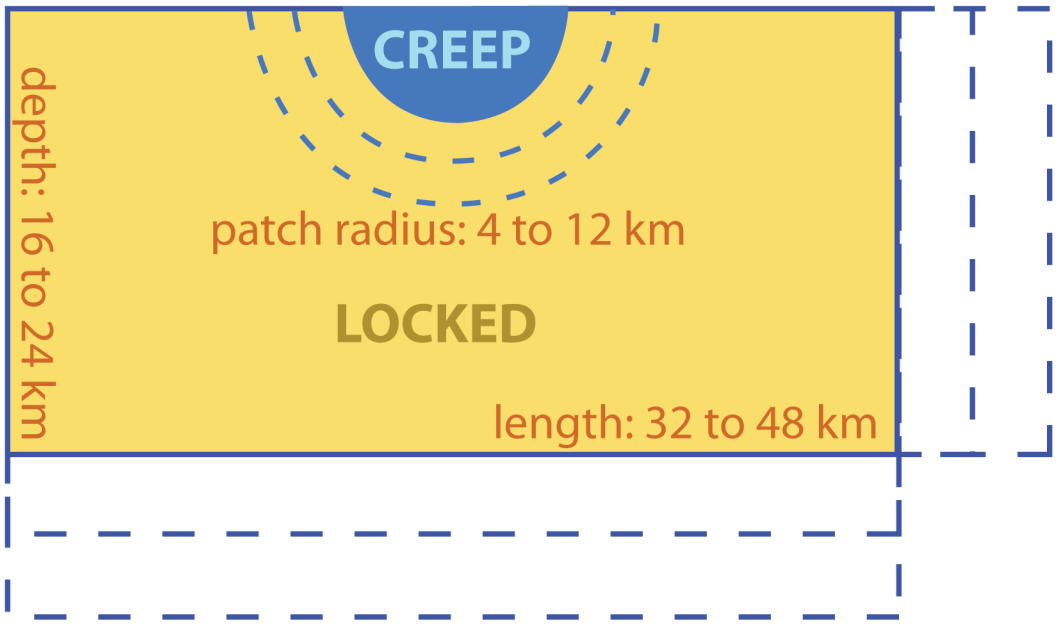

Figure 4.1. Cartoon of fault geometry, for models with a rate-strengthening patch embedded within an otherwise rate-weakening fault. Dotted lines indicate dimensions that we varied within our exploration of parameter space.

Figure 4.2.

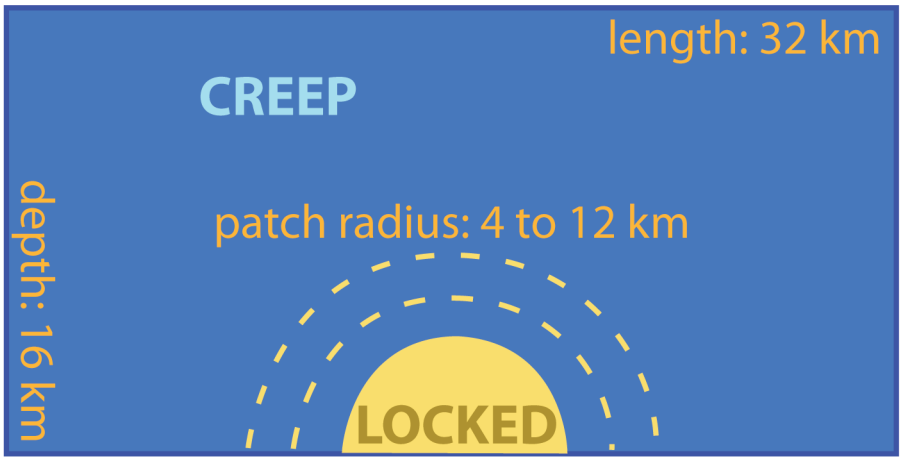

Figure 4.2. Cartoon of fault geometry, for models of a rate-weakening patch in an otherwise rate-strengthening fault. The radius of the locked patch is the only variable dimension here; the fault length and depth are fixed.

increased the radius of the creeping patch, thus keeping the nucleation point at the same distance from the edge of the creeping patch in all cases. Similarly, we tested for vertical directivity effects by conducting a set of models in which we increased the depth of the fault as we increased the radius of the creeping patch, and varied the nucleation point such that the distance between it and the edge of the creeping patch was the same in all cases.

Figure 4.2 shows the geometry of our models of a locked patch embedded within a creeping fault. In these models, we place a semi-circular rate-weakening patch at the base of the fault, also to represent a fault with measurable surface creep. This geometry is also more consistent with what is inferred about the Hayward Fault (Funning *et al*., 2007). As in the previous set of models, we tested locked patch radii of 4, 6, 8, 10, and 12 km while keeping the other fault dimensions constant. Nucleation in these models is forced at the center of the locked patch. Because rupture directivity in these cases is controlled by the size of the locked patch, we did not conduct models with variable fault length or basal depth in the locked-patch-within-creeping-fault case.

Results

Creeping Patch Within a Locked Fault

In the set of models in which the fault dimensions were kept constant but the radius of the creeping patch was variable, we find that the radius of the creeping patch controls both the ability of dynamic rupture to propagate across the entire length of the fault, and the ability of the creeping patch to sustain coseismic slip. Figure 4.3 plots the

Figure 4.3.

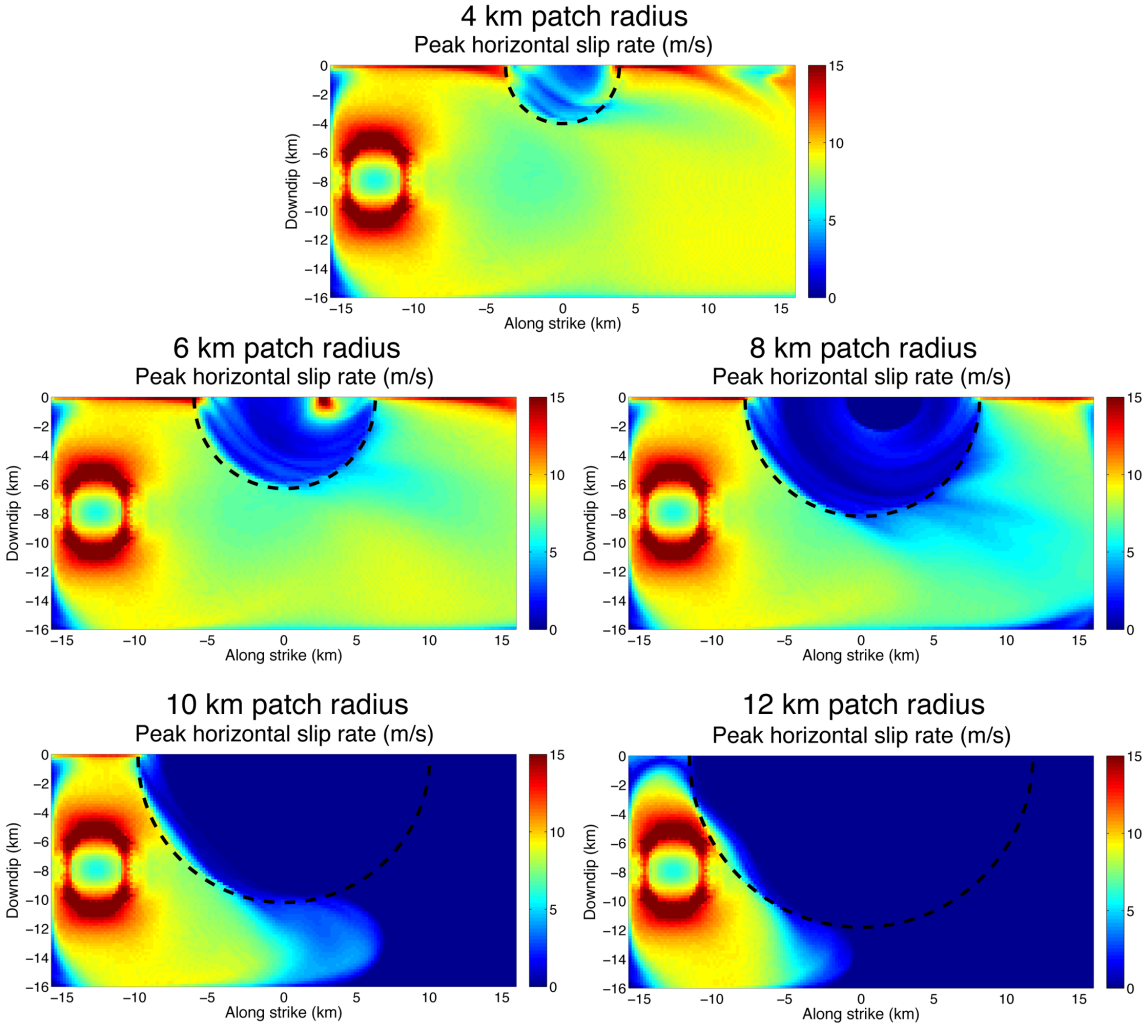

Figure 4.3. Plots of maximum horizontal slip rate for models of a rate-strengthening/creeping patch within an otherwise rate-weakening/locked fault. The dashed black line marks the edge of the creeping patch. Dynamic rupture progresses through the creeping patch in the 4 km radius model, whereas it wraps around the creeping patch and then propagates bilaterally inward in the 6 and 8 km radius models. The zone of high slip rate within the creeping patch in the 6 km radius model represents the coalescence of the rupture fronts propagating inward from either side. If the creeping patch greater than 8 km in radius, it prevents the rupture from propagating to the other end of the fault.

maximum slip rate sustained across the fault in these models, using the stronger rate-strengthening properties for the creeping patches. We find that, if the radius of the creeping patch is half, or less than half of the seismogenic thickness of the fault, rupture is able to propagate through the full strike of the fault. In these cases, the primary rupture through the locked part of the fault progresses along strike and wraps around the creeping patch, after which point slower slip propagates inward into the creeping patch. For radii of 4 and 6 km, the entire creeping patch sustains some coseismic slip, but slip does not reach the center of the patch in the models with an 8 km or greater patch radius. In models with a patch radius of greater than half the seismogenic thickness of the fault (10 and 12 km), rupture stops within the narrow locked zone between the edge of the creeping patch and the base of the fault. In these models, the left edge of the creeping patch, closer to the forced nucleation point, sustains some slow coseismic slip, but this does not progress as far into the creeping patch as in the models where dynamic rupture is able to wrap around the patch and then propagate inward. Using weaker rate-strengthening properties for the creeping patches did not have a first order effect on rupture's ability to propagate across the entire fault, though it did allow for the creeping patches to sustain more coseismic slip than in the models with stronger rate-strengthening properties.

Plots of maximum slip rate for the set of models in which we extended the length of the fault as we increased the radius of the creeping patch are shown in Figure 4.4. Allowing the rupture front to build up energy over the same distance from nucleation to the edge of the creeping patch, regardless of patch size, did not affect the ability of

Figure 4.4.

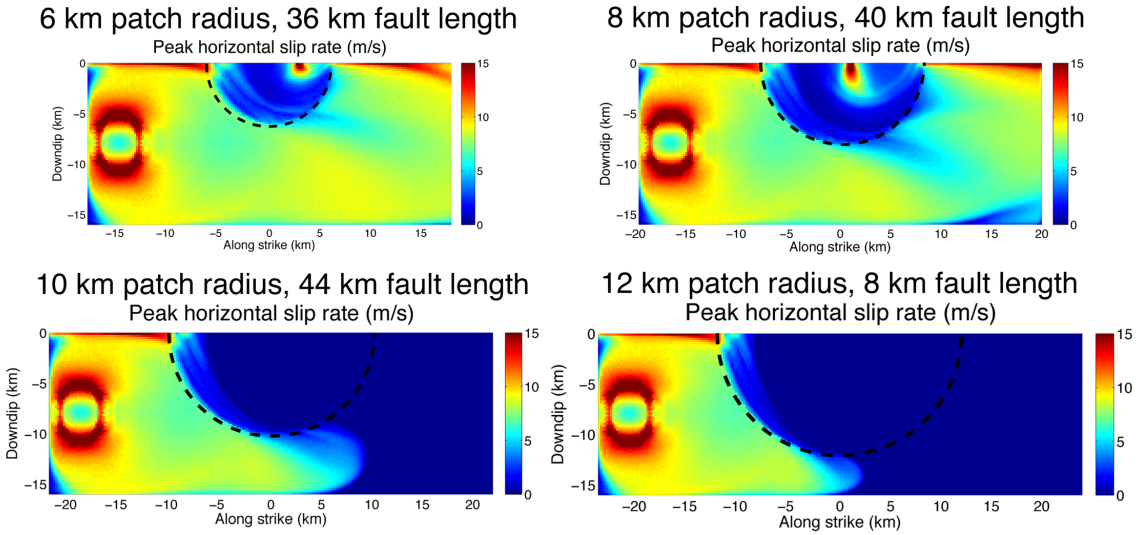

Figure 4.4. Plots of maximum horizontal slip rate for models of a rate-strengthening/creeping patch within an otherwise rate-weakening/locked fault, with the length of the fault scaled by the radius of the creeping patch. The dashed black line marks the edge of the creeping patch. Increasing the length of the fault has no first-order effect on rupture's ability to propagate along strike (compare to Figure 4.3), but the larger directivity effect that results from rupture propagating a larger distance before reaching the creeping patch allows for more coseismic slip within the creeping patch. The areas of particularly high slip rate within the creeping patch in the 6 and 8 km radius models represent the coalescence of two rupture fronts propagating inward from either side of the patch.

Figure 4.5.

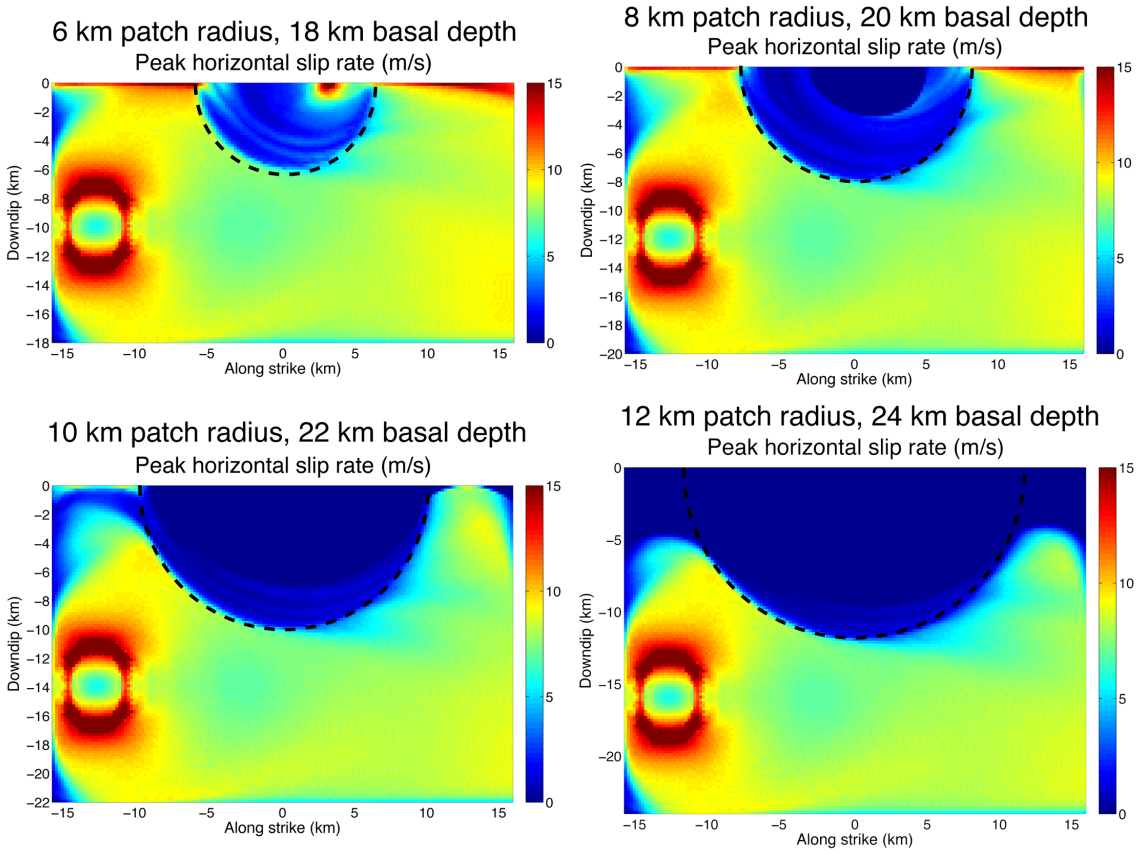

Figure 4.5. Plots of maximum horizontal slip rate for models of a rate-strengthening/creeping patch within an otherwise rate-weakening/locked fault, with the basal depth of the fault scaled by the radius of the creeping patch. The dashed black line marks the edge of the creeping patch. In all cases, rupture propagates along the full extent of the fault strike, but larger creeping patches prevent surface rupture. As in the set of models with a constant 16 km basal depth, smaller creeping patches sustain higher slip rates.

rupture to propagate across the entire fault. Creeping patch radii of greater than half the seismogenic thickness of the fault still arrested rupture propagation. The primary effect of extending the length of the fault was increased extent and amount of coseismic slip within the creeping patches.

The models in which we increased the depth of the fault as we increased the radius of the creeping patch are shown in Figure 4.5. Keeping the distance between the base of the creeping patch and the base of the fault fixed allowed rupture to propagate through the full strike of the fault in all cases. However, rupture was unable to propagate all the way to the surface of the fault in the models with the largest patch radii. Increasing the basal depth of the fault also has little effect on the ability of the creeping patch to sustain coseismic slip.

Locked Patch Within a Creeping Fault

The radius of a locked patch within a predominantly creeping fault has very little effect on the overall rupture behavior. In all of these models, shown in Figure 4.6, rupture propagated to the edges of the locked patch, then died out within the 1 km of creeping fault surrounding the locked patch. Even in the model with a 4 km locked patch radius, in which the radius of the forced nucleation zone was larger than the radius of the locked patch and dynamic rupture was forced into the rate-strengthening zone, rupture still came to a halt within 1 km of the edge of the forced nucleation zone. Implementing a weaker rate-strengthening effect for the creeping parts of the fault slightly increased how far coseismic slip was able to propagate into the creeping zone before coming to a halt, but

Figure 4.6.

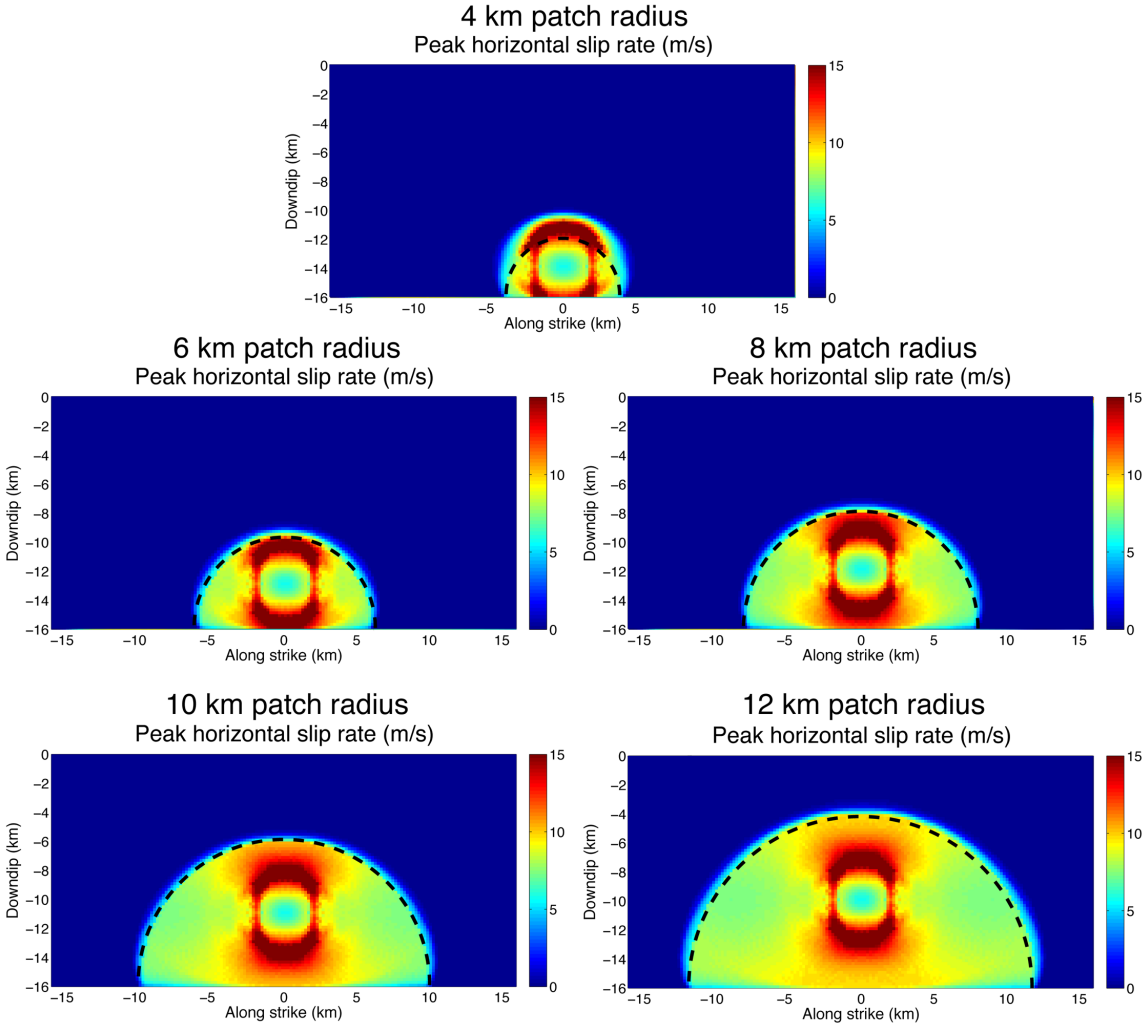

Figure 4.6. Plots of maximum horizontal slip rate for models of a rate-weakening/locked patch within an otherwise rate-strengthening/creeping fault. The dashed black line indicates the edge of the locked patch. Note that, regardless of the size of the locked patch, rupture does not propagate more than 1 km beyond the edge of the patch into the creeping zone. Note that, in the 4 km patch radius model, the size of the forced nucleation zone is larger than the size of the locked patch, but even forced propagation into the creeping part of the fault does not result in self-sustaining rupture outside of the forced nucleation zone.

this effect was not significant enough to allow full dynamic rupture through a rate-strengthening zone.

Discussion

In general, the dimensions of the creeping parts of a fault relative to the locked parts have a much stronger effect on the overall rupture behavior and extent than the specific frictional properties of the creeping patches do. In particular, there must be a critical width of locked fault through which full dynamic rupture can propagate around a creeping zone. If the narrowest dimension of the locked zone is between the base of the fault and the furthest down-dip edge of the creeping patch, as in the 10 and 12 km radius cases in Figure 4.3, along-strike rupture may be halted. Similarly, if the narrowest dimension is between the end of the fault and the nearest along-strike edge of the creeping patch, as in the 12 km radius case in Figure 4.5, rupture may be prevented from reaching the surface of the fault.

This effect is a result of how the energy budget of a rupture front is divided. A rupture propagating along a homogeneous rate-weakening fault builds up seismic wave energy ahead of the rupture front in the direction of rupture, and can spend most of that energy on seismic radiation and increasing its propagation speed, rather than on fracture energy or friction. Creeping patches with smaller radii do not pose much of an interruption to this buildup of energy, which is why fracturing and slipping into the rate-strengthening patch does not use so much of the energy budget such that none is left for propagation and radiation. However, a creeping patch with a large radius alters the

energy balance both by requiring more energy to go into fracturing through the creeping area, and by decreasing the area of fault that is building up more energy ahead of the rupture front. Thus, the rupture becomes less energetic overall, and is spending more of the remaining energy on fracture and less on propagation and radiation, which ultimately leads to the rupture dying out in the narrow locked zone and not propagating as far into the creeping patch.

As a test of this critical width effect, we conducted a model in which a creeping patch with a 12 km radius is embedded in a fault that is as long as the 12 km radius case in Figure 4.3 and as deep as the 12 km radius case in Figure 4.5, thus eliminating any major narrowing of the locked zone. In this model, the results of which are shown in Figure 4.7, rupture propagated from end to end of the fault, and from base to surface. This rupture front was able to build up enough energy that it was able to propagate much further into the creeping patch than in any of our other models.

The balance of the energy budget is also why the cases in which the rate-weakening part of the fault is completely surrounded by rate-strengthening all result in rupture stopping within a short distance of the edge of the locked patch. In these cases, the entire energy budget is redirected into fracture and friction when rupture reaches the rate-strengthening zone. Not only is there no more accumulation of energy ahead of an ongoing rupture front, but the rate-strengthening zone also resists fracture. The combination of these effects halts the rupture propagation almost immediately after it reaches the creeping zone.

Figure 4.7.

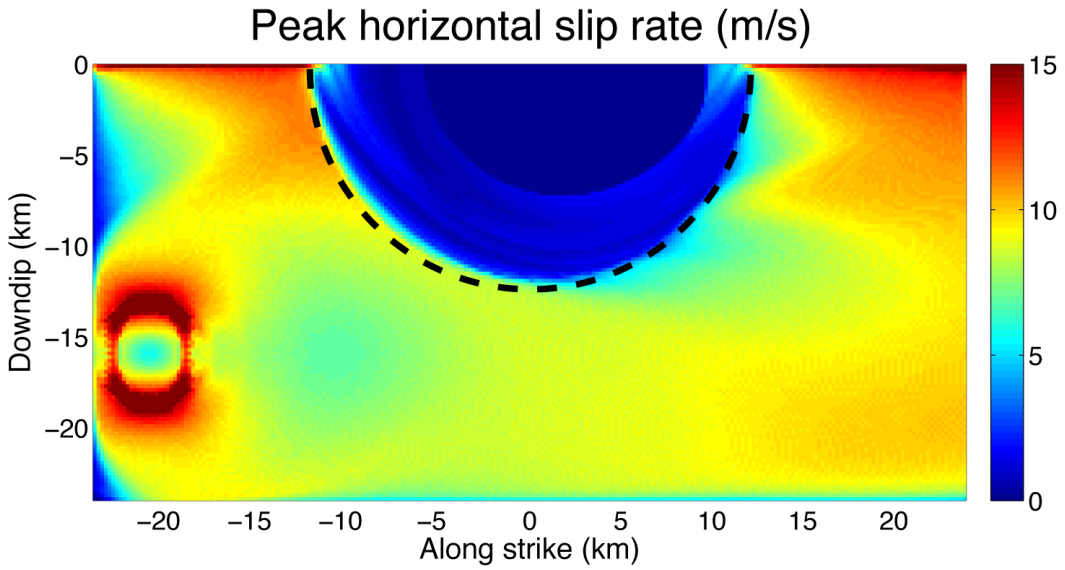

Figure 4.7. Maximum horizontal slip rate for a model with a rate-strengthening/creeping patch with a 12 km radius embedded in an otherwise rate-weakening/locked fault, with both the fault length and basal depth scaled up to accommodate the large patch radius. The edge of the creeping patch is indicated by the dashed black line. A 12 km patch radius arrested along-strike rupture in Figure 4.3, and up-dip rupture in Figure 4.5, but in this model, rupture is able to reach both the surface and the far end of the fault.

Conclusions

We find that the presence of a creeping patch within a locked fault, and vice versa, can have a controlling effect on the ability of rupture to propagate through the entire fault. In particular, the width of the locked zone with respect to the width of the creeping zone is the controlling factor. If the locked zone is too narrow, then the overall energy budget of the rupture decreases, and more of the remaining energy is spent on fracture as opposed to propagation and radiation, which can lead to arrest of the rupture front. In the case of a locked patch within a creeping fault, this reduction and re-balancing of the energy budget is almost instantaneous when rupture reaches the edge of the locked patch, which results in near immediate cessation of rupture propagation. We also find that some coseismic slip through a creeping zone is possible in cases where the rupture front is not forced to narrow much around the creeping zone, though the amount of slip is less than in locked areas, and the associated slip rate is slower.

While our models are extremely simplified when compared to a real-world fault, and while they do not account for the difference in stress and strain accumulation on a creeping zone as opposed to a locked one, nor for the effects of pore fluid pressurization, they still provide constraints as to possible rupture extents. In the case of the Hayward Fault, on which the locked patches are surrounded entirely by creep, dynamic rupture is likely to be confined in those locked patches, which means an end-to-end dynamic rupture of the entire fault is unlikely, and that observed surface displacement is more likely to be postseismic than coseismic. However, if the creeping patches of a given fault were small and surrounded by locked zones, they may be able to sustain coseismic slip.

Our models highlight the importance of knowing the geometry of the creeping and locked parts of a partially-creeping fault in assessing potential rupture lengths and amounts of coseismic surface displacement. We emphasize that any dynamic rupture models on partially-creeping faults should incorporate this complexity with as much detail as possible.

References

Andrews, D. J., and M. Barall (2011). Specifying initial stress for dynamic heterogeneous earthquake source models, *Bulletin of the Seismological Society of America* **101**, 2408-2417.

Barall, M. (2009). A grid-doubling technique for calculating dynamic three-dimensional spontaneous rupture on an earthquake fault, *Geophysical Journal International* **178**, 845–859.

Barbot, S., N. Lapusta, and J.-P. Avouac (2012). Under the hood of the earthquake machine: toward predictive modeling of the seismic cycle, *Science* **336**, 707-710.

Boatwright, J., and H. Bundock (2008), Modified Mercalli Intensity maps for the 1868 Hayward earthquake plotted in ShakeMap format, *Open File Report 2008-1127*, U.S. Geological Survey, Menlo Park, California.

Day, S. M., S. H. Gonzalez, R. Anooshehpoor, and J. N. Brune (2008). Scale-model and numerical simulations of near-fault seismic directivity, *Bulletin of the Seismological Society of America* **98**, 1186-1206.

Dieterich, J. H. (1978). Time-dependent friction and the mechanics of stick-slip, *Pure and Applied Geophysics* **116**, 790-806.

Funning, G. J., R. Burgmann, A. Ferretti, and F. Novali (2007). Asperities on the Hayward Fault resolved by PS-InSAR, GPS and boundary element modeling, *EOS Transactions* **88**, S23C-04.

Gilchrist, J. J., J. H. Dieterich, K. B. Richards-Dinger, and D. D. Oglesby (2012). "Using a multi-cycle earthquake simulator to specify initial conditions for modeling rupture dynamics." American Geophysical Union Fall Meeting, Moscone Center, San Francisco, California. Conference presentation.

Harris, R. A., and S. M. Day (1993). Dynamics of fault interaction: parallel strike-slip faults, *Journal of Geophysical Research* **98,** 4461-4472.

Kame, N., J. R. Rice, and R. Dmowska (2003). Effects of pre-stress state and rupture velocity on dynamic fault branching, *Journal of Geophysical Research* **108,** 2265, doi: 10.1029/2002JB002189.

Kozdon, J. E., and E. M. Dunham (2013). Rupture to the trench: dynamic rupture simulations of the 11 March 2011 Tohoku earthquake, *Bulletin of the Seismological Society of America* **103**, 1275-1289.

Lienkaemper, J. J., J. S. Galehouse, and R. W. Simpson (2001), Long-term monitoring of creep rate along the Hayward fault and evidence for a lasting creep response to 1989 Loma Prieta earthquake, *Geophysical Research Letters* **28**, 2265–2268.

Lienkaemper, J. J., and P. L. Williams (2008), A record of large earthquakes on the southern Hayward fault for the past 1800 years, *Bulletin of the Seismological Society of America* **97**, 1803–1819.

Lozos, J. C., D. D. Oglesby, B. Duan, and S. G. Wesnousky (2011a). The effects of fault bends on rupture propagation: a geometrical parameter study, *Bulletin of the Seismological Society of America* **101***,* 385-398.

Lozos, J. C., J. H. Dieterich, and D. D. Oglesby (2011b). "The effects of d_0 on rupture propagation on geometrically-complex faults." Seismological Society of America Annual Meeting, Memphis Marriott Downtown Hotel, Memphis, Tennessee. Conference presentation.

Magistrale, H., and S. M. Day (1999). 3D simulations of multi-segment thrust fault rupture, *Geophysical Research Letters* **26,** 2093-2096.

McFarland, F. S., J. J. Lienkaemper, and S. J. Caskey (2009), Data from theodolite measurements of creep rates on San Francisco Bay region faults, California: 1979-2009, *Open File Report 2009-1119*, U.S. Geological Survey, Menlo Park, California.

Noda, H., and N. Lapusta (2013). Stable creeping fault segments can become destructive as a result of dynamic weakening, *Nature* **493**, 518-521.

Oglesby, D. D. (2005). The dynamics of strike-slip step-overs with linking dip-slip faults, *Bulletin of the Seismological Society of America* **95,** 1604-1622.

Ruina, A. (1983). Slip instability and state variable friction laws*, Journal of Geophysical Research* **88**, 10359-10370.

Ryan, K. J. (2012). Dynamic models of earthquake rupture on fault stepovers and dip-slip faults using various friction formulations, MS thesis, University of California, Riverside.

Ryan, K. J., D. D. Oglesby, and E. L. Geist (2013). "Modeling rupture with heterogeneous prestress and through stable sliding zones, and implications for an Alaskan-Aleutian megathrust earthquake." Seismological Society of America Annual Meeting, Salt Palace Convention Center, Salt Lake City, Utah. Conference presentation.

Yu, E., and P. Segall (1996). Slip in the 1868 Hayward earthquake from the analysis of historical triangulation data, *Journal of Geophysical Research* **101**, 16,101–16,118.

Conclusion

The effects of fault zone complexity have long been a focus of research within the sub-field of earthquake rupture dynamics. The present work investigates four different aspects of fault zone complexity, and affirms in all cases that complexity can have a controlling effect on the extent of rupture, the details of rupture behavior, and the resulting ground motion.

Our investigation of geometrical effects, in the more simplified case of a stepover consisting of two or three planar segments, or in the extremely complex case of the northern San Jacinto Fault, corroborates past work showing that geometry alone can control rupture behavior (e.g. Harris and Day, 1993; Magistrale and Day, 1999; Kame et al. 2003; Oglesby, 2005; Oglesby, 2008; Lozos *et al.*, 2011). However, our work continues to break down the common interpretation that rupture is more easily able to negotiate an extensional stepover or bend than a compressional one of the same size. We find that the orientation of the faults within a regional stress field, and their orientation relative to one another, contributes just as large of an effect as both dynamic and static compression and extension do. We also find that small geometrical features, such a short bends or intermediate fault segments within a larger stepover, can also have a controlling effect on rupture through the larger fault system. Past work on faults with small-scale geometrical complexities produce very heterogeneous rupture behaviors and stress distributions (Dieterich and Smith, 2009; Dunham *et al*., 2011; Shi and Day, 2013), but these studies specifically isolate the effects of these small complexities. Our work

combines small-scale and large-scale geometrical complexities, and shows that small features can control overall rupture extent and behavior just as much as large ones do.

Similiarly, our work on the effect of complex initial stress conditions builds upon existing work on this topic by combining different scales and types of complexity. Past work has shown that geometrically-induced stress heterogeneity (Dieterich and Smith, 2009), the heterogeneity that comes from how a regional stress field resolves onto different sections of a bent fault (Lozos *et al*., 2011), and a random stochastic stress distribution (Oglesby and Day, 2002; Andrews and Barall, 2011) can all control slip patterns and rupture extent. In all of these cases, it is the spacing and relative intensity of the contrasts in stress, stress drop, and fault strength (S), rather than the specific values of all of those parameters, that affects the rupture behavior. We find that a combination of all of these effects also produces a very complex stress distribution. While it is still the spacing and intensity of the stress contrasts that controls rupture behavior in our models, we find that leaving out one type of stress complexity, versus including as many as realistically possible, produces a different stress distribution that results in different rupture characteristics.

By incorporating a complex velocity structure into our dynamic rupture models, we support a conclusion that is common between kinematic modeling studies of ruptures on faults within realistic geologic settings: the velocity structure has a strong effect on the intensity and distribution of strong ground motion, particularly in areas not immediately adjacent to the fault (Olsen *et al*., 2006; Jones *et al*., 2008; Graves *et al*., 2011). These effects are apparent in our dynamic models, even with a velocity structure that is clipped

such that we are able to resolve ground motions of up to 1 Hz with an element size of 200 m. We also find that whether or not a model of a complex fault is placed in its realistic material setting may make the difference between whether or not rupture is able to negotiate major geometrical complexities in the fault trace; this is due to changes in the energy budget of the rupture front as it encounters a sharp contrast in material properties. This effect will likely be even more significant in dynamic models with a higher spatial resolution, since the velocity structure would not need to be smoothed out as much in order to resolve 1 Hz ground motions.

Our models of faults with rate-strengthening patches within rate-weakening zones and vice versa, and our investigation of the effect of the size of the slip weakening parameter, emphasize the importance of frictional regime and fault weakening behavior in rupture propagation. We find that a contrast in frictional/weakening properties can serve as a barrier to rupture by directing more of the energy budget into fracture and friction than into propagation and radiation, and also by decreasing the overall energy concentration by interrupting directivity. However, we find that dynamic stress changes can still induce some coseismic slip even within rate-strengthening zones. These findings are corroborated by models of contrasting frictional weakening/strengthening regimes in subduction zones (Noda and Lapusta, 2013; Kozdon and Dunham, 2013; Ryan *et al*., 2013), though we are the first to extend this type of modeling into the realm of strike-slip faults. We also show that the way in which weakening (or strengthening) is parameterized within a model can control the abruptness of the redistribution of the energy budget of a rupture front, which can in turn control the extent of rupture. Thus,

choice of parameterization is important, even though it is difficult to infer which parameterization is most correct for real faults.

Though our work addresses several different aspects of fault complexity and its effect on rupture behavior, we can still make several overarching points that are borne out by all of our results. First, we find that rupture extent is controlled largely by the shape and distribution of heterogeneity, and by the intensity of contrast between adjacent patches, rather than by the specific intensity of any one parameter. In order for rupture to continue along a fault, it must have some critical width of favorable on-fault properties through which to propagate. If an unfavorable part of a fault system – be it a bend that is unfavorably oriented within a stress field, a stepover or discontinuity in the fault trace, a patch of particularly high fault strength, or a rate-strengthening zone – is small enough, rupture will either propagate through it or jump over it; or, if the unfavorable zone is surrounded by favorable parts of the fault, rupture may be able to propagate around it. It is only when the unfavorable zone is too large, or when the surrounding favorable zones are too small, that rupture propagation is arrested.

Second, the critical size of a zone of unfavorable fault properties needed to stop rupture, or the critical size of a zone of favorable properties needed to allow rupture to continue, is directly related to the energy budget of the rupture front. Negotiating an unfavorable patch of any type requires more energy to be directed into fracture and friction than into forward propagation and seismic radiation. The barrier also breaks directivity, which means the rupture front is no longer building up energy due to seismic radiation ahead of the rupture front in the direction of propagation. Thus, if an

unfavorable barrier is large enough that it redirects the entire energy budget into fracture and friction while significantly depleting the energy, rupture may die out. The amount of the energy budget that is redirected into fracture and friction, and the rate at which energy depletes once the rupture is in the unfavorable area, depends on the way in which on-fault weakening properties are parameterized, further emphasizing the importance of choosing values for these parameters that are informed by best inferences of real-world properties.

Lastly, while each individual type of fault zone complexity investigated within this study contributes to rupture behavior, ground motion, and to the overall extent of rupture, when many levels of realistic complexity are combined into a single model, it is difficult to separate out the individual effects of each component from the resulting rupture. That said, leaving out one type of heterogeneity may drastically alter the rupture behavior, even if the specific effect of that parameter is not individually identifiable outside of its interactions with other types of heterogeneity. Thus, we feel that it is important to incorporate as many levels of realistic complexity as feasible into models of both historic and forward scenario events on real faults. There is still much room for modeling that isolates the effects of individual parameters, or of the interactions between selected simplified types of heterogeneity, on the physics of rupture. However, when assessing the potential rupture and ground motion hazard of a specific fault zone, it is advisable to incorporate as much observational and geological information about the geometry, stress state, distribution of asperities and barriers, and surrounding material setting into the model as possible, in order to produce the most plausible description of that fault's rupture behavior and related hazard.

References

Andrews, D. J., and M. Barall (2011). Specifying initial stress for dynamic heterogeneous earthquake source models, *Bulletin of the Seismological Society of America* **101**, 2408-2417.

Dieterich, J. H., and D. E. Smith (2009). Nonplanar faults: mechanics of slip and off-fault damage, *Pure and Applied Geophysics* **166**, 1799-1816.

Dunham, E. M., D. Belanger, L. Cong, and J. E. Kozdon (2011). Earthquake ruptures with strongly rate-weakening friction and off-fault plasticity, part 2: nonplanar faults, *Bulletin of the Seismological Society of America* **101**, 2308-2322.

Graves, R., T. H. Jordan, S. Callaghan, E. Deelman, E. Field, G. Juve, C. Kesselman, P. Maechling, G. Mehta, K. Milner, D. Okaya, P. Small, and K. Vahi (2011). CyberShake: a physics-based seismic hazard model for southern California, *Pure and Applied Geophysics* **168**, 367-381.

Harris, R. A., and S. M. Day (1993). Dynamics of fault interaction: parallel strike-slip faults, *Journal of Geophysical Research* **98,** 4461-4472.

Jones, L. M., R. Bernknopf, D. Cox, J. Goltz, K. Hudnut, D. Mileti, S. Perry, D. Ponti, K. Porter, M. Reichle, H. Seligson, K. Shoaf, J. Treiman, and A. Wein (2008). The ShakeOut scenario, *U.S. Geological Survey Open File Report 2008-1150*.

Kame, N., J. R. Rice, and R. Dmowska (2003). Effects of pre-stress state and rupture velocity on dynamic fault branching, *Journal of Geophysical Research* **108,** 2265, doi: 10.1029/2002JB002189.

Kozdon, J. E., and E. M. Dunham (2013). Rupture to the trench: dynamic rupture simulations of the 11 March 2011 Tohoku earthquake, *Bulletin of the Seismological Society of America* **103**, 1275-1289.

Lozos, J. C., D. D. Oglesby, B. Duan, and S. G. Wesnousky (2011). The effects of fault bends on rupture propagation: a geometrical parameter study, *Bulletin of the Seismological Society of America* **101***,* 385-398.

Magistrale, H., and S. M. Day (1999). 3D simulations of multi-segment thrust fault rupture, *Geophysical Research Letters* **26,** 2093-2096.

Noda, H., and N. Lapusta (2013). Stable creeping fault segments can become destructive as a result of dynamic weakening, *Nature* **493**, 518-521.

Oglesby, D. D., and S. M. Day (2002). Stochastic fault stress: implications for fault dynamics and ground motion, *Bulletin of the Seismological Society of America* **92**, 3006-3021.

Oglesby, D. D. (2005). The dynamics of strike-slip step-overs with linking dip-slip faults, *Bulletin of the Seismological Society of America* **95,** 1604-1622.

Oglesby, D. D. (2008). Rupture termination and jump on parallel offset faults, *Bulletin of the Seismological Society of America* **98**, 440-447.

Olsen, K. B., S. M. Day, J. B. Minster, Y. Cui, A. Chourasia, M. Faerman, R. Moore, P. Maechling, and T. Jordan (2006). Strong shaking in Los Angeles expected from southern San Andreas earthquake, *Geophysical Research Letters* **33**, doi: 10.1029/2005GL025472.

Ryan, K. J., D. D. Oglesby, and E. L. Geist (2013). "Modeling rupture with heterogeneous prestress and through stable sliding zones, and implications for an Alaskan-Aleutian megathrust earthquake." Seismological Society of America Annual Meeting, Salt Palace Convention Center, Salt Lake City, Utah. Conference presentation.

Shi, Z., and S. M. Day (2013). "Validation of dynamic rupture simulations for high-frequency ground motion." Seismological Society of America Annual Meeting, Salt Palace Convention Center, Salt Lake City, Utah. Conference presentation.